FIU Wall of Wind
NHERI Experimental Facility

Wind-Induced Loads on Roof Overhangs
Project# B83FC1
(Year 2)

Submitted to:

Florida Building Commission

Florida Department of Business and Professional Regulation

Mo Madani, Program Manager

Building Codes and Standards 2555 North Shumard Road
Tallahassee, Florida 32399

Laboratory for Wind Engineering Research (LWER), Extreme Events Institute (EEI)

Florida International University (FIU)

Prepared by:

Project PI: Ioannis Zisis, Associate Professor, CEE, Florida International University, USA

Project Co-PI: Ted Stathopoulos, Professor, BCEE, Concordia University, Canada

Graduate Research Assistant: Karim Mostafa, CEE, Florida International University, USA

Date: June 2022

Contents

List of Figures

List of Tables

EXECUTIVE SUMMARY

The Laboratory for Wind Engineering Research (LWER) of the Extreme Events Institute (EEI) at Florida International University (FIU) was commissioned by the Florida Building Commission / Florida Department of Business and Professional Regulation to investigate the wind-induced loads on roof overhangs of low-rise residential buildings. The large-scale experimental campaign was carried out at the Wall of Wind (WOW) Research Experimental Facility in two phases. The first phase was carried out in 2021 and composed of two 1:10 scaled models (2 ft and 6 ft inclined overhangs) of a low-rise hip roof building with roof slope 4:12. Phase 2 which has been carried out in 2022 composed of six 1:10 scaled models of a low-rise hip roof building with two different roof slopes (i.e., 4:12 and 6:12). The detailed description of the six models is discussed in this report. In addition, this report describes the experimental and analytical tasks conducted and concludes on the research findings.

The research showed that the 2 ft overhang experienced higher suction coefficients at the edges compared to the 4 ft and 6 ft overhangs. In addition, the results confirmed that, for all models, soffit pressure coefficients may be taken as the adjacent wall external pressure, as stated by ASCE7-16 for the case of positive pressure coefficients. On the contrary, negative pressure coefficients (i.e., suction) were not well correlated between the soffit and the wall. The width of the overhang did not seem to have a considerable effect on the positive pressure coefficient on walls and soffit. However, by carrying out correlation and regression analysis between soffit pressure taps and upper wall taps, the 6 ft soffit seemed to be less correlated with the wall upper taps, than the 2 ft and 4 ft soffits. Moreover, the research showed that the 4:12 roof slope experienced higher suction compared to the 6:12 roof slope. Area averaged pressure coefficients for overhangs and adjacent roof areas, were compared to the GC_p plots in ASCE 7-10, ASCE 7-16, and ASCE 7-22 for each specified zone. The provision is less conservative compared to the experimental testing for most of the cases. A codification study has been carried out and design guidelines are recommended for hip roof with overhangs and adjacent walls.

1. Introduction

An overhang is an unenclosed continuation of the roof surface. Particularly on low-rise residential applications, overhangs may be open or covered by a soffit and may be cantilevered or supported. Most of the foundational belief about overhangs seems to suggest that overhangs extend no more than 2 ft, whereas, in Florida, overhangs are often much longer and are necessary for energy efficiency and livability in this semi-tropical climate. Overhangs in Florida can be cantilevered 6 ft or more, or supported, as on a terrace or porch, for 10 to 12 ft or more.

Low-rise buildings are greatly affected by extreme wind events. The risk of wind-induced failure is particularly increased on roofs and roof overhangs. The latter are commonly used in residential and industrial buildings for weather protection against wind, snow, rain, and sun. Roof overhangs are prone to damage because they are subjected to wind from both the upper and bottom surfaces (soffit). They are vulnerable to uplift forces that in some cases could trigger local or more severe failure on the roof. Researchers at CSTB [Centre Scientifique et Technique du Bâtiment (Center for Building Science and Technology)] suggested to limit the length of overhangs to 20 in especially for small slope roofs, Taher (2007). Nevertheless, in warmer and sunny climates, it is common to use extended overhangs that go beyond the 2 ft and even reach 6 ft. Extended overhangs resemble a roof extension like a canopy or a patio cover that is attached to the main structure. Recent studies showed that canopies may experience lower wind loads compared to those specified for roof overhangs on ASCE 7 (Zisis and Stathopoulos 2010, Candelario et al. 2014, Zisis et al. 2017).

ASCE 7-16 (2017) provides methods for analysis of the loads on overhangs, both for main wind force resisting systems (MWFRS) and component and cladding (C&C) loads, but the commentary does not provide any information as to the maximum length of overhang for which this analysis is valid. In section 30.9, it states that the pressure on the bottom covering of the roof overhang is the external pressure coefficient on the adjacent wall surface as implemented by Vickery (2008). This assumption was adopted more recently in the ASCE 7-16 (2017). The most recent version ASCE 7-22 (2022) has the same assumption. In earlier versions of ASCE 7, for instance in ASCE 7 (2010), the overhang pressures considered the net pressure applied on these elements from simultaneous contributions from both the top and bottom surfaces of the overhang. Moreover, this may be an adequate assumption for a 2 ft overhang, but the pressure on the bottom surface of a 4ft or 6ft or 12ft overhang may not be a simple one-to-one wall-to-overhang pressure equivalent. The research that was done for canopies (ASCE 7-16 section 30.11), suggests that this may not be the case (Candelario et al. 2014, Zisis et al. 2017). Most importantly the research that led to the revised provisions of ASCE 7-16 did not consider any building model with roof overhangs.

The last three recent versions of ASCE 7 have different procedures regarding the design of roof overhangs. These major differences are discussed in detail later this report. In this project, wind tunnel testing using large-scale models with different overhang widths was carried out. The project was divided into two phases. In phase 1, which was carried out in 2021 (Zisis et al. 2021), large scale wind tunnel experiments were conducted at the Wall of Wind at Florida International University for two models of a residential building of hip roof with different overhang width (i.e. 2 ft and 6 ft) for a hip roof building with slope 4:12, eave height of 24 ft and horizontal dimensions of 40 ft by 50 ft (full scale). Peak local surface wind coefficients were measured for walls, soffits, and roofs with overhangs for both model cases. Moreover, area averaged pressure coefficients were measured for different combinations of taps and were compared to the GC_p plots in ASCE 7-16. In addition to local and area averaged pressure coefficients, correlation coefficients and

regression analyses were considered to assess the correlation of soffit pressure coefficients to pressure coefficients of wall upper taps. The findings showed that the 2 ft overhang experienced higher suction coefficients at the edges compared to the 6 ft overhang. In addition, the results confirmed that, for both models, soffit positive pressure coefficients may be taken as the adjacent wall external pressure, as stated by ASCE7-16, while for negative pressure this assumption may not be valid. Area-averaged pressure analysis was carried out and compared to the GC_p plots in ASCE 7-16. The standard was less conservative compared to the experimental results regarding most of the cases. Thus, the experimental testing carried out in this phase was used for an enhanced and more comprehensive codification study that included data from both phases. More details about the results and finding from phase 1 can be found in 'phase 1 final report' that is available online on floridabuilding.org (Zisis et al. 2021). In addition, data from phase 1 testing have been published online on Designsafe - Data Depot (Mostafa et al. 2022). The data from this phase will be available online on Designsafe-Data Depot later in June 2022.

In phase 2, which was conducted in 2022, large scale wind tunnel tests were carried out on six models of different overhang widths and roof slope. It is important to investigate how the pressures on the wall relate to the overhang and for what distance. In addition, it is important to investigate at what point does the wall pressure cease to affect the overhang of different width. Finally, the experimental results are compared with ASCE 7-22, ASCE 7-16, and ASCE 7-10 in terms of area averaging pressure analysis to investigate the pressure gradients on single and groups of taps on the overhangs.

This report is divided into three main parts; first the physical testing, including the model design, pressure tap instrumentation, test setup, and test protocols, second the experimental results, data analysis and findings, and finally a proposal from a codification study that could be implemented in future ASCE 7 wind provisions and other building codes of practice.

2. Experimental setup and test protocol

This section comprises the experimental test setup that was conducted at the Wall of Wind (WOW) Experimental Facility at Florida International University (FIU) (Gan Chowdhury et al. 2016) in February 2022. The 12-fan WOW is the largest and most powerful university research facility of its kind and can simulate a Category 5 hurricane – the highest rating on the Saffir-Simpson Hurricane Wind Scale. In 2015, the National Science Foundation (NSF) has designated the Wall of Wind as one of the nation's major "Experimental Facilities" (EF) under the Natural Hazards Engineering Research Infrastructure (NHERI) program as a distributed, multi-user national facility that provides the natural hazards research community with access to research infrastructure. The WOW EF is managed by FIU's Extreme Events Institute (EEI).

2.1.Model layouts and dimensions

Discussions were held with an informal advisory group of building code officials and truss manufacturing companies before phase 2 testing. It was concluded that priority should be given to the most common layouts that exist in current residential construction. Thus, a hip roof building layout was selected, with an eave height of 24 ft and horizontal dimensions of 40 ft by 50 ft (full scale). The slope of the roofs was either 4:12 to continue what had been tested on phase 1, or 6:12, which is associated with phase 2 testing only. The building dimensions are the same with those

tested in phase 1 and phase 2 and at the same scale of 1:10 for all the models. The six models were named from Model A to F, and the details of each model are as follows. Model A has a roof slope 4:12 and an inclined overhang with width of 4 ft, which is one of the most common widths suggested by the truss manufacturing industry, covered underneath with a horizontal soffit. It is important to mention that model A continues on the two models that were tested in phase 1 (2 ft and 6 ft). Models B, C and D have a roof slope 6:12 with an inclined overhang width of 2 ft, 4 ft, and 6 ft respectively, covered underneath with a horizontal soffit. The last two models (models E and F) have a roof slope 6:12 and inclined overhang width of 2 ft and 4 ft, respectively, with no cover underneath (i.e., with no horizontal soffit). Model E and F were tested for the purpose of comparison with models B and C in terms of the difference between covered and uncovered soffit. Drawings of the six models are shown in Figures 1 to 6 with model scale dimensions in inches. Table 1 shows the scales for the different parameters in test setup and Table 1 shows the prototype and model dimensions.

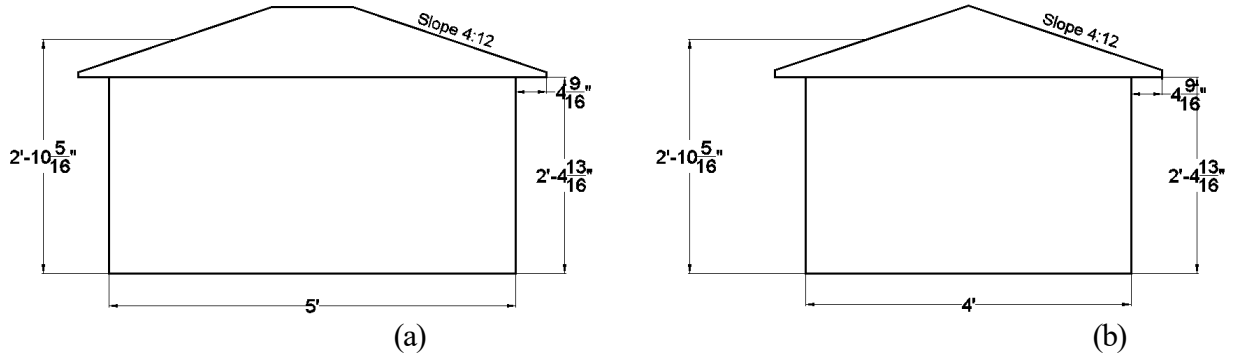

Figure 1 Model A layout (a) Elevation View (b) Side View

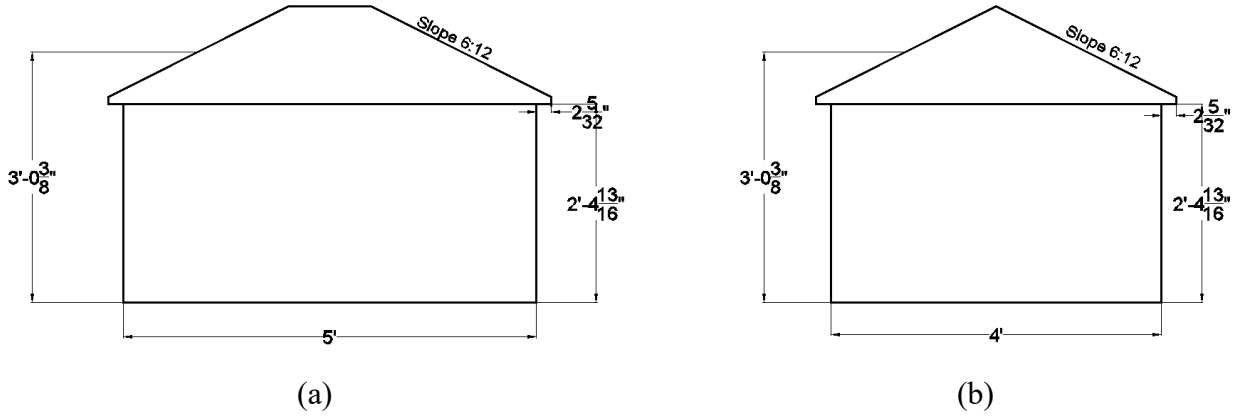

Figure 2 Model B layout (a) Elevation View (b) Side View

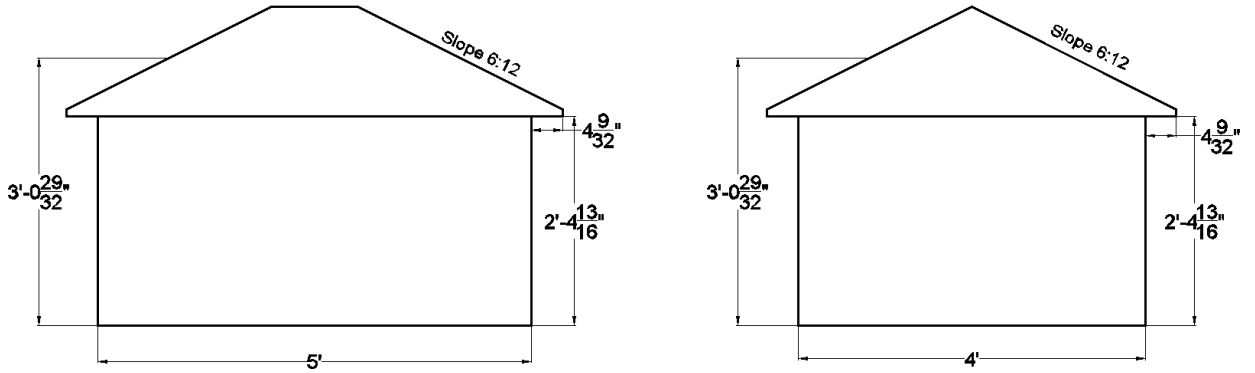

(a) (b)

Figure 3 Model C layout (a) Elevation View (b) Side View

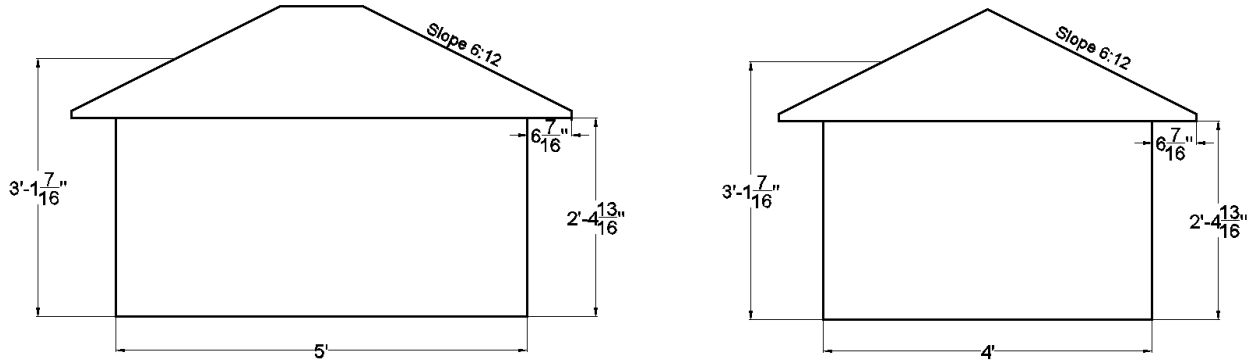

(a) (b)

Figure 4 Model D layout (a) Elevation View (b) Side View

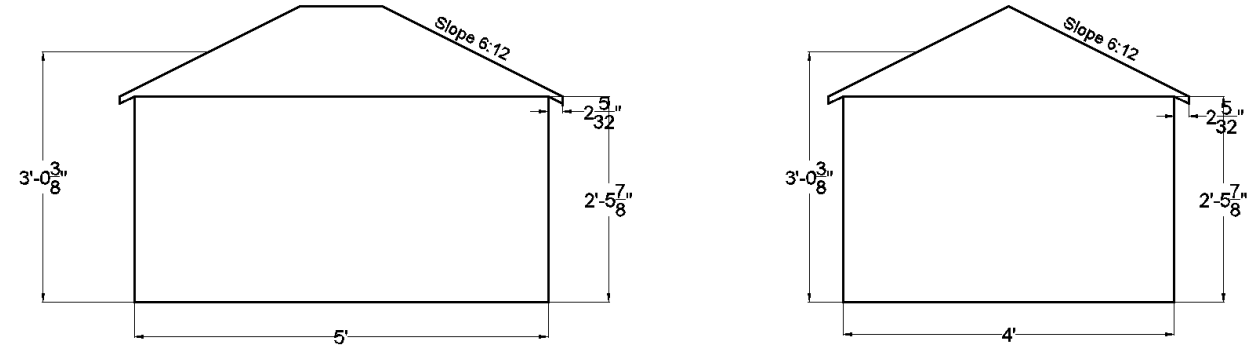

(a) (b)

Figure 5 Model E layout (a) Elevation View (b) Side View

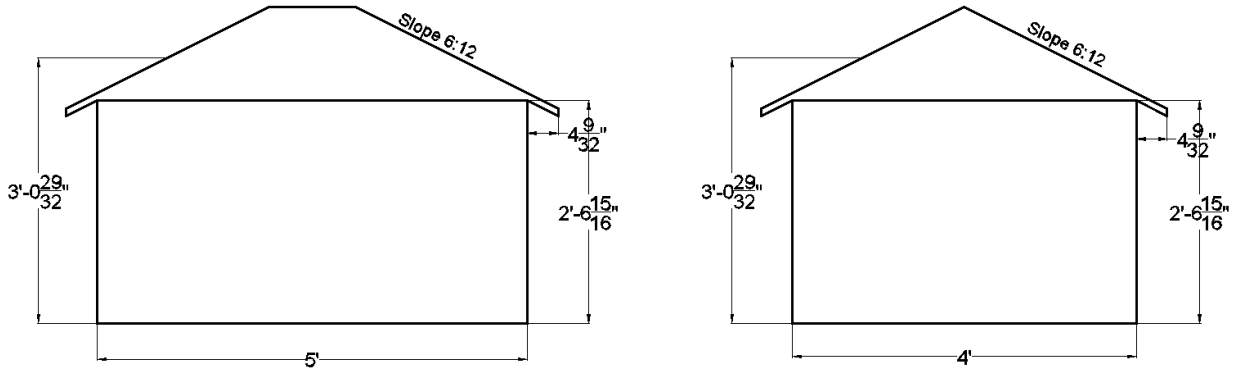

(a) (b)

Figure 6 Model F layout (a) Elevation View (b) Side View

Table 1. Prototype and model dimensions

Model	***Model***	***Roof Slope***	***Building Dimensions***		***Scale***	***Model Dimensions***		***Notes***
			L x W x h	*Overhang*		*L x W x h*	*Inclined Overhang*	
			(ft)	*(ft)*		*(ft)*	*(in)*	
A	*Hip Roof*	*4:12 (18.4°)*	*50 x 40 x 24*	*4*	*1:10*	*5 x 4 x 2.4*	*4.8*	*With horizontal soffit*
B		*6:12 (26.3°)*		*2*	*1:10*		*2.4*	
C				*4*			*4.8*	
D				*6*			*7.2*	
E				*2*			*2.4*	*No horizontal soffit*
F				*4*			*4.8*	

2.2.Instrumentation and test protocol

Pressure taps were added on the walls, the top surface of overhangs and the bottom surface of soffits, as well as on the roof area adjacent to overhangs to be placed within zone 3 and 2e as specified in ASCE 7-16, as shown in Figure 7. The variable a is defined in ASCE 7-10 and ASCE 7-16 as follows; the smaller of 10% of the least horizontal dimension (shall not include any overhang distance) or 0.4h, where h is the roof mean height, and a shall not be less than either 4% of the least horizontal dimension or 3 ft. - note that during the design and construction of the models, ASCE 7-22 was not published. Each model had a different number of pressure taps according to its dimensions (Table 2). Pressure tap locations are shown in Figures 9 as a sample for model B. The pressure taps were connected to a sensitive pressure scanning system (Scanivalve ZOC33). The test was conducted for 40 wind direction for each model (i.e., 0° → 360° with increments of 10 degrees plus the four corners as shown in Figure 8) with a target wind speed of 40 mph. The sampling time for each direction was 60 seconds and the sampling frequency was 520 Hz. The six models were tested for an open terrain exposure (i.e., category 'C'). Figure 10 shows one of the models (model B) placed on the WOW's turntable. Table 3 shows the testing measurement parameters.

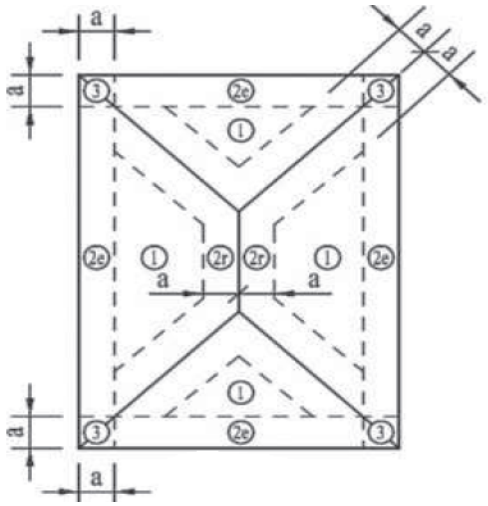

Figure 7 Assigned zones for hip roof in ASCE 7-16

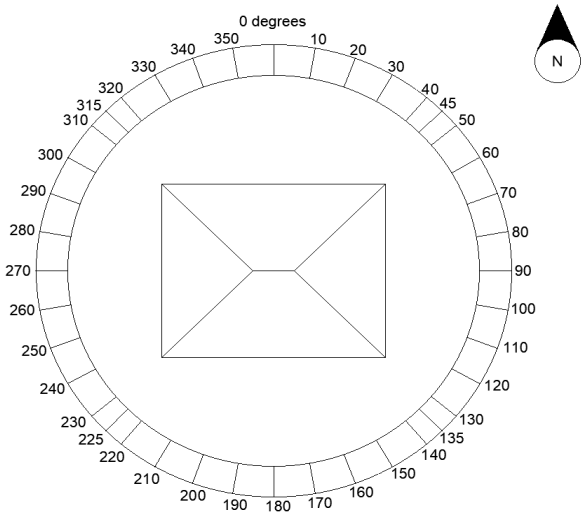

Figure 8 Wind directions tested at the WOW

Table 2. Number of pressure taps in each model

Model	Pressure taps on roofs	Pressure taps on soffits	Pressure taps on walls	Total Number of Pressure Taps
A	112	92	100	304
B	106	72	100	278
C	112	92	100	304
D	136	116	100	352
E	106	72	120	298
F	112	92	120	324

Table 3. Measurement configurations and parameters

Model Scale	1:10
Sampling frequency	520 Hz
Sampling period	60 s
Test angles	0º:10º:360º, 45º, 135º, 225º and 315º
Upstream exposure	Open
Nominal wind speed at reference height	Varies depend on each model roof mean height

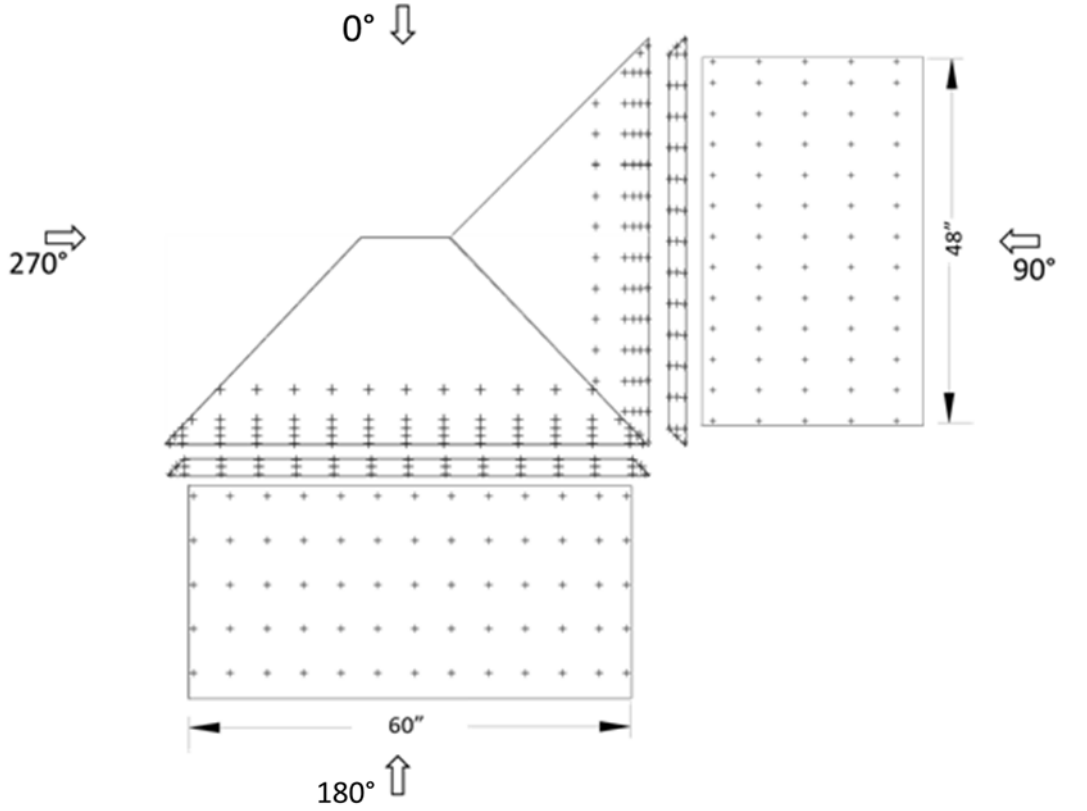

Figure 9 Sample Pressure tap layout for Model B on walls, soffits, and roof with overhangs

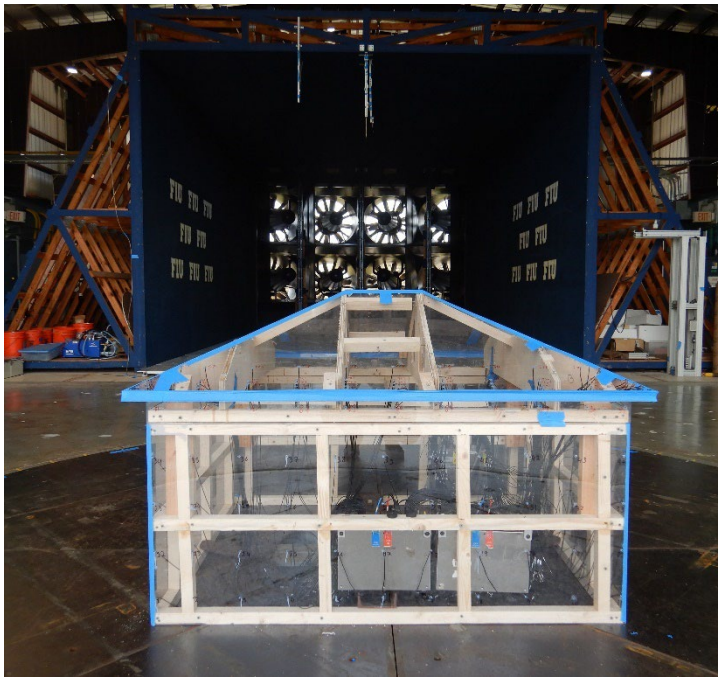

Figure 10 Photograph for testing Model B on the turntable at the Wall of Wind

3. Results and discussion

Data analyses was performed on the data acquired from the conducted experimental testing. The acquired raw data for each pressure tap measure the pressure difference between the pressure at the tap location and the static pressure at the WOW in psf. First, the data went through a transfer function for correction of the tubing distortion - a onetime process done for any wind testing project using flexible tubing to connect pressure taps to the pressure scanners. The pressure tubing was a regular Alphawire single black tubing (PVC 105-16) of an internal diameter 0.0.53 in. The tap side length that was used for all the pressure taps was 49 in, while the connector side was 12 in. The transfer function was applied according to the used tap side length. The transfer function process consists of a Labview code generating random white noise data as analog signals to a pressure signal generator (i.e., audio amplifier). The distortion of pressure signals caused by the tubing is compensated for using the inverse transfer function method described (Irwin et al. 1979) and a low pass filter at 250 Hz is applied. The transfer function causes the deviation RMS between the long tubing data and short tubing data to reach $2x10^{-4}$. Afterwards, a post-test Partial Turbulence Simulation (PTS) was performed to account for the missing low frequency part of the spectrum (Mooneghi et al. 2016; Moravej 2018). The PTS is an analytical method based on quasi-steady assumptions relying on the match of the non-dimensional power spectrum of the longitudinal turbulence and the large-scale and full-scale spectrum for high frequencies. The entire spectrum is obtained using gaussian probability distribution for the low-frequency effects with the high frequency data obtained during testing in the wind tunnel. The peak pressure coefficient is estimated by dividing the sample time (60 sec) into subintervals where peak values could be treated as independent, while the full-scale sampling time of one hour is a sufficient sampling time to achieve stable statistics when measuring fluctuating wind loads. The number of sub-intervals used was 100 (the max number that can be used was 180 according to some calculated values related to the time ratio and cut off frequency as specified in the PTS approach), and the time of each subinterval was 0.6 sec. Table 4 shows the parameters used for PTS for open terrain.

Table 4. PTS parameters for open terrain

	Prototype		Model	
Iu% (Turbulence Intensity)	Iu_p	21.65	Iu_m	8.30
Lu (Length Spectrum) (m)	Lu_p	72.50	Lu_m	0.2394
H (Roof height) (m)	b_p	8.763	b_m	0.8763
V (m/s)	U_p	66.1	U_m	20.90
test time (minutes)	T_p	60	T_m	1

3.1. Wind speed and turbulence intensity profiles.

Wind speed profile measurements have been taken for the open terrain simulations before testing. A single terrain exposure was generated in the wind tunnel corresponding to one surface roughness length, zo = 0.02 m (0.065 ft) for open terrain (exposure C). Different iterations were generated at the WOW to adjust the automated roughness element and spires angles to match ESDU wind. The wind spectrum was compared to the Von Karman spectrum at full scale for open terrain (Figure 11) before and after applying the PTS shown as uncompensated and compensated spectrum, respectively. Note that for open terrain zo ranges from 0.03 ft to 0.49 ft according to table C26.7-

1 in ASCE7-16. The PTS approach accounts for the deviation between the normalized area under the curve for the wind tunnel spectrum and Von Karman spectrum, as described in the ASCE 49-21 standard (ASCE 2022) as shown in Figure 12.

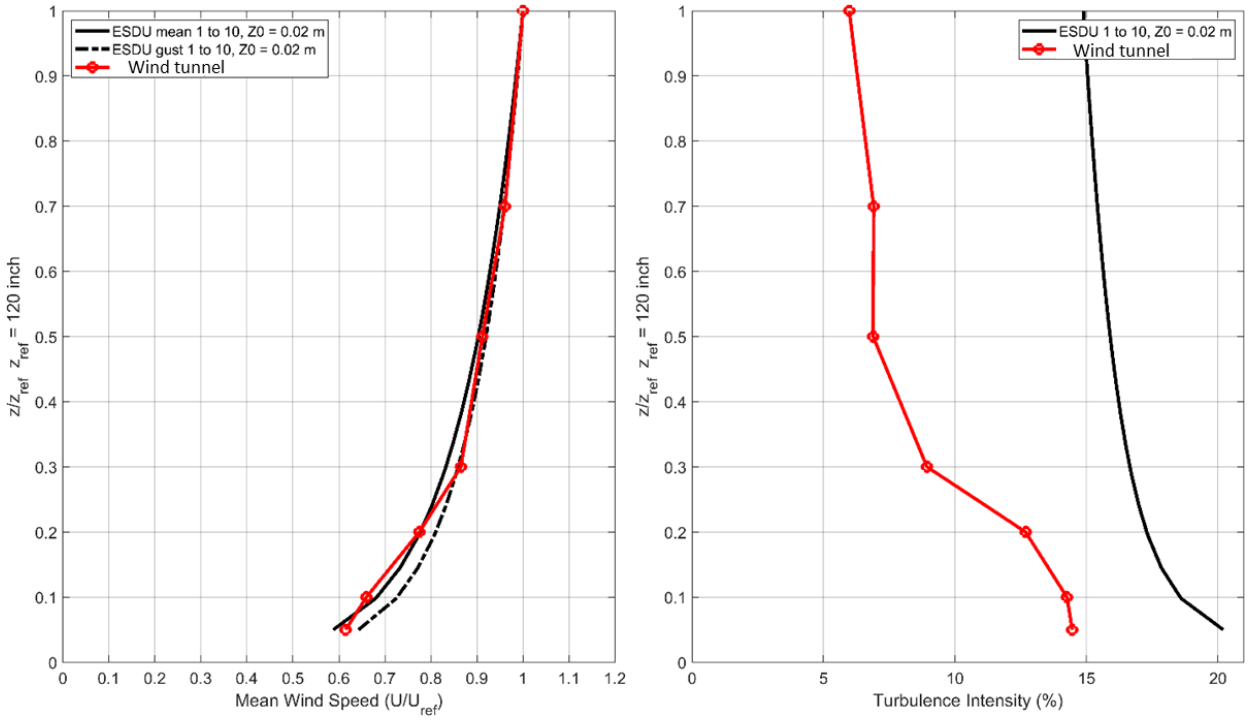

Figure 11 Wind speed and turbulence intensity profile for open terrain setup for 1:10 scale.

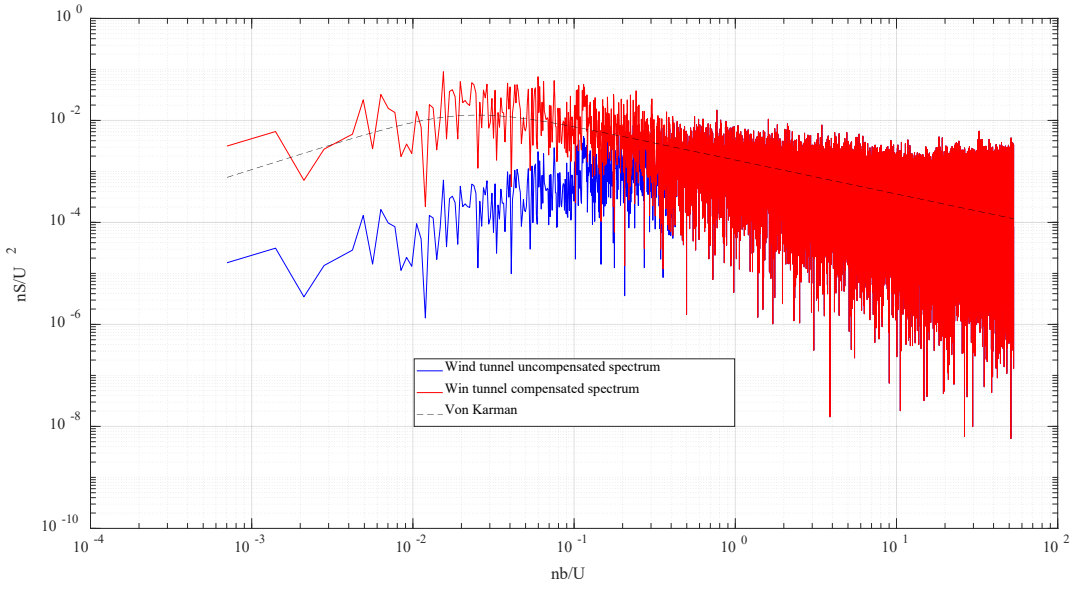

Figure 12 Wind spectra at roof mean height 36.5 inch for open terrain

3.2.Pressure Results

As mentioned earlier, the pressure scanning modules used in the aerodynamic test measure the relative pressure in psf. These pressure values are presented here as normalized pressure coefficients (C_p) computed using equation (1), where ΔP is the relative pressure at the tap location, ρ is the air density $1.225\ kg/m^3$, V_{ref} corresponds to the mean wind speed at mean roof height (34.5 in). Consequently, statistical pressure coefficient parameters were also computed by using their corresponding pressure change parameters, as shown in equations (2) and (3). Peak pressure coefficients are referred to the minimum (highest suction/negative pressure) and maximum (highest positive pressure). In a partial turbulence simulation, the testing sample time (60 sec) was divided into subintervals of sufficient duration that peak values occur in them. The peak pressure is calculated as a function of the peak pressure coefficient occurred during the subinterval, the resultant wind speed for that subinterval and flow density (Moravej et al. 2019). The resultant wind speed composed of the mean velocity over the subinterval and each of the low frequency turbulent velocity component, u_L, u_V, u_W. The partial turbulence simulation method uses Fisher Tippet Type 1 distribution in estimating the probability of the peak pressure coefficient for not exceeding that peak pressure coefficient in the subinterval. The peak pressure coefficient for each interval is calculated based on the peak pressure and the mean velocity of the full sample period with full spectrum turbulence and it is based on mean hourly dynamic pressure. The peak pressure coefficient for 3 sec is obtained by rescaling using equation 4 which is based on 3-second gust dynamic pressure. Importantly, note that for any positive sign represents a pressure directed towards the surface while a negative sign represents a pressure directed away from surface (suction). Throughout this report, peak pressure coefficients were identified either as local (single tap) or area-averaged (two or more taps).

$$Cp = \frac{\Delta P}{0.5\ \rho\ V_{ref}{}^2} \quad (1)$$

$$C_{p\,mean} = \frac{P_{mean}}{0.5\rho V_H^2} \quad (2)$$

$$C_{p\,peak} = \frac{P_{peak}}{0.5\rho V_H^2} \quad (3)$$

$$Cp_{peak\ 3-\sec} = Cp_{peak}\ (\frac{V_H}{V_{3-sec}})^{\ 2} \quad (4)$$

Where, V_{ref} is the reference wind speed at any specified height, V_H is the wind speed at roof mean height, V_{3-sec} is the peak wind speed averaged over 3 sec.

In total, 40 wind directions were tested to determine the peak max and min C_p for each pressure tap. For any pressure tap, the time history comprises of min, max and mean C_p at any wind direction. Specifically, some wind directions were more critical than others. For instance, at the south side at a wind direction of 180˚, which is the windward direction for that side, the wall and the soffit were exposed predominantly to positive pressure while the roof and the overhang were exposed to suction. Sample C_p contour of the roof with overhang for the south side of models B, C, and D plots are shown in Figure 13, and of soffits, as shown in Figure 14, and of walls, as shown in Figure 15. The contour plots for soffit are not shown, as there are not significant values there.

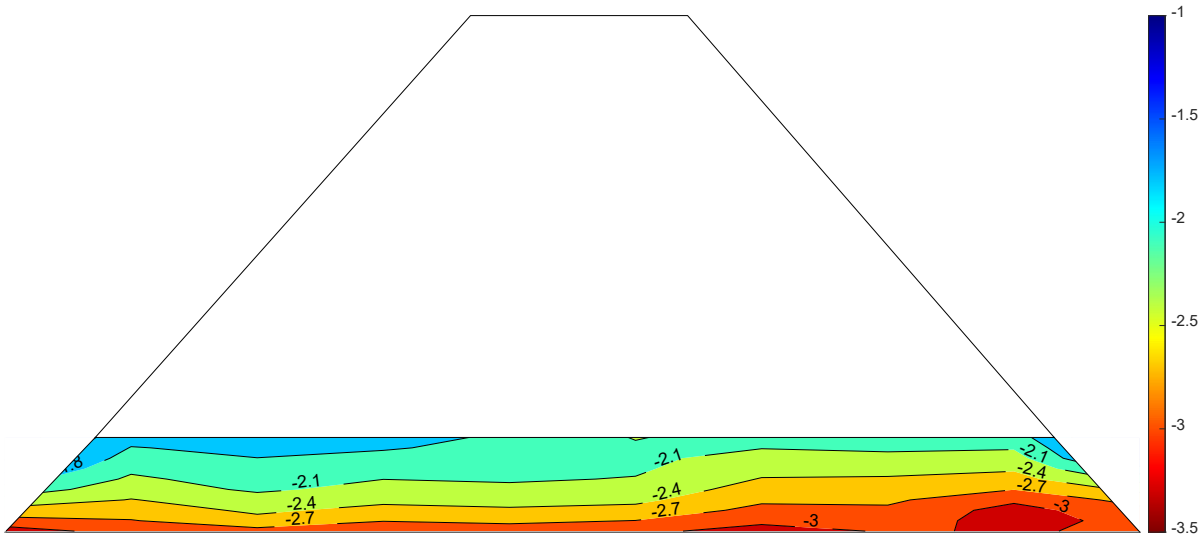

(a)

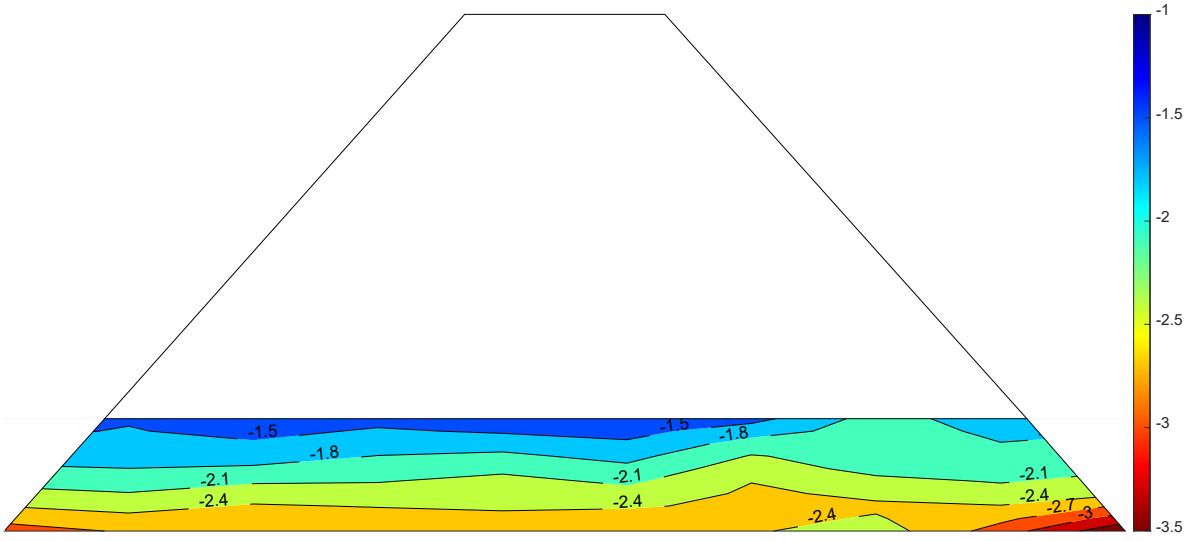

(b)

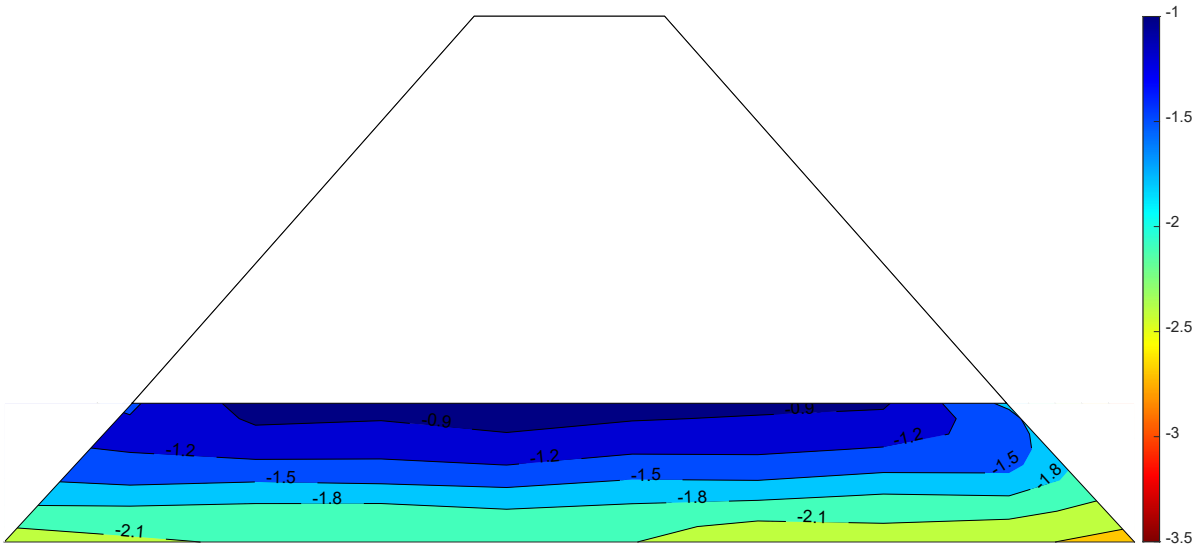

(c)

Figure 13 Min Peak C_p for South Roof at wind direction of 180° (a) Model B (b) Model C (c) Model D

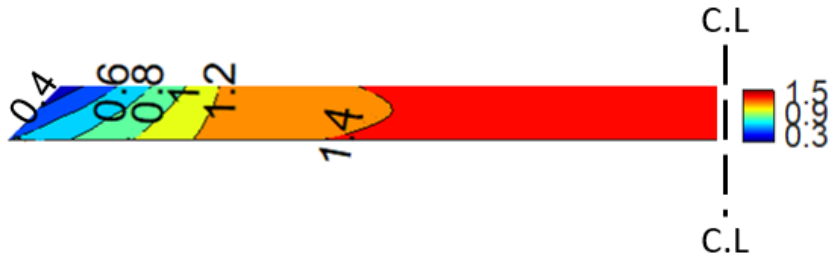

(a)

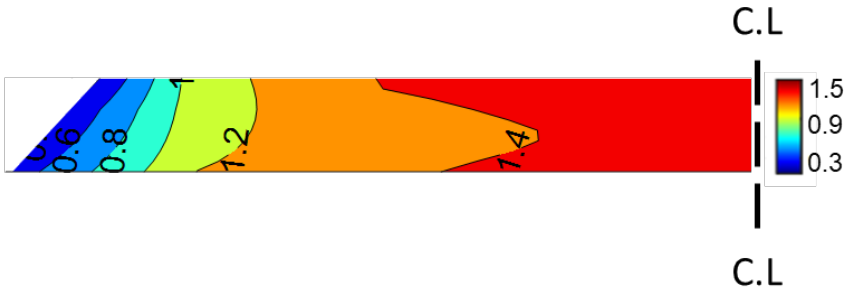

(b)

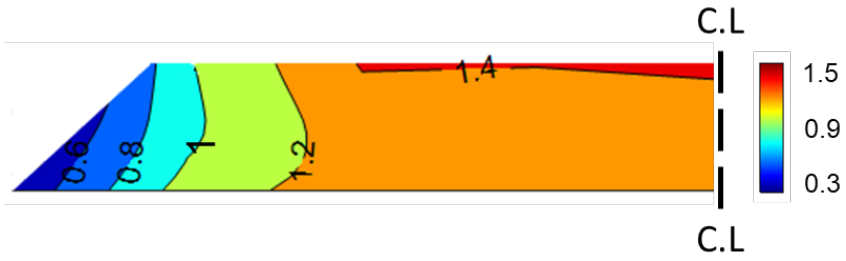

(c)

Figure 14 Max Peak Cp for South Soffit at wind direction of 180° (a) Model B (b) Model C (c) Model D

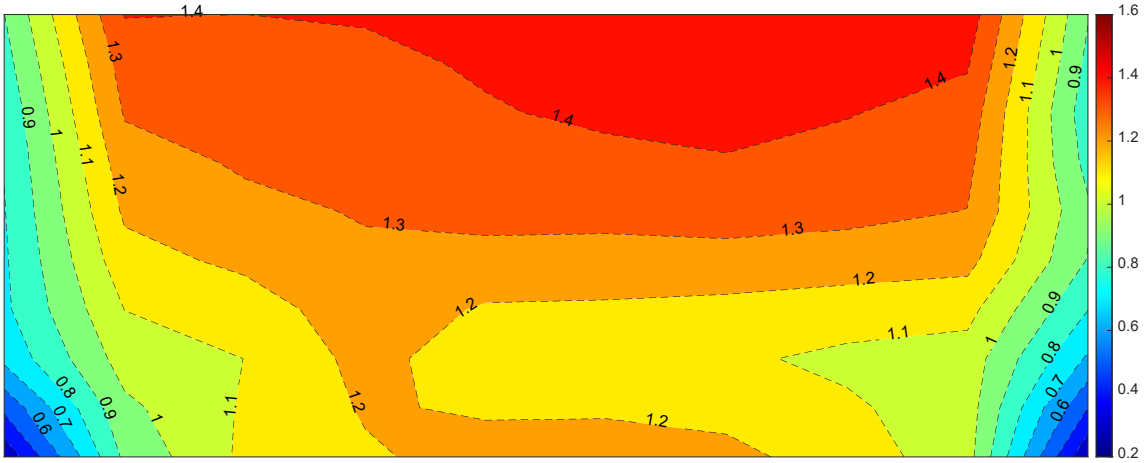

(a)

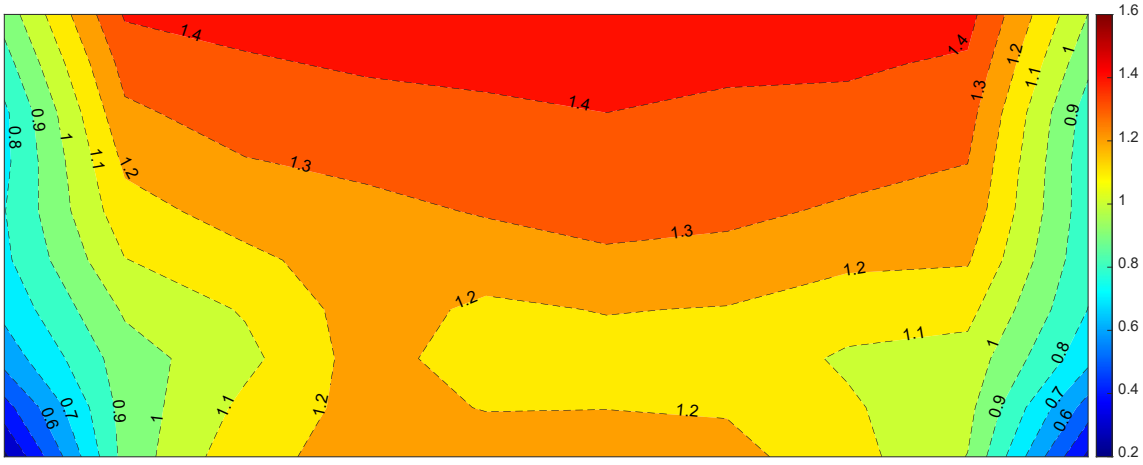

(b)

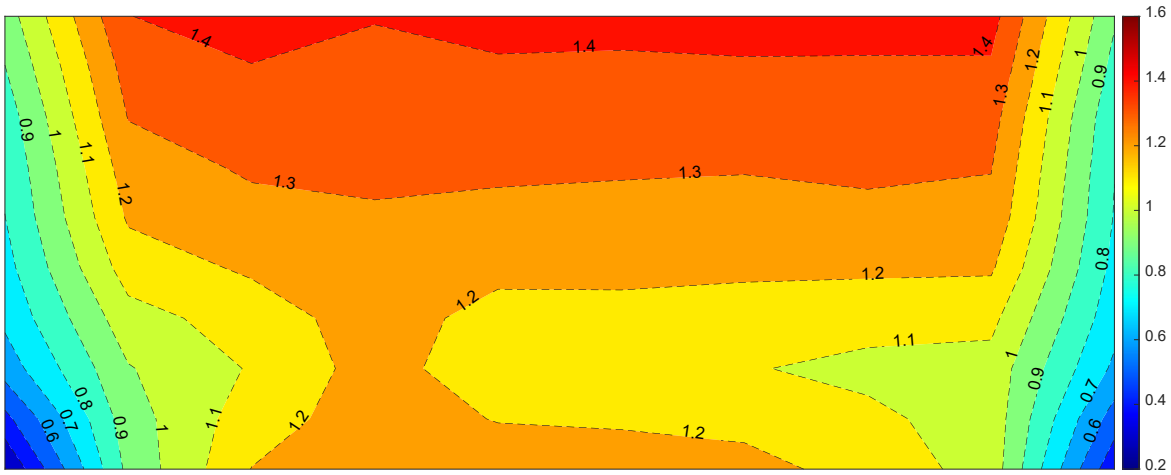

(c)

Figure 15 Max Peak Cp for South Wall at wind direction of 180º (a) Model B (b) Model C (c) Model D

3.3. Correlation of Pressures on Soffits and Adjacent Walls

The pressure taps in walls and soffits were placed with equal spacing, to compare the C_p of upper taps on the wall with the adjacent taps on the soffit using correlation and regression analysis. For all the figures that include the wall and the soffit, the shorter side of the soffit is the wall side (lower side), and the longer side of the soffit is the edge side (upper side). The taps shown in the dashed box in Figure 16 used as sample taps for a comparison between soffits and wall pressure fluctuations along wind directions, while the taps in the solid box used to derive the correlation coefficients, correlation contour plots, and perform the regression analysis.

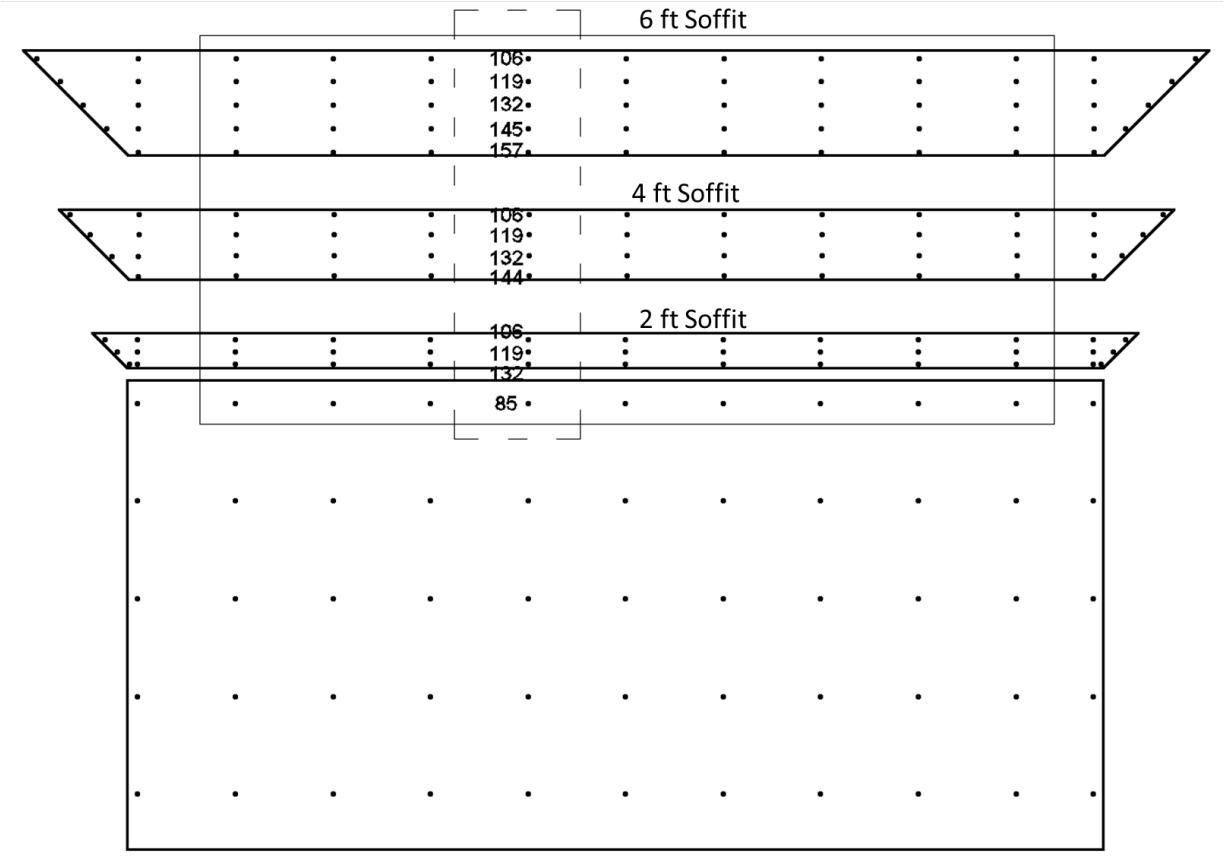

Figure 16 Pressure taps instrumentation on south wall and soffit Models B, C, and D

3.3.1. Pressure fluctuations at the upper taps of the soffit/wall

One of the upper taps in south wall (tap 85) was used to display the similarity in pressure fluctuations between the upper taps of the wall with the corresponding taps in the soffit (Figure 16). The peak max and peak min pressure coefficients of one of the upper taps in south wall (taps 85) were compared with the adjacent soffit taps (106, 119 and 132), (106, 119, 132 and 144), (106, 119 132, 145 and 157) of model B, C and D, respectively for the 40 wind directions. Figure 17 displays the peak max and peak min for the chosen wall and soffit taps for all wind directions. It is apparent that the peak max C_p's were similar along the adjacent taps in all wind directions. In contrast, the peak min C_p's used to slightly change for soffit taps located away from the wall. For instance, for wind directions from 135º to 225º, the wall and soffit taps were mainly exposed to positive pressure, thus, the peak min C_p ranged from 0 to -0.5, while the positive C_{ps} values were very similar and ranged from 0.6 to 1.45. This supports the assumption in ASCE 7-16 and ASCE 7-22 that the pressure coefficient at the bottom covering of the roof overhang shall be taken as the external pressure coefficient on the adjacent wall surface. The edge pressure taps in the soffit experienced more suction compared to the middle or the inner row. The soffit exposed to more turbulence underneath and this turbulence increased near the edge where more separation occurs. Consequently, pressure taps at the soffit edge had higher peak min C_p than the middle and inner taps. It is important to note that tap 85 on the wall is not the middle tap and shifted towards one of the sides, thus the pressure fluctuations are not symmetric between 90˚ and 270˚

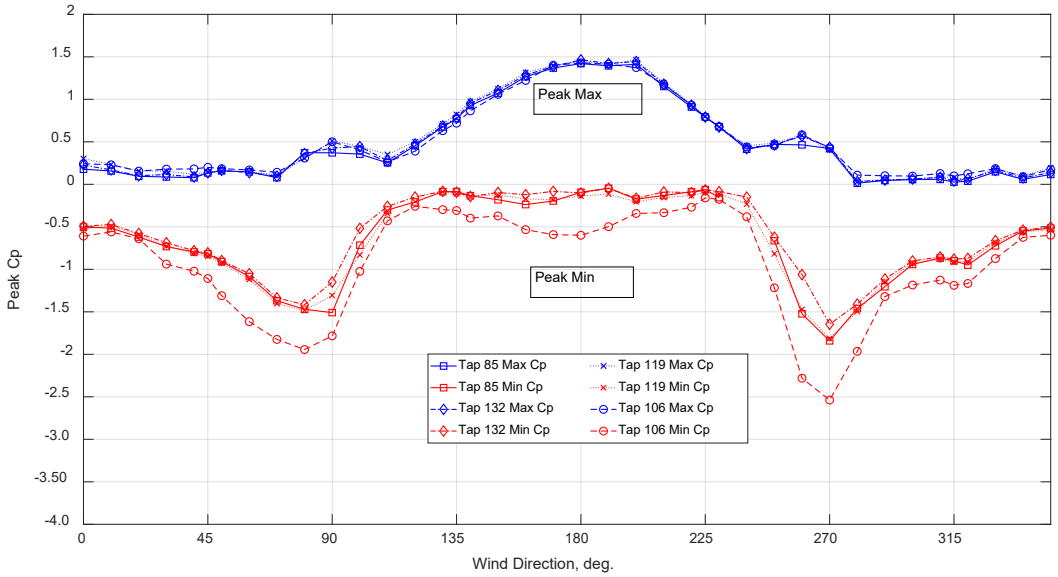
Peak Max
Peak Min
Tap 85 Max Cp
Tap 85 Min Cp
Tap 132 Max Cp
Tap 132 Min Cp
Tap 119 Max Cp
Tap 119 Min Cp
Tap 106 Max Cp
Tap 106 Min Cp
Peak Cp
Wind Direction, deg.

(a)

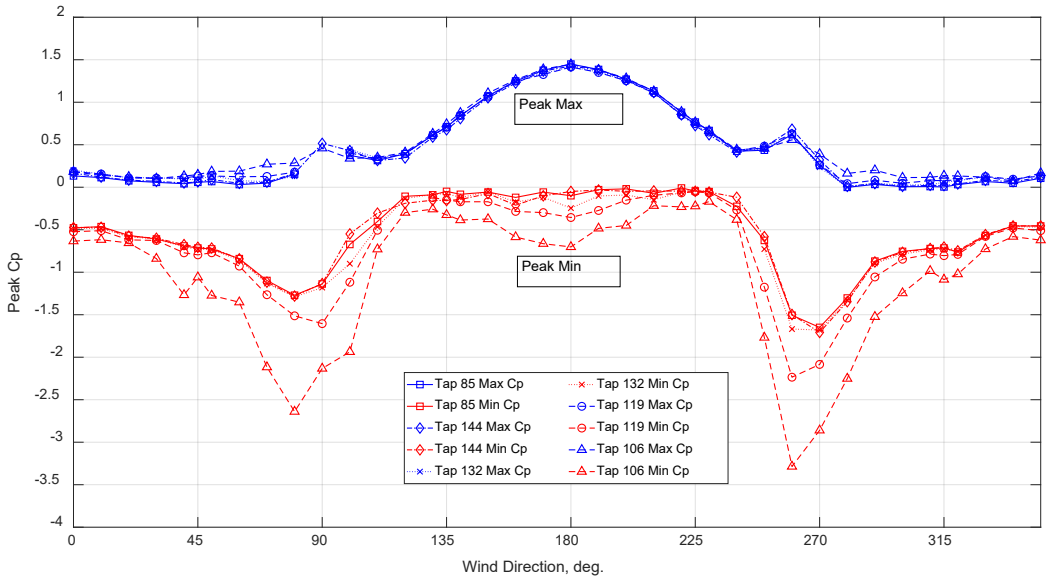
Peak Max
Peak Min
Tap 85 Max Cp
Tap 85 Min Cp
Tap 144 Max Cp
Tap 144 Min Cp
Tap 132 Max Cp
Tap 132 Min Cp
Tap 119 Max Cp
Tap 119 Min Cp
Tap 106 Max Cp
Tap 106 Min Cp
Peak Cp
Wind Direction, deg.

(b)

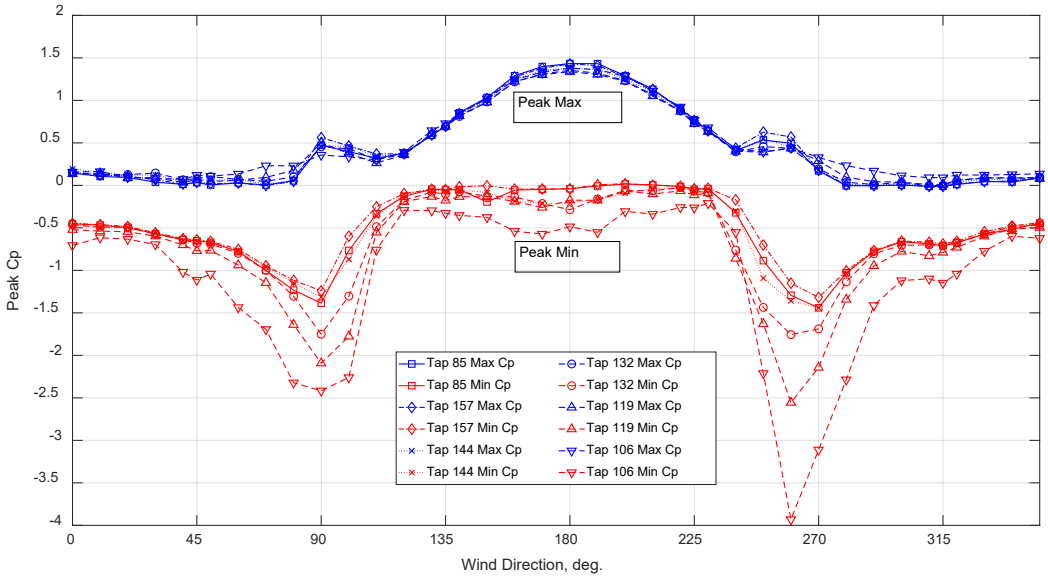

(c)

Figure 17 Peak Max and Peak Min for one of the upper wall taps with adjacent soffit taps for (a) Model B (b) Model C (c) Model D

3.3.2. Regression Analysis and Correlation Coefficients

One of the objectives of this research study, was to correlate the effect of wall pressure to the soffit pressure and investigate how the width of soffit would affect this correlation. The three middle upper taps in the walls for both models that used before in displaying the peak max and min C_p were used to display their correlation coefficient. Correlation coefficients are used to measure the relation between two variables and one of the most common forms is the Pearson's correlation (R factor) which ranges from 0 (no correlation) to 1/-1 (perfect correlation). This factor follows equation (5) and was used later in Regression analysis as well.

$$R = \frac{\Sigma(x_i-\bar{x})(y_i-\bar{y})}{\sqrt{\Sigma(x_i-\bar{x})^2\Sigma(y_i-\bar{y})^2}} \quad (5)$$

Regression analysis was done on the wall upper taps and soffit taps for model B, C and D. Regression analysis was done for getting the relationship between the pressure coefficients of the soffit taps with the wall taps. This relationship either shows a decrease or increase of the pressure coefficient for each row of the soffits compared to pressure coefficients of the walls. For all the models, the corner taps for walls and soffit were not considered in correlation as shown in Figure 16, only the taps inside the solid box included in correlation, because the separation of the flow occurs at the corner of the building, so the C_p of these taps have lower values compared to other taps and may not be significant to be correlated together. For model B, the first row is the one next to the wall and the third row is the outer edge row, similarly for model C and D, the first row is the row adjacent to the walls and the fourth and fifth rows are the edge rows, respectively. The positive peak pressures were well correlated for the near and far rows for all the models, while for the negative peak pressure, R-squared value significantly decrease as the taps locate far from the

wall, especially for wider soffits. It is apparent from the regression plots, as shown in Figure 18 to Figure 20, that the slope for the positive peak pressure coefficient in all the models is close to 1 and this supports the assumption in ASCE 7-16 and ASCE 7-22. However, for peak negative pressure coefficients the soffit and wall taps are not well correlated, and the slope is not close to 1 due to the divergence of peak negative pressure coefficients for the soffit and wall soffit

To validate the current findings, the results were compared to one of the few relevant studies that was identified in the literature (Vickery 2008). The linear regression model match well with (Vickery 2008) for positive pressure coefficients, and negative pressure for model B as shown in Figure 18a. Vickery (2008) investigated a soffit with width of 1.67 ft which is corresponding to the first two rows of soffit taps for model A. Therefore, by comparing the experimental results with that study, the regression and correlation analysis look very similar, while divergence started to happen in row 3 which is at the edge of 2 ft soffit as shown in Figure 18b. Models C and D which have a soffit width of 4 ft and 6 ft were deemed to be too different in terms of peak negative pressure coefficients compared with Vickery (2008), while peak positive pressures still match well, even by increasing overhang width as shown in Figures 19 and 20.

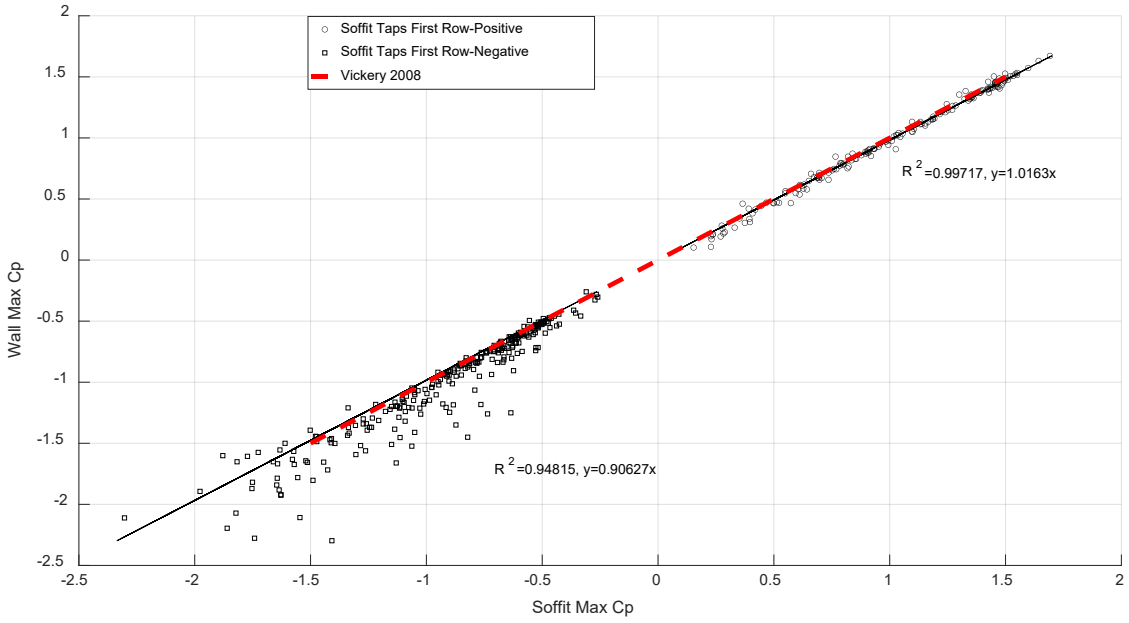

(a)

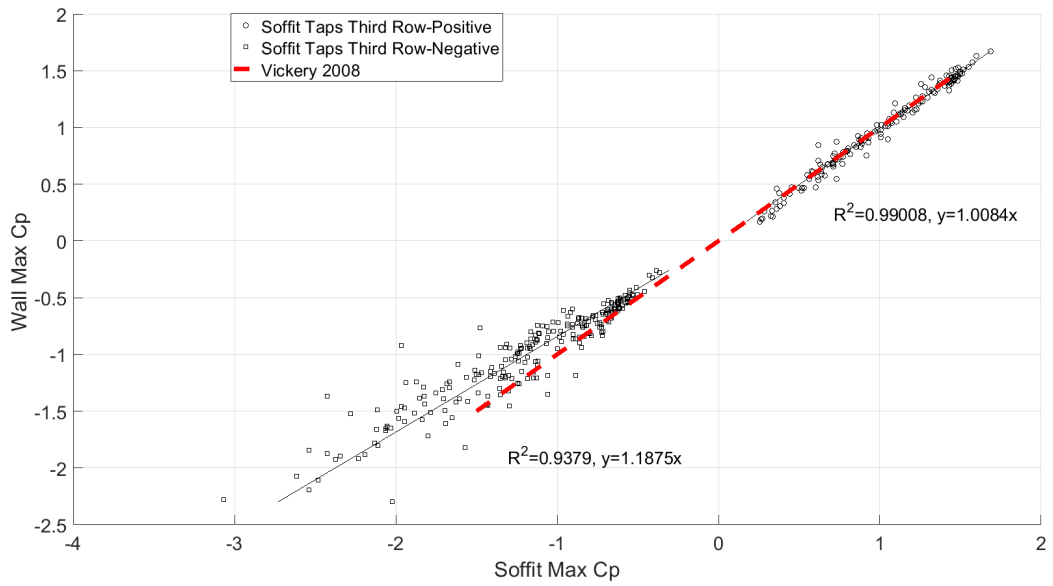

(b)

Figure 18 Linear Regression Relation between Upper Taps in South Wall and (a) first row of taps (b) third row of taps in soffit for model B

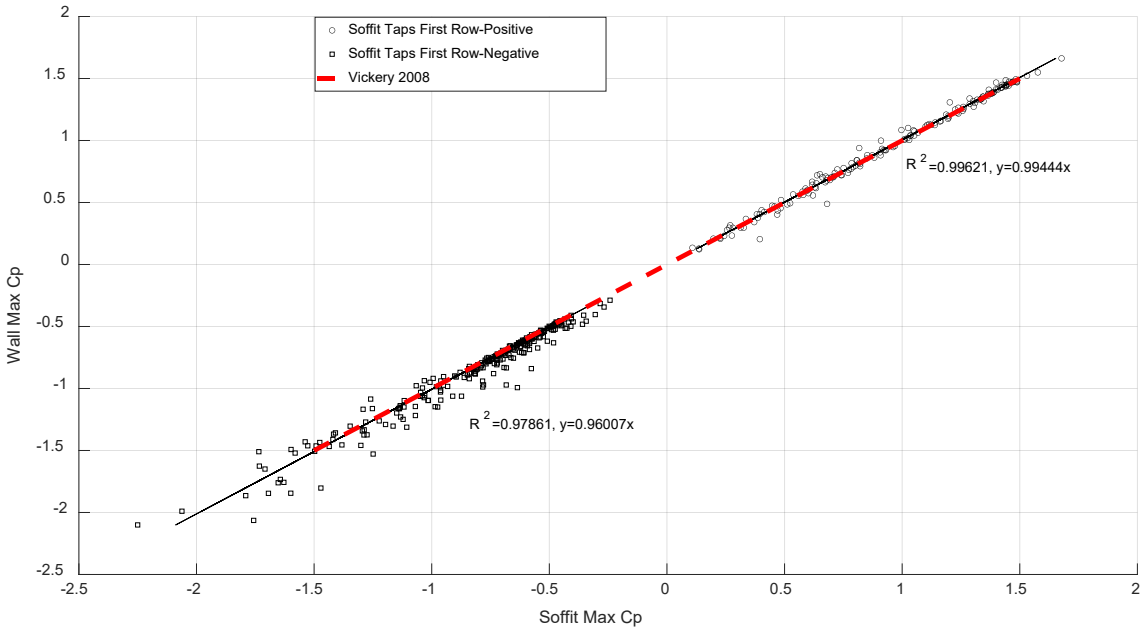

(a)

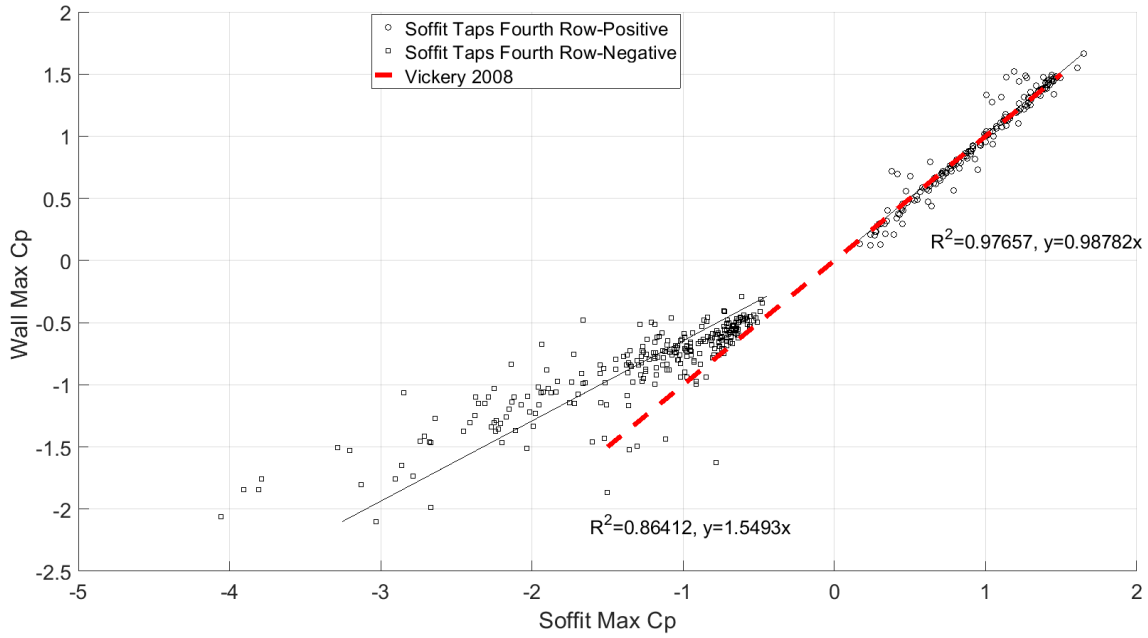

(b)

Figure 19 Linear Regression Relation between Upper Taps in South Wall and (a) first row of taps (b) fourth row of taps in soffit for model C

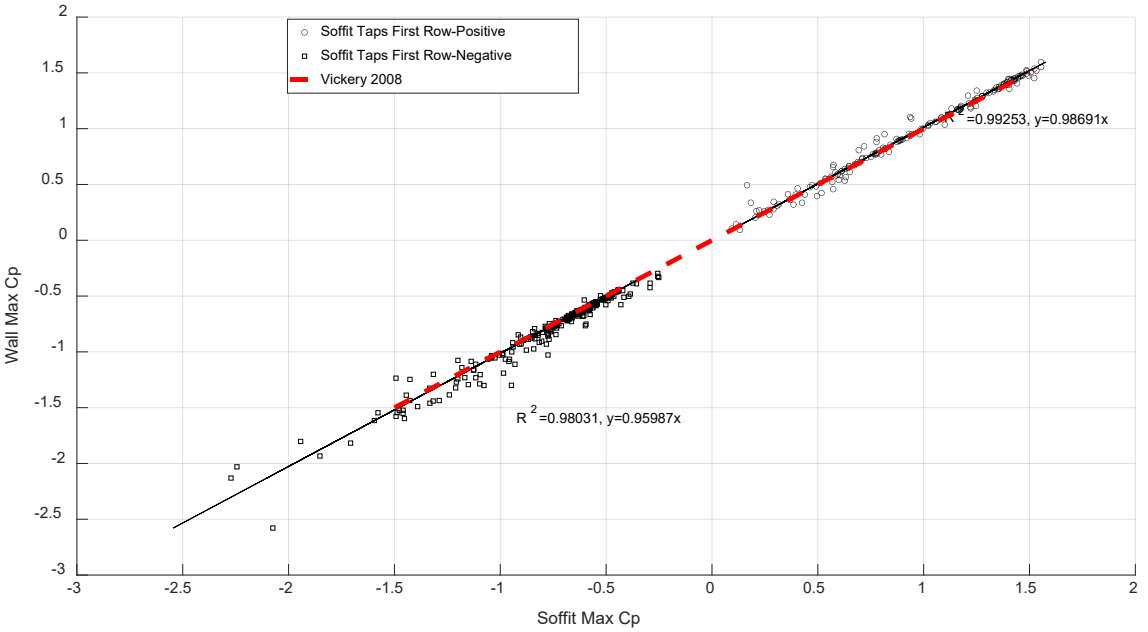

(a)

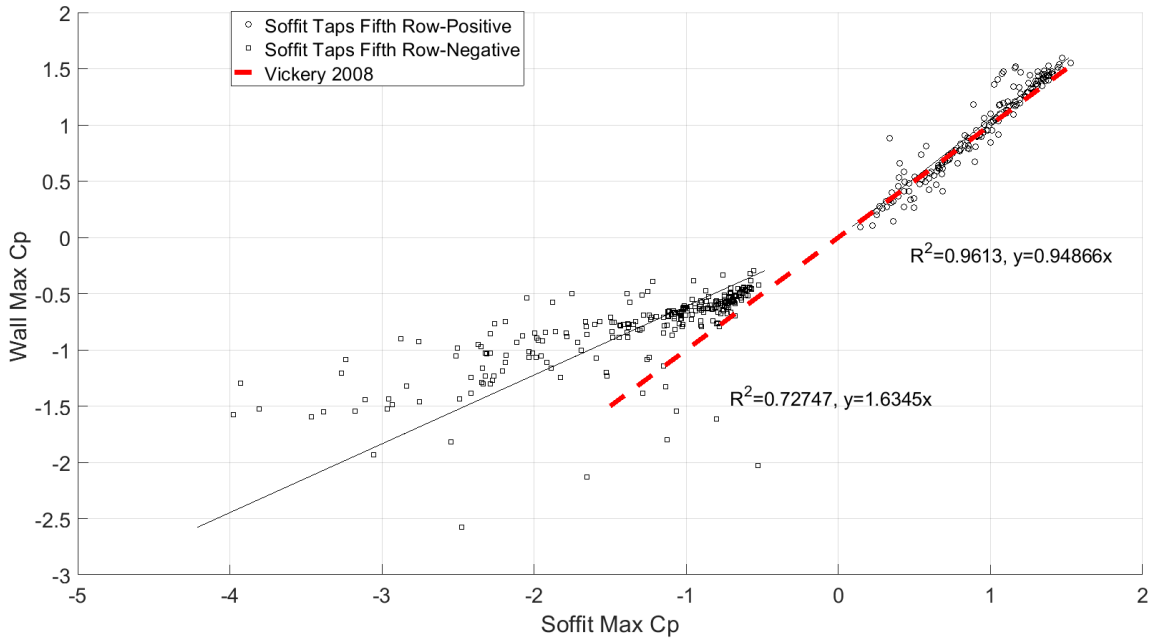

(b)

Figure 20 Linear Regression Relation between Upper Taps in South Wall and (a) first row of taps (b) fifth row of taps in soffit for model D

Beside regression analyses, correlation coefficients were analyzed between the C_p time series of soffit taps with upper wall taps as shown in the solid box in Figure 16. Figure 21 to Figure 23 provide correlation coefficient contour plots for south soffit for model B, C, and D, respectively, for four wind directions (0˚, 90˚, 180˚ and 270˚). For all the soffit plots the wall side is the upper side of the plots, and the soffit edge is the lower side of the plots. Generally, wall taps are well correlated with soffit taps near to the wall. The R factor ranges from 0.68 to 0.98 for model B and C, and ranges from 0.6 to 0.96 for model D. The highest correlation occurred when the south wall and the adjacent soffit were at the windward (wind direction 180°) or in the wake region (wind direction 0°), i.e., the wall and the soffit were exposed to predominantly positive pressure or predominantly suction, respectively. Model B and C show almost the same correlation coefficient when the models placed in the windward (180º degree), and the correlation coefficient at the corner significantly decrease for model D when placed in the windward direction. The correlation coefficients for models B and C are significantly higher at the outer edges compared to model D, for all other shown directions. This indicates that the correlation coefficients for wider overhang significantly decrease compared to narrower overhangs, especially when the taps are exposed to suctions. For instance, at wind direction 90° and 270°, suction occurred at the south and separations caused more turbulence underneath the soffit that cause reduction in correlation coefficients. It was concluded that the soffit pressure is less correlated with the wall at the outer edges compared to the near wall surfaces.

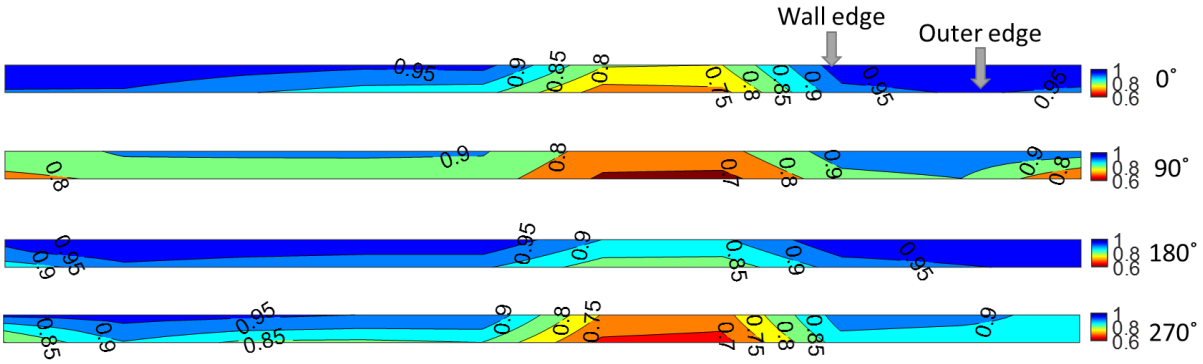

Figure 21 Correlation Coefficients contour plots for south soffit – Model B

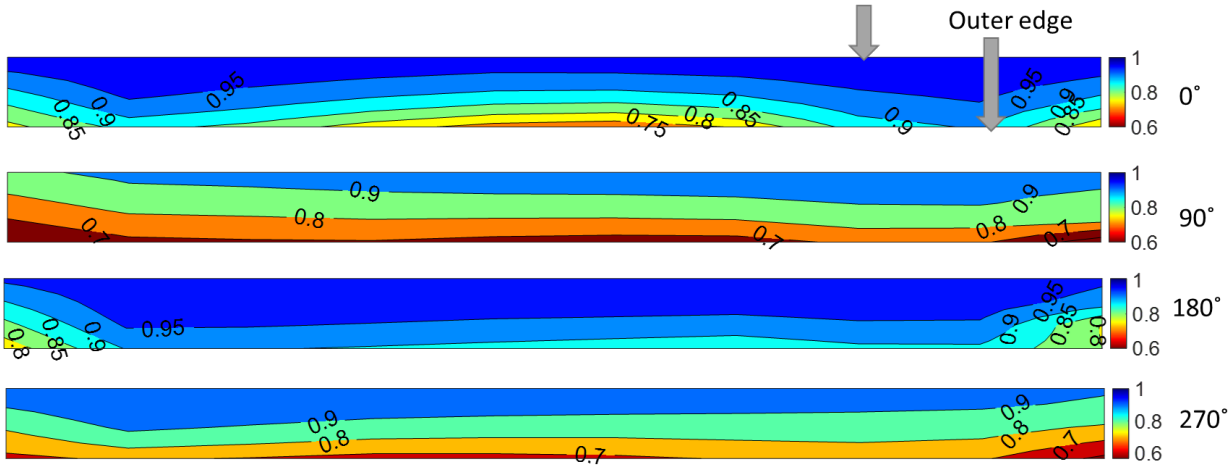

Figure 22 Correlation Coefficients contour plots for south soffit – Model C

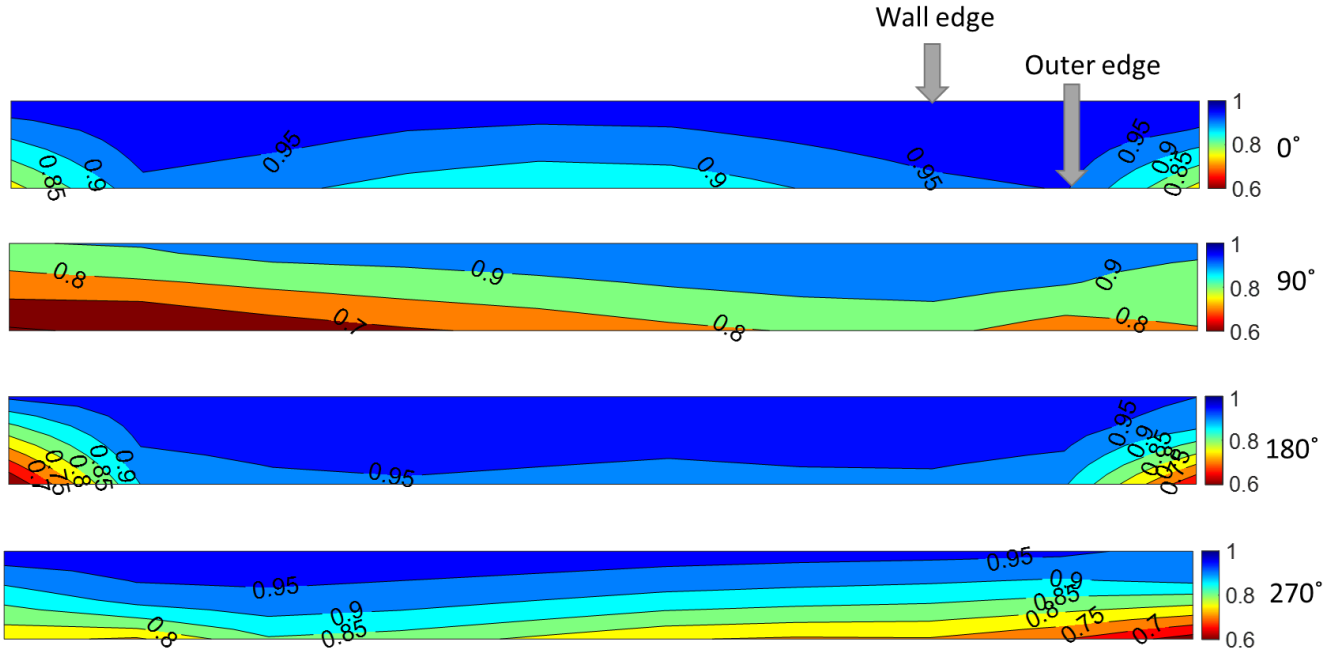

Figure 23 Correlation Coefficients contour plots for south soffit – Model D

3.4.Overhangs with covered and uncovered soffits

Among this phase of experimental testing, wind tunnel tests were carried out on two additional models (models E and F) which have the same roof slope and overhang widths with models B and C, respectively, but with uncovered soffits as shown in Figures 5 and 6. The aim of testing these two models was to investigate the effect of uncovered soffits (inclined soffits) on pressure coefficients variation compared to covered soffits (horizontal soffits). In addition, it was important to analyze the uplift forces and uplift pressures among the covered and uncovered soffits. Data analyses which included correlation coefficients, regression analysis, peak pressure coefficients, and uplift forces was carried out on these two models. Overall, it was found that there is not much difference between the two soffit cases in terms of regression analysis, peak pressure coefficients and correlation coefficients. Some of the performed data analyses for models E and F are shown in Appendix A.

A comparison between the uplift forces for the two models was also carried out. First, the uplift forces were calculated for each pressure tap as a function of the net pressure coefficient between the upper and lower surface of the overhang and the tap tributary area using equation 6. The wind-induced pressure is a function of the applied wind speed; thus, a wind speed of 156 mph which is a category 5 hurricane was used in calculating the forces. It is important to note that the comparison between the uplift pressure for different overhangs is not affected by the assigned value of wind speed, while the magnitude of each uplift force/pressure is affected by the applied wind speed value. For instance, at wind direction of 180˚, the uplift pressures are -221 lb/ft^2 and -198 lb/ft^2 for models B and C, respectively as shown in Figure 24. These values are dependent on the wind speed but in terms of comparison between the uplift pressure, model B is exposed to higher uplift pressure than model C regardless the wind speed value. The uplift pressure over the total surface

area of the overhangs is calculated as the summation of forces for each pressure tap over the summation of the tributary areas for all pressure taps. This procedure was applied for all the 40 wind directions. The uplift pressures were plotted with the wind direction, as shown in Figures 24 to 27. It is apparent that for the same overhang width, the uplift pressures over the total surface area of the overhangs are similar for covered and uncovered soffits. Clearly, the 2 ft overhang is exposed to higher uplift pressures compared to the 4 ft overhang, and this was expected due to the smaller surface area of the 2 ft overhang.

$$F_{L(i)\theta} = C_{p(i)\theta} * 0.5 * \rho * V^2 * A_i \quad (6)$$

$$P = \frac{\sum_i^n F_L}{\sum A_i} \quad (7)$$

where, F_L is the uplift force for tap (i) at wind direction (θ), $C_{p(i)\theta}$ is the 3-sec peak net pressure coefficient for the upper taps and the lower taps on the same location on the overhangs at wind direction (θ), ρ is the air density, V is the wind speed, A_i is the tributary area of tap (i), and P is the uplift pressure at the total surface area of the overhang.

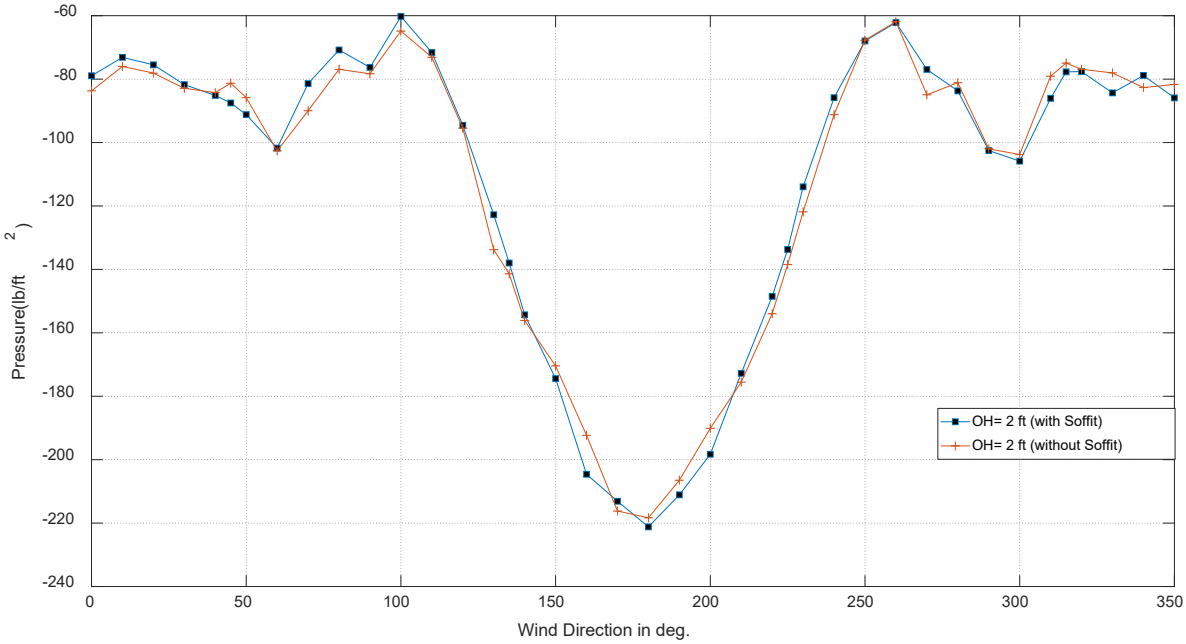

Figure 24 Uplift pressure over the 2 ft overhang surface area along wind directions for covered and uncovered soffits

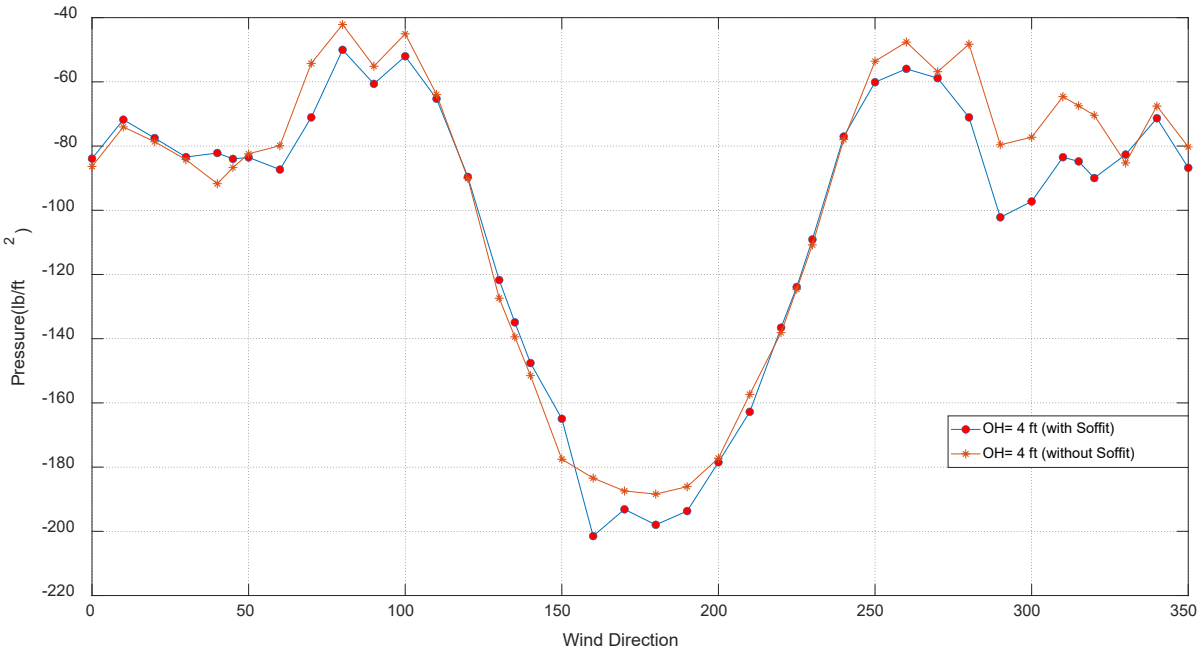

Figure 25 Uplift pressure over the 4 ft overhang surface area along wind directions for covered and uncovered soffits

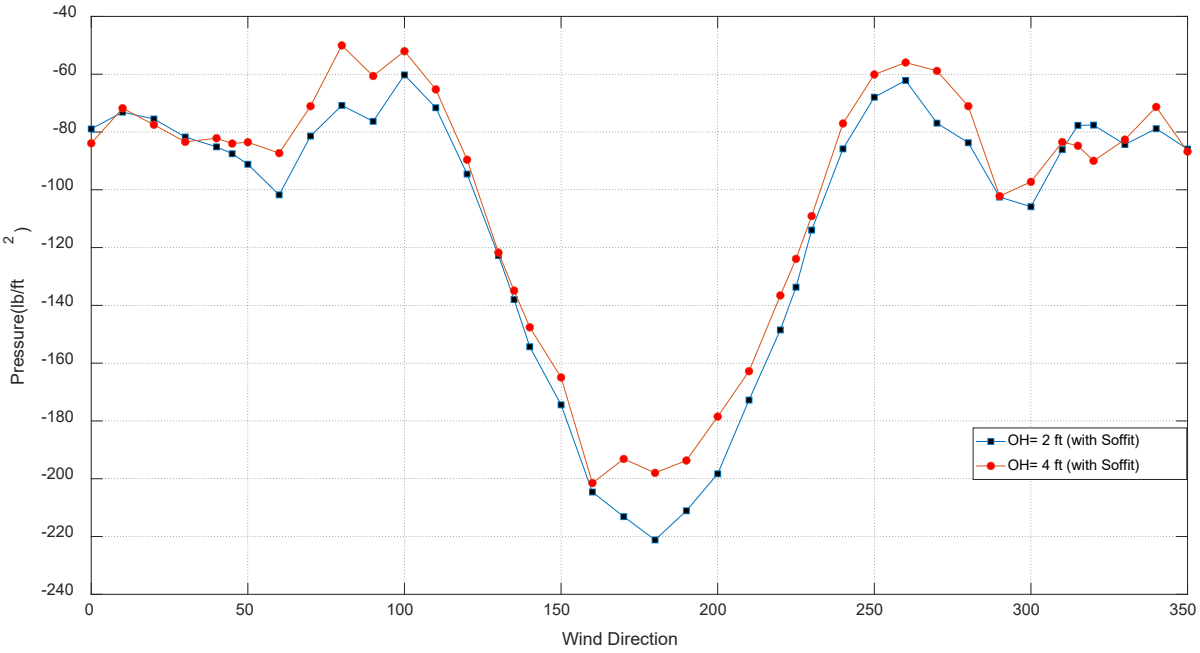

Figure 26 Uplift pressure over the 2 ft and 4 ft overhang surface area along wind directions for covered soffits

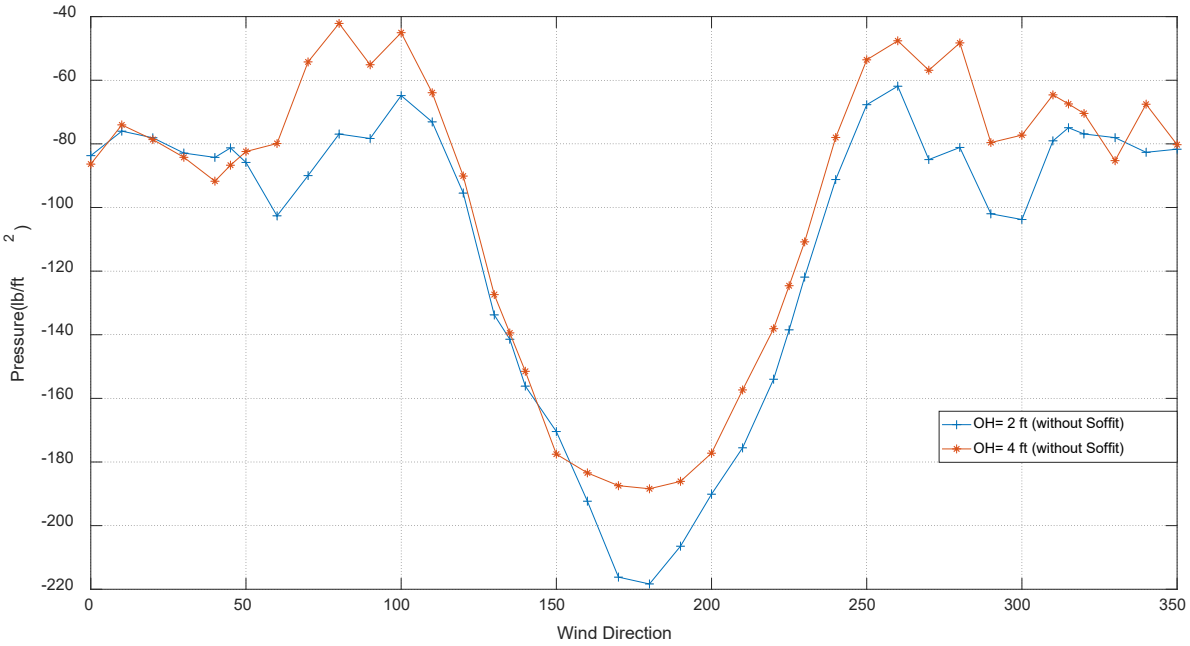

Figure 27 Uplift pressure over the 2 ft and 4 ft overhang surface area along wind direction for uncovered soffits

3.5.Area Averaged pressure coefficients

3.5.1 Comparisons with ASCE 7-10 & ASCE 7-16

Area-averaged pressure analysis was done to investigate further the pressure gradients on single or groups of taps on the overhangs and walls. Moreover, the area-averaged C_p values are an important input for codification purposes. According to (Simiu and Yeo 2019) when pressure taps are placed in an orthogonal pattern, the tributary area for each tap is approximated by rectangular areas, while for non-orthogonal pressure tap patterns the tributary area should be calculated using Voronoi diagrams which are derived from Delaunay triangulation. Samples of different combinations and sets for area-averaged are shown in Appendix B**.**

The area-averaged peak C_p values were computed for each wind direction by considering single or multiple sets of pressure taps and assign them to their corresponding tributary area. GC_p are calculated first in which the tributary area A_i for each tap i inside the desired averaged area at any wind direction θ is multiplied by its wind pressure coefficient time history $Cp_i(\theta, t)$, then the sum is divided by the summation of all the tributary area for the selected taps of interest following equation 8 (Simiu 2011), then using PTS to calculate the peak 3 sec as complied with equation 4. Area averaged pressure taps were considered according to the specified zones for hip roof of slope 20˚ to 27˚ in ASCE 7-16 and ASCE 7-22 as shown in Figure 7 and Figure 33, respectively.

$$GCp_{av}(\theta, t) = \frac{\sum_i Cp_i(\theta,t)\, A_i}{\sum_i A_i} \quad (8)$$

The experimental results for overhang's peak net pressure coefficient in terms of effective area were plotted and compared to ASCE 7-16 and ASCE 7-10 GC_p plots. Zone 2 in ASCE 7-10 (Figure

28) was defined later in ASCE 7-16 as zones 2e and 2r (Figure 7). The net pressure coefficient was calculated as the algebraic sum of the overhang's top surface and the overhang's bottom surface (soffit). In ASCE 7-16, there are two GC_p plots for hip roof of slope 7˚ to 20˚ with overhangs, one for h/B ≥ 0.8 and the other for h/B ≤ 0.5, where h is the roof mean height and B is the horizontal dimension of the building normal to wind direction. There are no separate plots for different h/B for the hip roof of slope 26.6 ˚ (i.e., between 20˚ and 27˚).

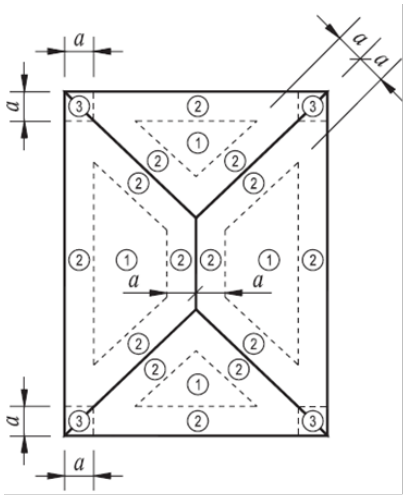

Figure 28 Assigned zones for hip roof in ASCE 7-16

As expected, both plots show the expected monotonically decreasing relationship between the effective area and the magnitude of the net pressure coefficients. According to the dimension of all the models 40 ft x 50 ft x 28.75 ft, h/B for south side is 0.57 and for east side is 0.71 for model A in phase 2 testing (i.e., roof angle of 18.4˚). Most of the peak net GC_p values for both south and east sides were above the upper bound of the plot (-2.9) and (-2.5) respectively, as shown in Figure 29, while for zone 3 only local point exceeded the upper bound of ASCE 7-16 (-3.1) and ASCE 7-10 (-3.7) as shown in Figure 30. For models B to F (i.e., roof angle of 26.3˚), there are no specific plots for different h/B for roof angle between 20˚ to 27˚, thus all the plots comprise the peak net GC_p values for both south and east sides together. For zone 2e, many local and area averaged pressure taps were above the upper bound for ASCE 7-16 (-2.5) and ASCE 7-10 (-2.1), as shown in Figure 31. It is important to note that the smallest effective wind area is based on local pressure for one tap. For zone 3, most of the GC_p values for all the models were entirely below the upper bound for ASCE 7-16 (-3.1) and ASCE 7-10 (-3.7) with some local points of one tap exceeding the upper bound for only model B as shown in Figure 30a. This may suggest that ASCE 7-16 is less conservative compared to the experimental testing regarding zone 2e for any overhang width, while regarding zone 3 it is less conservative compared to experimental testing only for short overhang width (i.e., 2 ft).

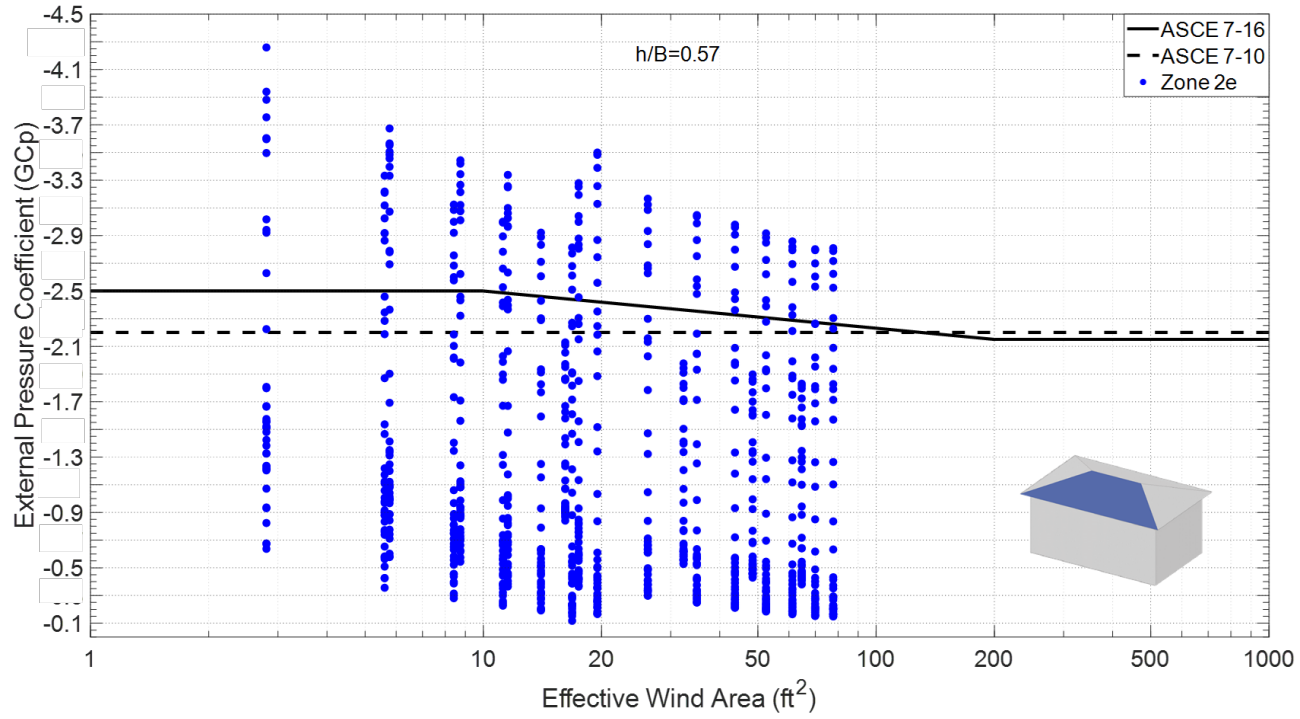

(a)

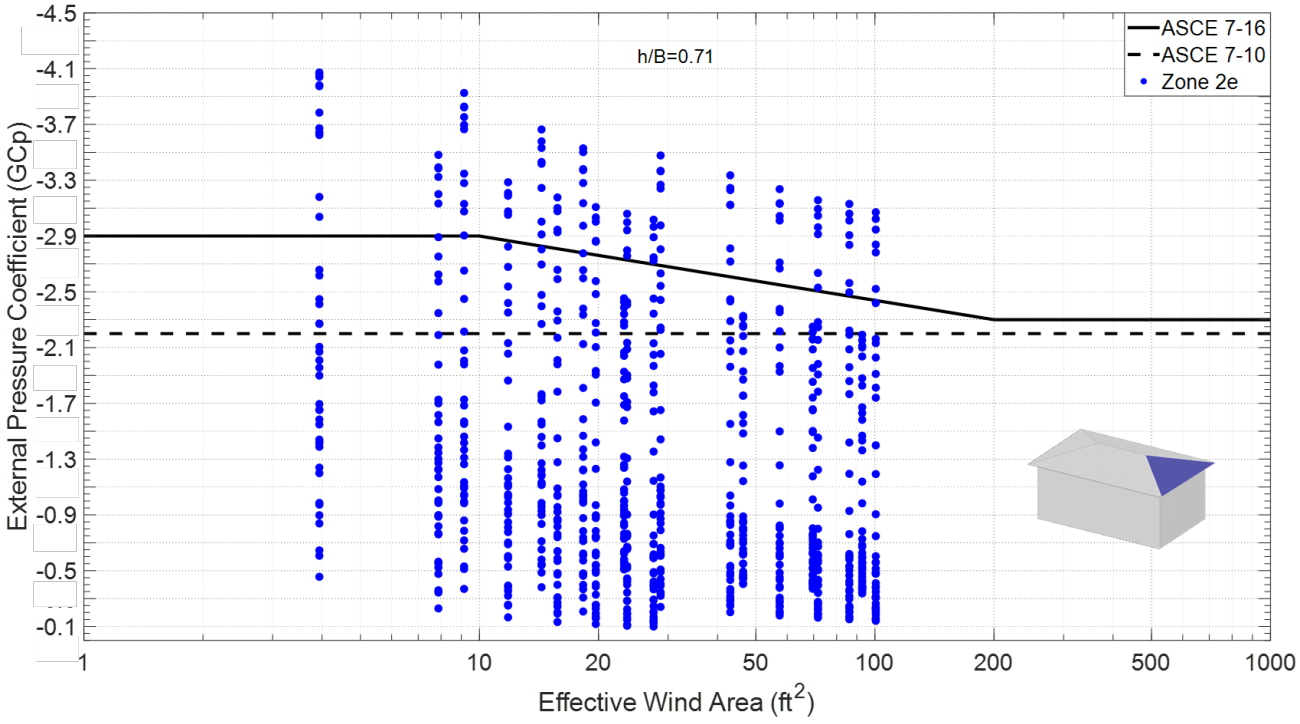

(b)

Figure 29 Critical area-averaged net pressure coefficient for zone 2e compared to GC_p plot in ASCE 7-16 and ASCE 7-10 (a) Model A- South side (b) Model A- East side

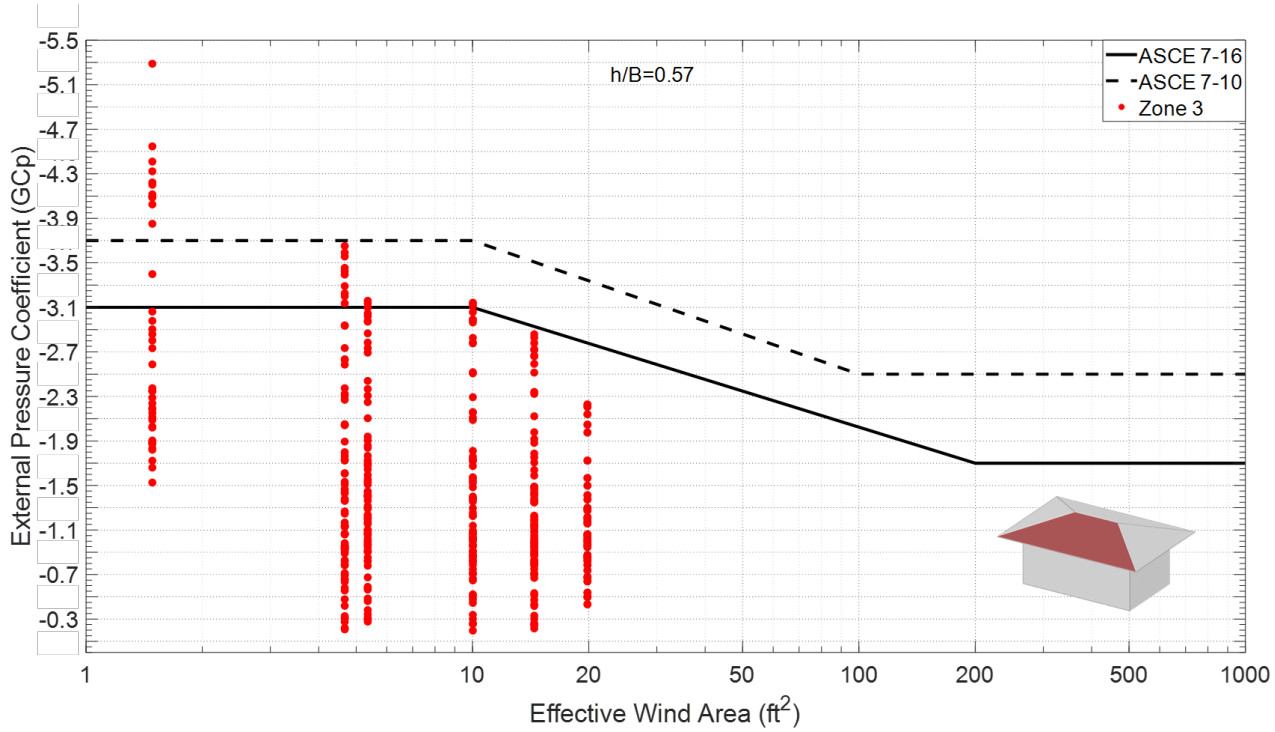

(a)

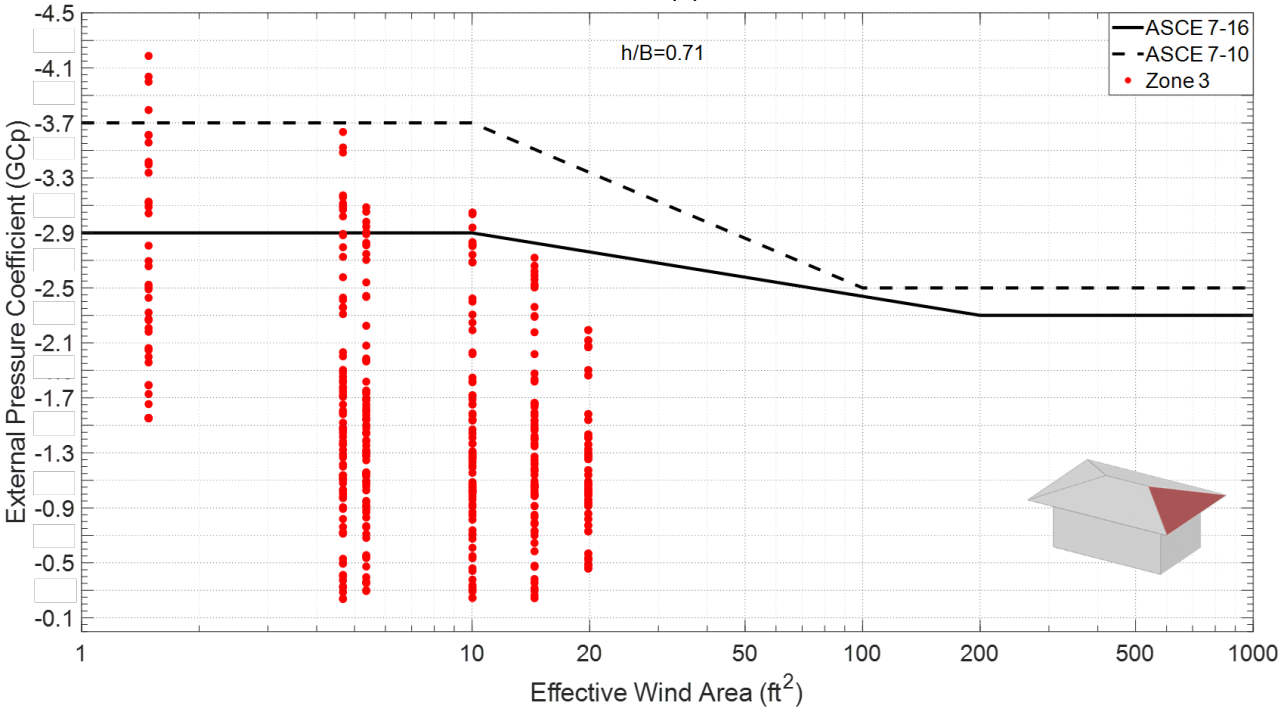

(b)

Figure 30 Critical area-averaged net pressure coefficient for zone 3 compared to GC_p plot in ASCE 7-16 and ASCE 7-10 (a) Model A- South side (b) Model A- East side

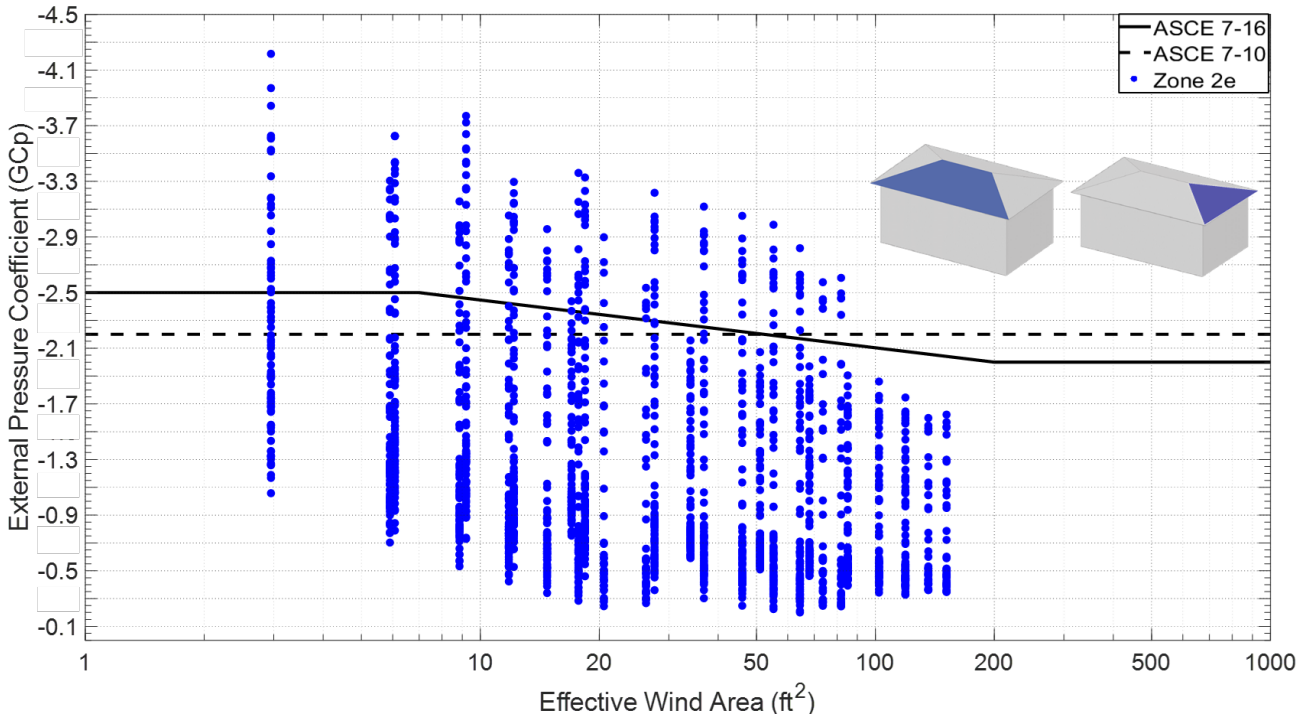
ASCE 7-16
ASCE 7-10
Zone 2e
External Pressure Coefficient (GCp)
-4.5
-4.1
-3.7
-3.3
-2.9
-2.5
-2.1
-1.7
-1.3
-0.9
-0.5
-0.1
1
10
20
50
100
200
500
1000
Effective Wind Area (ft2)

(a)

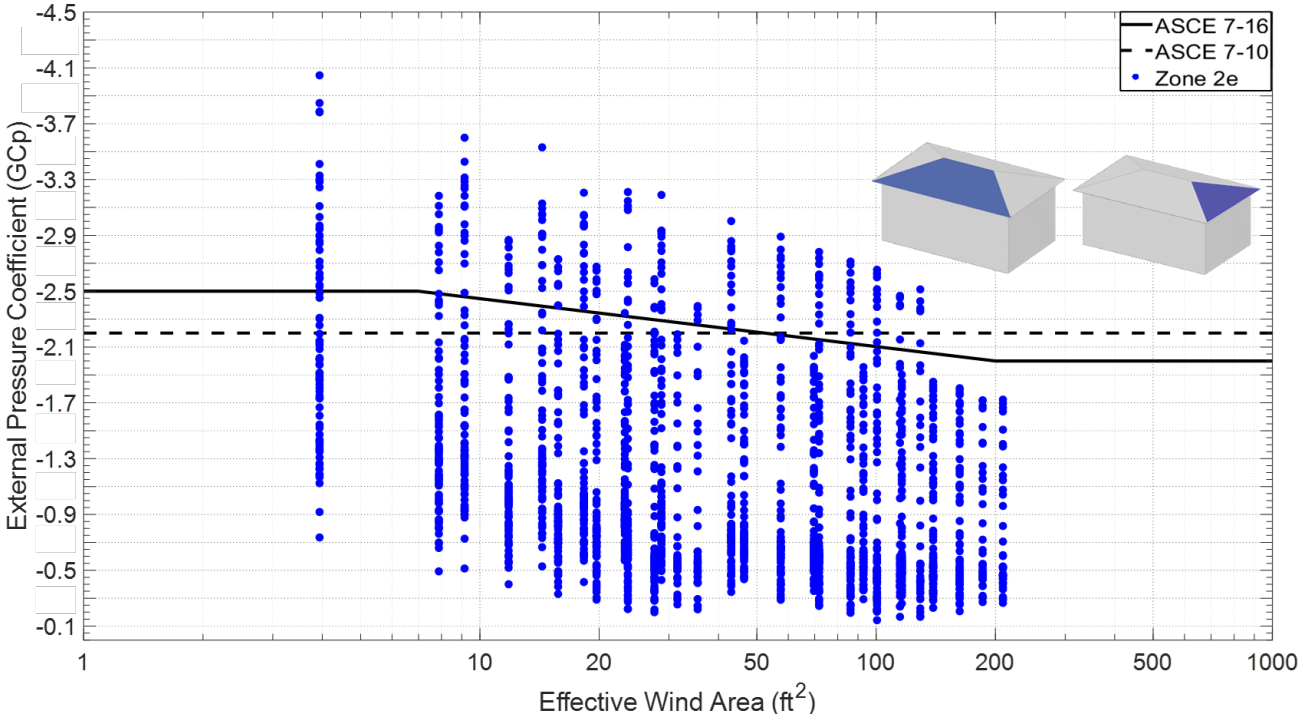
ASCE 7-16
ASCE 7-10
Zone 2e
External Pressure Coefficient (GCp)
-4.5
-4.1
-3.7
-3.3
-2.9
-2.5
-2.1
-1.7
-1.3
-0.9
-0.5
-0.1
1
10
20
50
100
200
500
1000
Effective Wind Area (ft2)

(b)

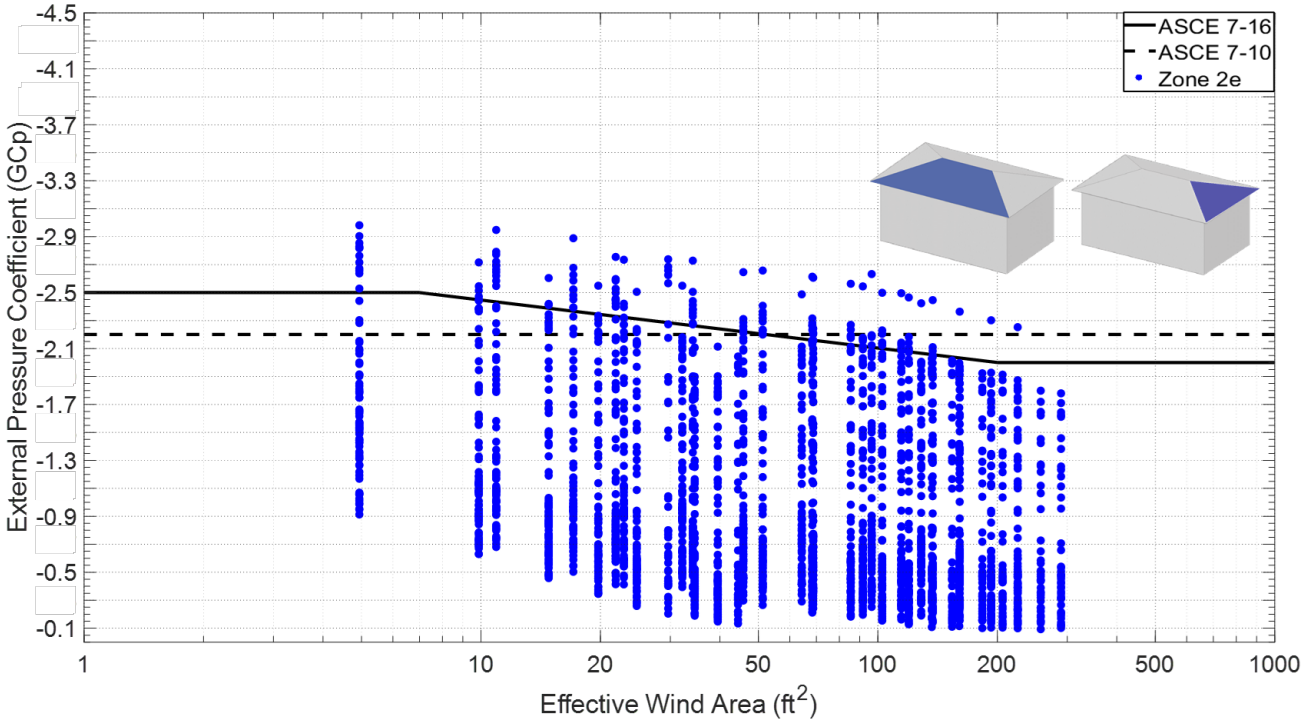
ASCE 7-16
ASCE 7-10
Zone 2e
External Pressure Coefficient (GCp)
-4.5
-4.1
-3.7
-3.3
-2.9
-2.5
-2.1
-1.7
-1.3
-0.9
-0.5
-0.1
1
10
20
50
100
200
500
1000
Effective Wind Area (ft2)

(c)

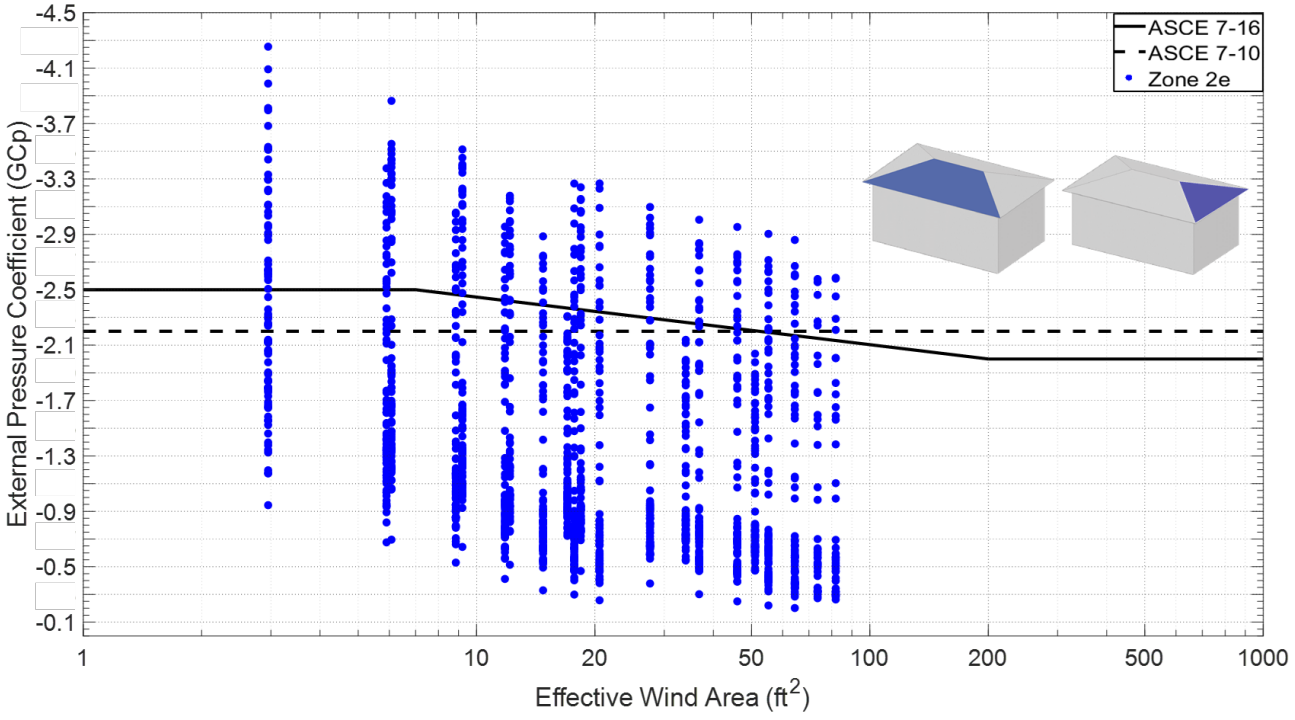
ASCE 7-16
ASCE 7-10
Zone 2e
External Pressure Coefficient (GCp)
-4.5
-4.1
-3.7
-3.3
-2.9
-2.5
-2.1
-1.7
-1.3
-0.9
-0.5
-0.1
1
10
20
50
100
200
500
1000
Effective Wind Area (ft2)

(e)

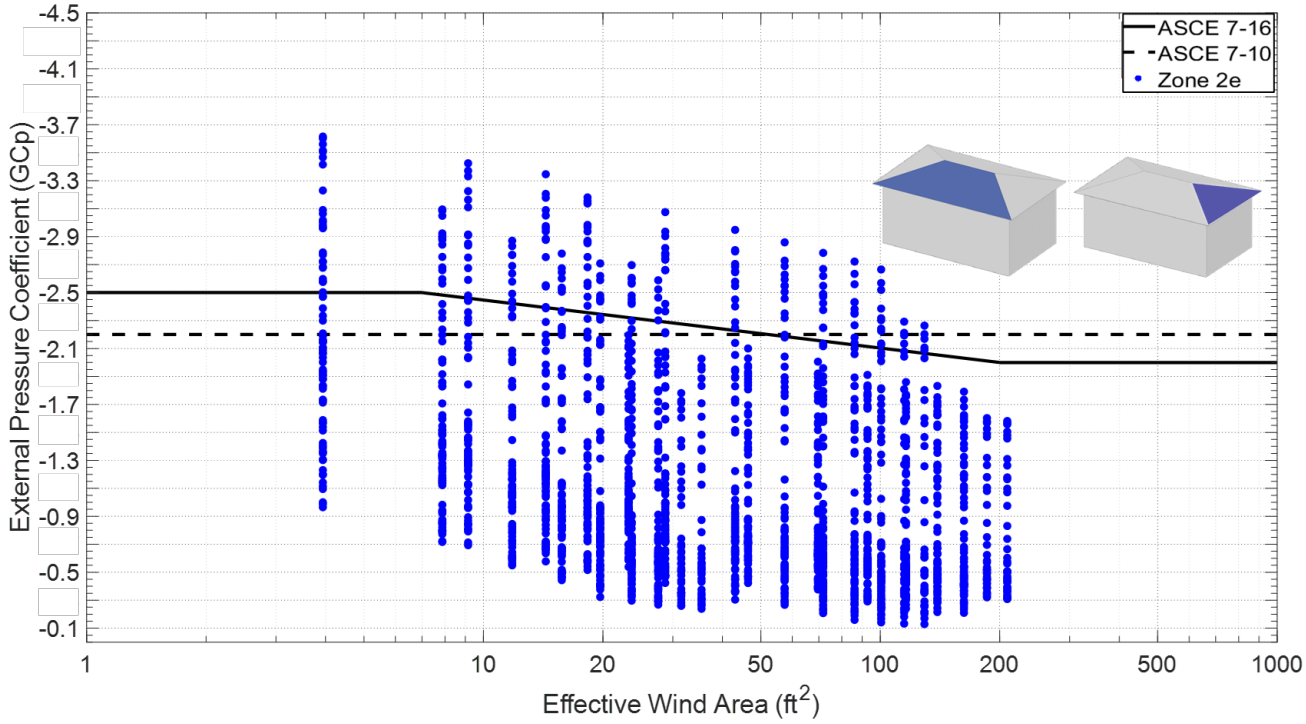

(f)

Figure 31 Critical area-averaged net pressure coefficient for zone 2e compared to GC_p plot in ASCE 7-16 and ASCE 7-10 (a) Model B (b) Model C (c) Model D (d) Model E (f) Model F

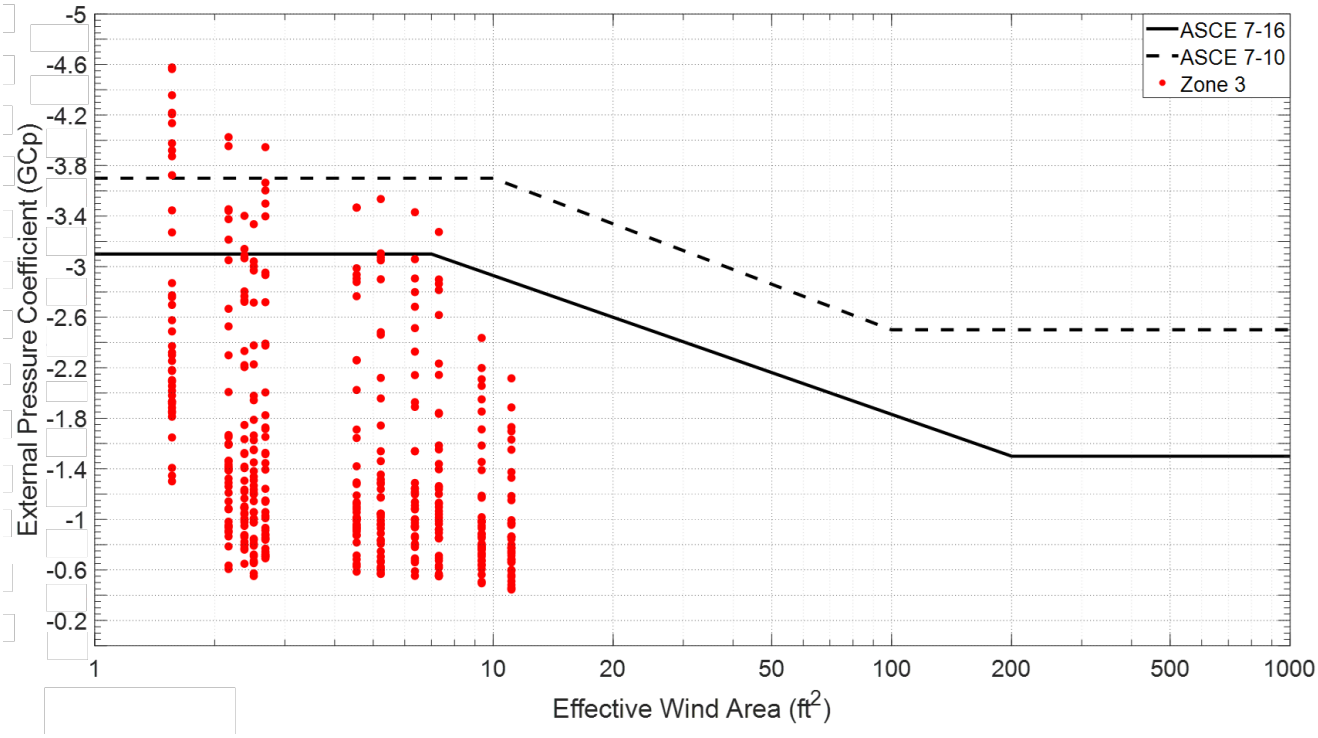

(a)

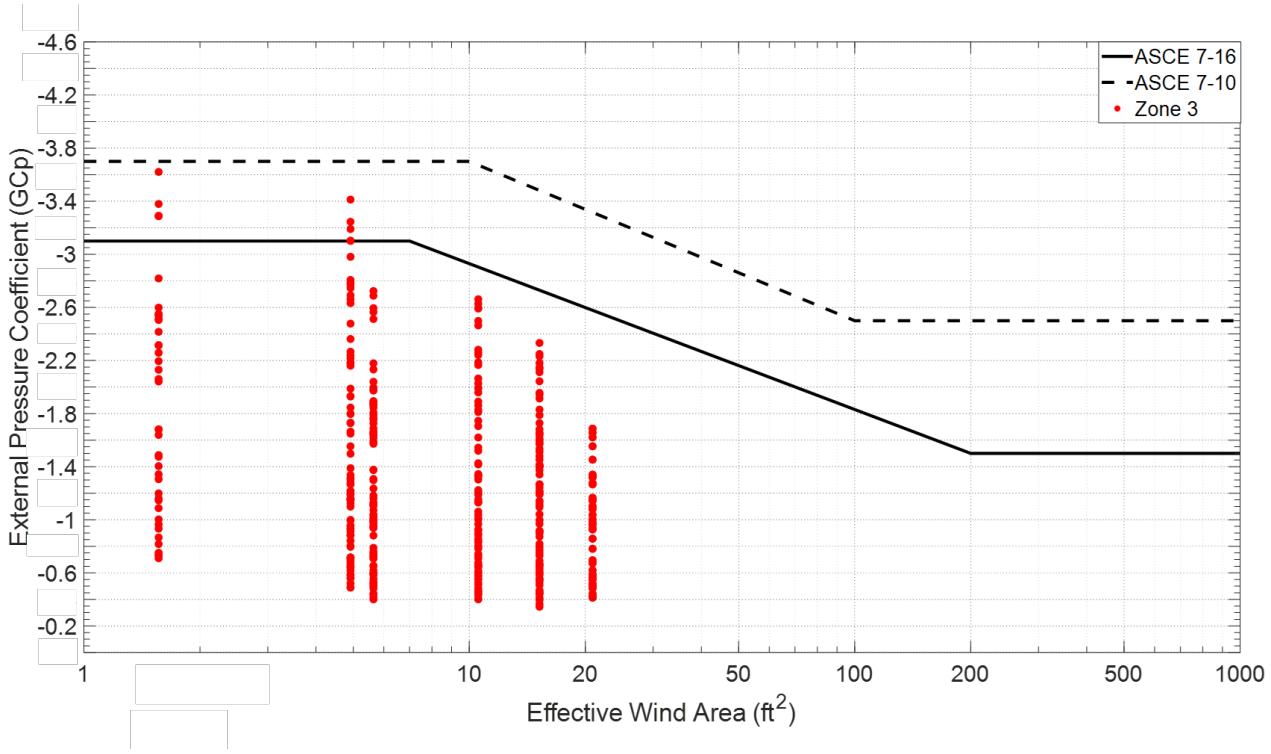

(b)

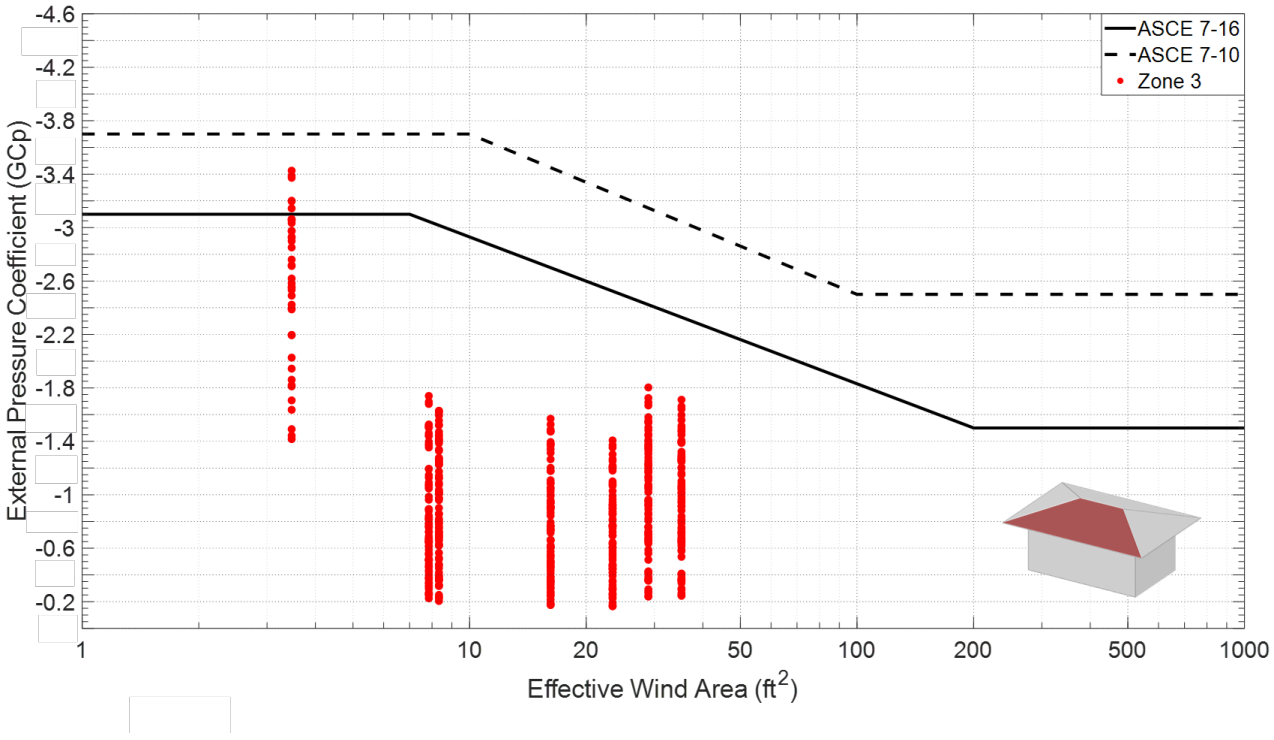

(c)

Figure 32 Critical area-averaged net pressure coefficient for zone 3 compared to GC_p plot in ASCE 7-16 and ASCE 7-10 for (a) Model B (b) Model C (c) Model D

3.5.2. Comparison with ASCE 7-22

In addition to the comparison made with ASCE 7-10 & ASCE 7-16, the experimental results for overhang's peak net pressure coefficient were plotted and compared to ASCE 7-22 GC_p plots (Figure 35). The zoning criterion is different between ASCE 7-22 and ASCE 7-10/7-16, both the edge and the corner are specified as zone 3 instead of zone 2/2e. The upper bound shown in Figure 35 for ASCE 7-22 is calculated as the sum of negative upper bound for the GC_p plot for the applicable roof surface and the positive upper bound for GC_p plot for the wall surface with x grid of [1 10 100 500 1000]. The x grids for GC_p plots of walls in ASCE 7-22 is [1 10 500 1000], while for hip roofs of angle 20˚ to 27˚ is [1 10 100 1000], thus in Figure 32 the ASCE 7-22 boundary was drawn to account for all the x grid between both GC_p plots for walls and roofs. It is important to note that positive pressure for the wall and soffit (towards the surface) is in the same direction as the negative pressure for the roof overhangs (away from the surface).

All the plots in Figure 35 show the expected monotonically decreasing relationship between the effective area and the magnitude of the net pressure coefficients. For model B, magnitudes of most of the tap combinations were above the upper bound (-3.4). For models C and D most of the peak net GC_p values were below the upper bound of the plot (-3.4) with some points exceeding the upper bound for smaller tributary areas or single local tap. This may suggest that ASCE 7-22 is less conservative compared to the experimental testing regarding zone 3 for short overhang width only (i.e., 2 ft). It is apparent that ASCE 7-22 is more conservative compared to ASCE 7-10 and ASCE 7-16, though some revisions appear to still be necessary.

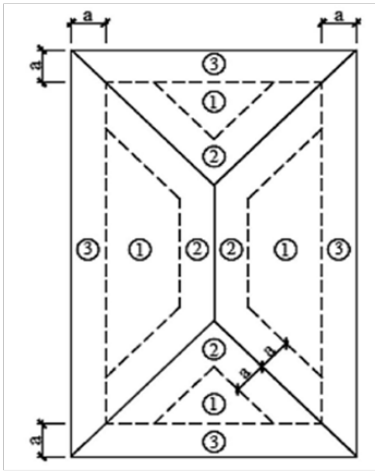

Figure 33 Assigned zones for hip roof in ASCE 7-22

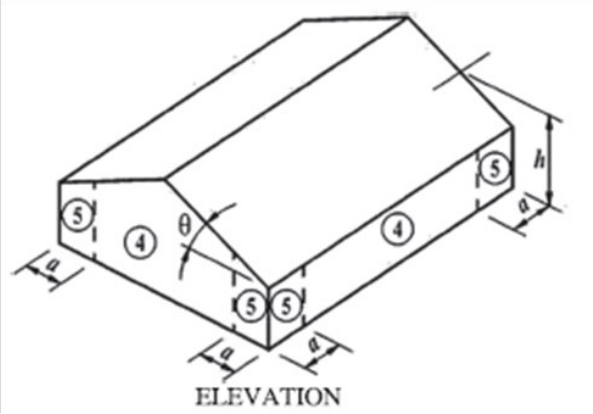

Figure 34 Assigned zones for walls in ASCE 7-22; same for ASCE 7-10 and ASCE 7-16

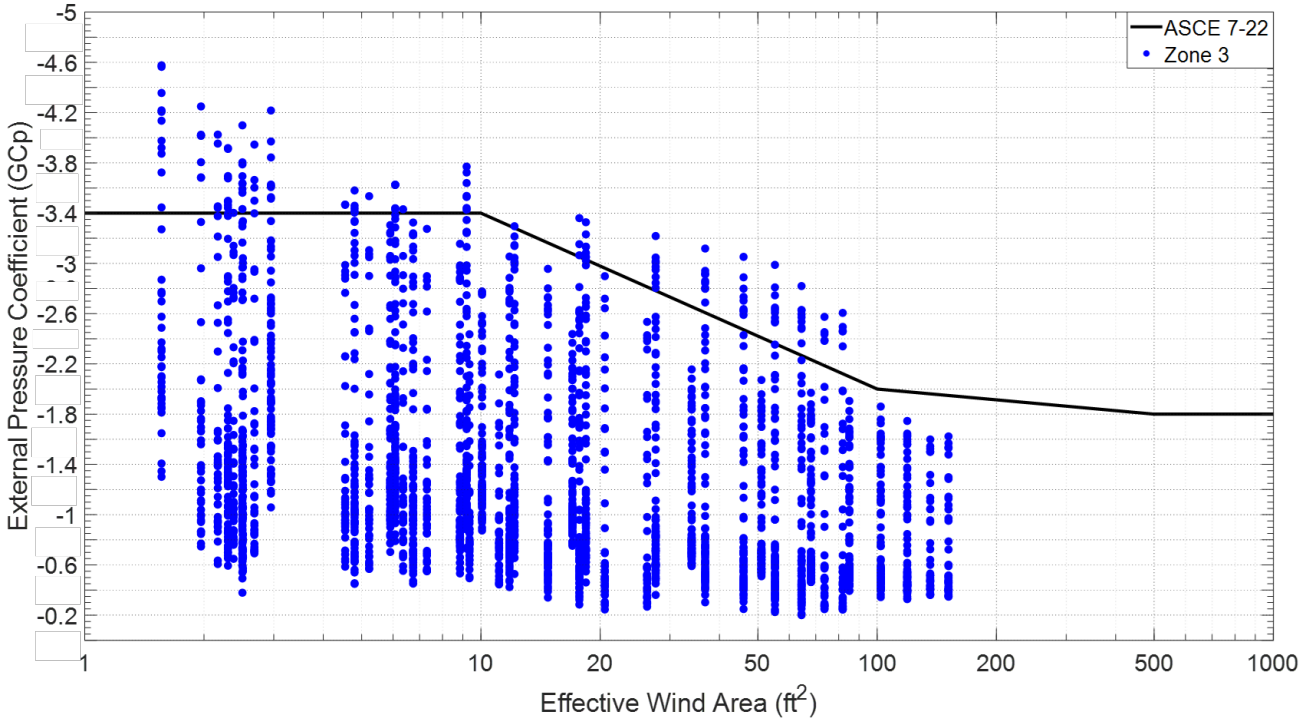
ASCE 7-22
Zone 3
External Pressure Coefficient (GCp)
-5
-4.6
-4.2
-3.8
-3.4
-3
-2.6
-2.2
-1.8
-1.4
-1
-0.6
-0.2
1
10
20
50
100
200
500
1000
Effective Wind Area (ft2)

(a)

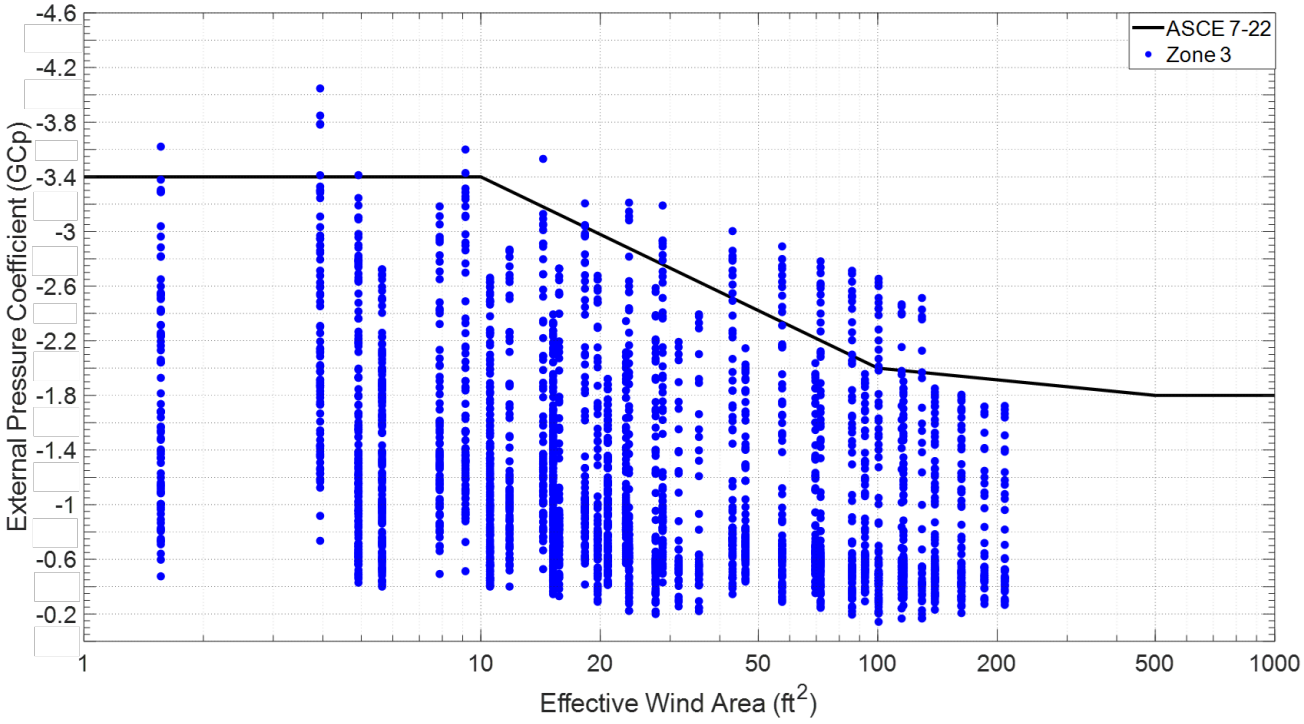
ASCE 7-22
Zone 3
External Pressure Coefficient (GCp)
-4.6
-4.2
-3.8
-3.4
-3
-2.6
-2.2
-1.8
-1.4
-1
-0.6
-0.2
1
10
20
50
100
200
500
1000
Effective Wind Area (ft2)

(b)

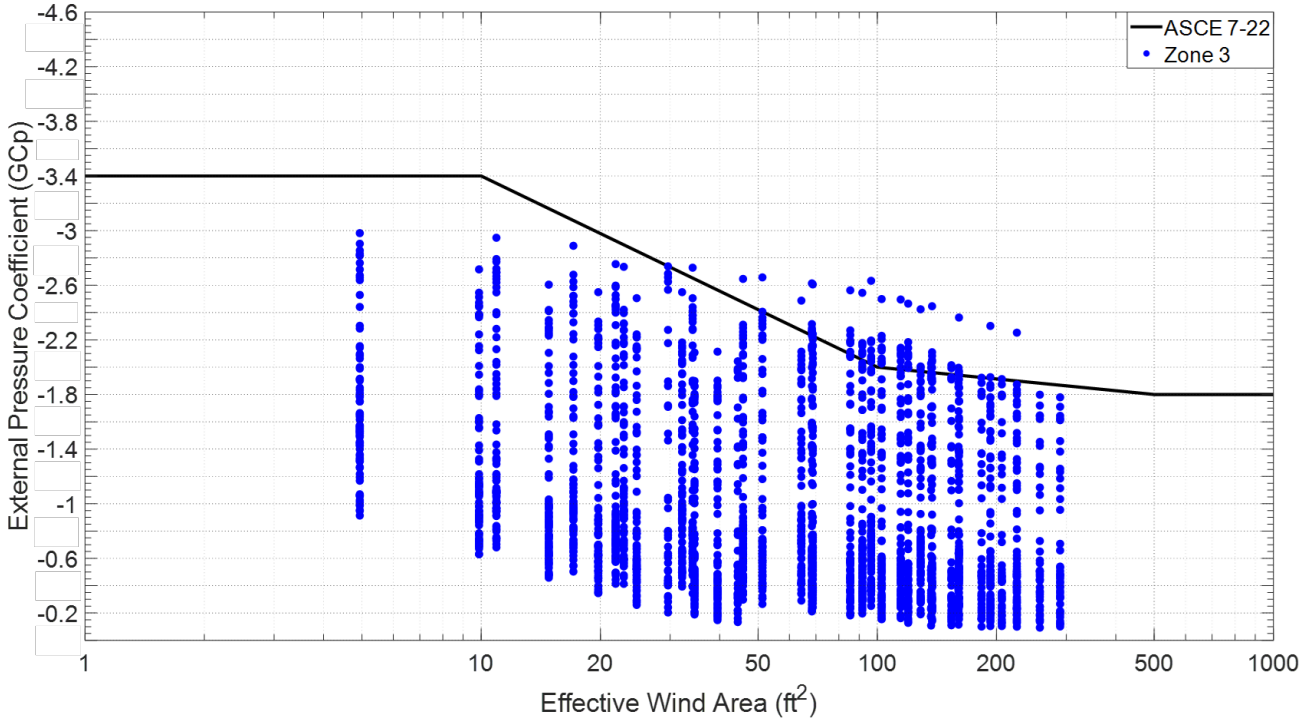

(c)

Figure 35 Critical area-averaged net pressure coefficient for zone 3 compared to GC_p plot in ASCE 7-22 for (a) Model B (b) Model C (c) Model D

In addition to the analysis of hip roofs, area-averaged pressure analysis for walls was done to investigate further the pressure gradients on single or groups of taps among the walls. The same procedures, as overhangs, were followed for the analysis of the external pressure coefficient at the walls. The area of the wall is divided into zone 4 and zone 5 as specified in ASCE 7 (7-10, 7-16, and 7-22), where zone 5 is the edge zone of width 'a' and zone 4 is the remaining area of the wall, as shown in Figure 32.

There is not a significant difference among the peak min and peak max pressure coefficients on the adjacent wall of different roof overhang widths for the same roof slope. However, there is such a variation between the peak pressure coefficients among the wall surface for different roof angles slopes (i.e., 18.4˚, 26.6˚). Figure 36 shows the critical area-averaged external pressure coefficient for zone 4 and 5 for adjacent walls for all overhang widths. For both roofs, most of the GC_p values were between the upper boundary (peak min) and lower boundary (peak max) of GC_p plots as specified in ASCE 7-22. However, GC_p values of some local taps or combination of small areas have exceeded these boundaries. For instance, the GC_p values among zone 5 reach peak min of -3.0 and -2.5 for roof angles of 18.4˚ and 26.6˚, respectively, and reach peak max of 1.9 for both slopes. For zone 4, the GC_p values reach a peak min of -2.3 and peak max of 1.4 for both slopes. Therefore, this may suggest that the code provision is less conservative compared to the experimental results regarding both zones 4 and 5. It is important to note that the slope of the roof has no effect on the wall positive pressure coefficients when the walls are located in the windward direction but have more considerable effect for other wind directions where suction occurs. As can be seen in Figure 36, the peak max pressure coefficients among the walls for both roof slopes

are almost the same (2.0), while the peak min pressure coefficient for adjacent walls is -3.0 and -2.5 for roof slope of 18.4˚ and 26.6˚, respectively.

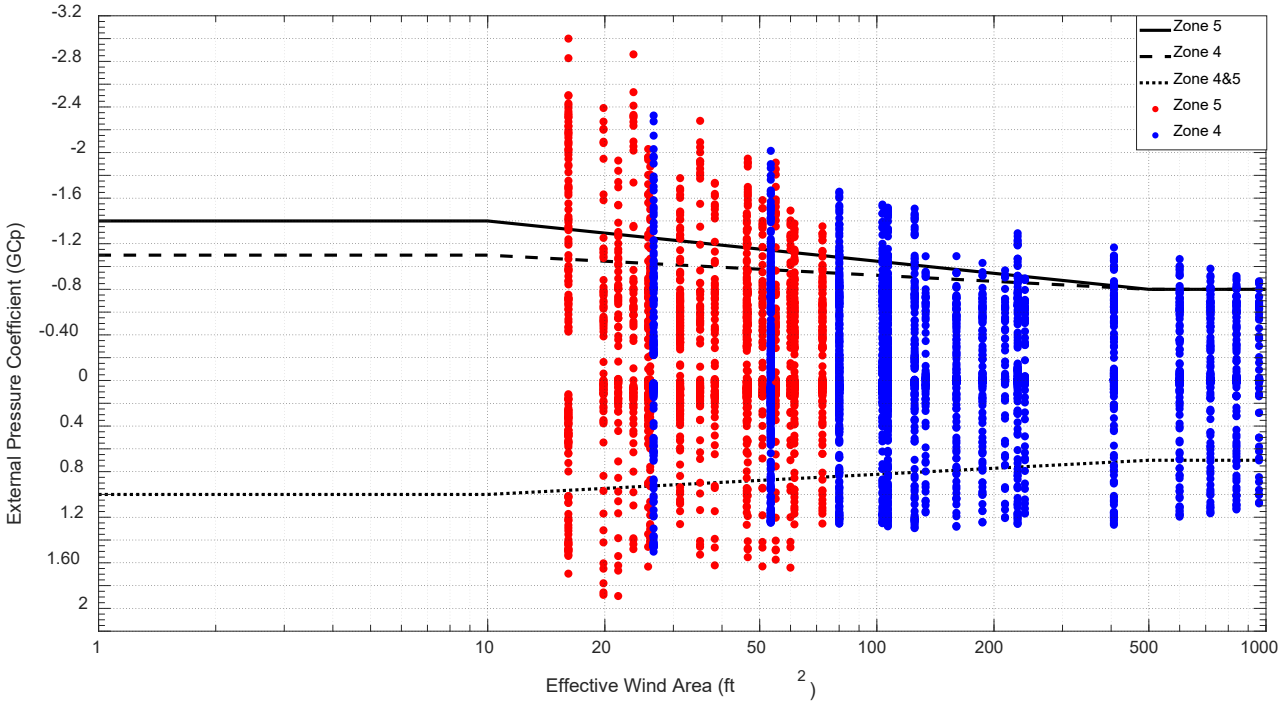

(a)

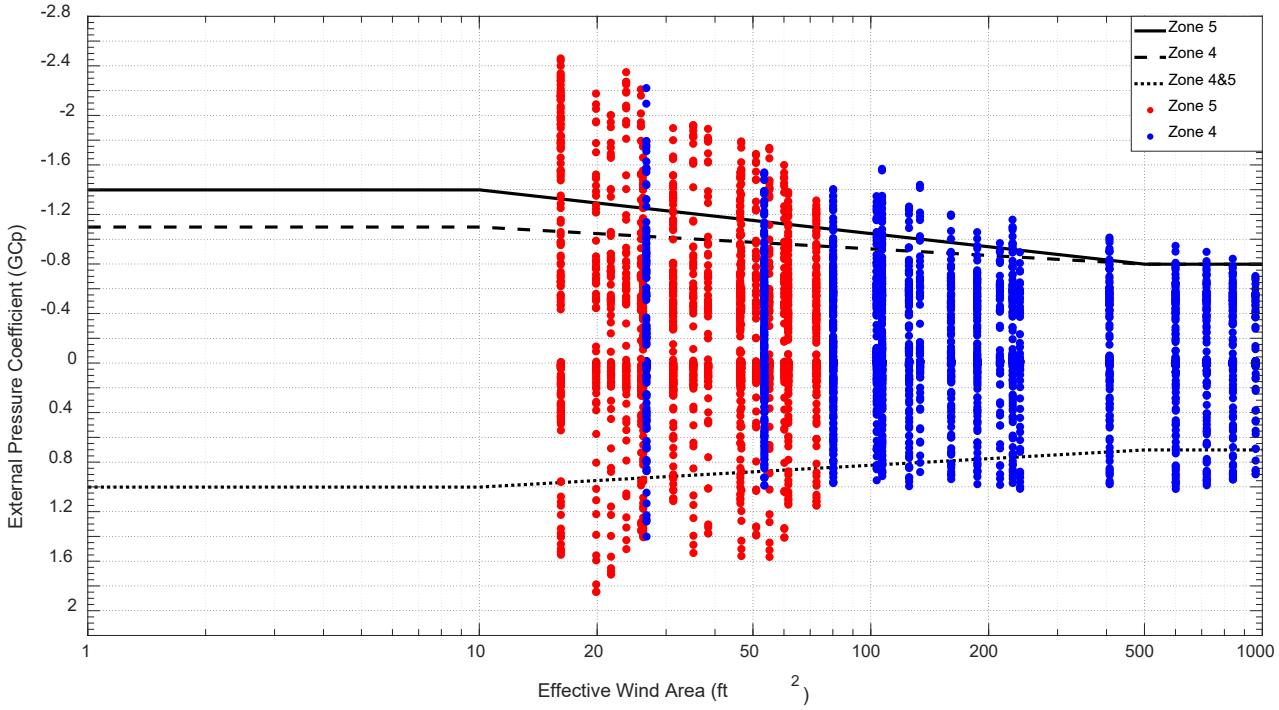

(b)

Figure 36 Critical area-averaged external pressure coefficient for zone 4 and 5 for walls compared to GC_p plot in ASCE 7-22 for (a) roof angle 18.4˚ (b) roof angle 26.6˚

3.6. Toward Codification

The area-averaged pressure analysis for the experimental data with GC_p plots, compared with the last three versions of ASCE 7 (7-10, 7-16, and 7-22), for both roof overhangs and adjacent walls was shown in the previous sections and in Phase 1 final report (Zisis et al. 2021). Based on this parametric study, it is apparent that none of the upper boundary for the GC_p plots of the latest three versions of ASCE 7 was entirely adequate when compared to the experimental results in terms of design guidelines. Thus, proposed design provisions for GC_p plots for roof with overhangs, and for walls as well, are generated from the envelopes of the experimental data obtained from this parametric study.

The three different versions of ASCE 7 in terms of roof overhangs design guidelines are studied towards codification purposes. There are some major differences related to the design of roof overhangs between the recently released version of ASCE 7-22 and the previous two versions (ASCE 7-10 and ASCE 7-16) in terms of zoning criteria for the roof surface, and the GC_p plots with effective wind area. For instance, zones 2 and 2e in ASCE 7-10 and ASCE 7-16 respectively, were assigned with the corners under zone 3 in ASCE 7-22, as shown in Figure 37. In addition, the two versions of ASCE 7-10 and 7-16 have separate plots for GC_p with effective wind area for roofs with overhangs, while in ASCE 7-22 there are no separate plots for overhangs. Though, in ASCE 7-22 the net pressure coefficient for roof overhangs is calculated as the sum of the GC_p of the overhang's top and bottom surfaces, where the GC_p of the top surface is the same as the applicable roof surface, while the GC_p of the overhang's bottom surface is the same as the adjacent wall surface (Figure 34), and there are no specified GC_p plots according to different h/B in ASCE 7-22, similar to those included in ASCE 7-16. Furthermore, ASCE 7-10 has assigned roof angle from 7˚ to 27˚ for both gable/hip roofs under the same category, which has been changed later in ASCE 7-16/7-22 to have different plots for gable roofs and hip roofs separately and to have separate plots for slope 7˚ to 20˚ and for slope 20˚ to 27˚.

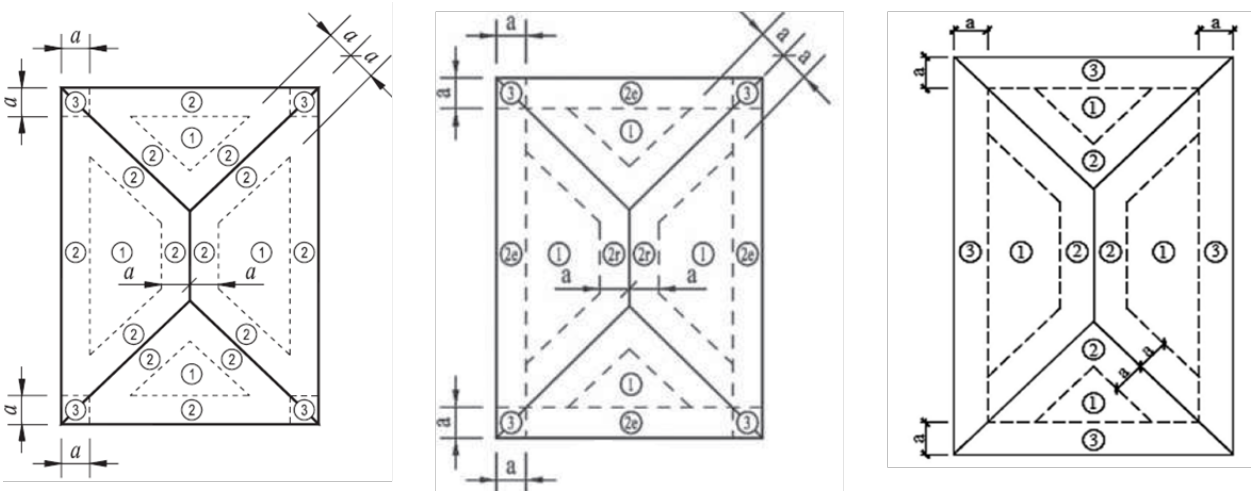

(a) (b) (c)

Figure 37 Assigned zones for hip roof in (a) ASCE 7-10 (b) ASCE 7-16 (c) ASCE 7-22

Envelope lines were superimposed onto each plot of each case to confine underneath all the GC_p value. All the envelope lines of the same category, which are either of the same roof slope or the same assigned zone on roof surface or wall surface, were combined in one plot as shown in Figures 38 and 39. The same for walls, the envelope lines were plotted according to the peak GC_p values for each case as shown in Figure 40. However, the GC_p plot for wall as specified in ASCE 7 is not affected by roof shape or slope or overhang width.

Consequently, the peak min envelope line for each plot was defined as the proposed boundary which is similar to the approach in a previous codification work (Davenport et al. 1985). Following this approach will assure that all the GC_p values from the experimental results will not exceed the proposed boundary. The peak min GC_p value for the proposed boundary for roof angle 18.4˚ is -4.6 and -6 for zone 2 and zone 3, respectively, and for roof angle 26.6˚ is -4.3 and -4.6 for zone 2 and zone 3, respectively, as shown in Figures 38 and 39. Therefore, it is suggested not to assign both the edge and the corner of the roofs into a single zone (i.e. zone 3) as specified in ASCE 7-22. Furthermore, there are not significant changes between the envelope lines based on h/B, as specified in ASCE 7-16. Therefore, it is suggested to follow the approach of ASCE 7-22 and ASCE 7-10 for eliminating h/B criteria that were specified only in ASCE 7-16. In addition, it is important to keep the assigned categories for roof slopes as specified in ASCE 7-16 and ASCE 7-22 (i.e., 7˚ to 20˚ and 20˚ to 27˚). No changes are suggested to be applied on the GC_p peak max boundary for roof overhangs, from ASCE 7-22. It is important to note that GC_p plots for roof overhangs in ASCE 7-10 and ASCE 7-16 do not include the peak max boundary. For walls, the peak min GC_p value for the envelope lines are -2.6 and -3.2 for zone 4 and zone 5, respectively, while the peak max GC_p value for both zones is 1.8. It is suggested not to change the defined zoning criteria for walls, but it is recommended to revise the GC_p plot with the new proposed boundaries for both max and min GC_p.

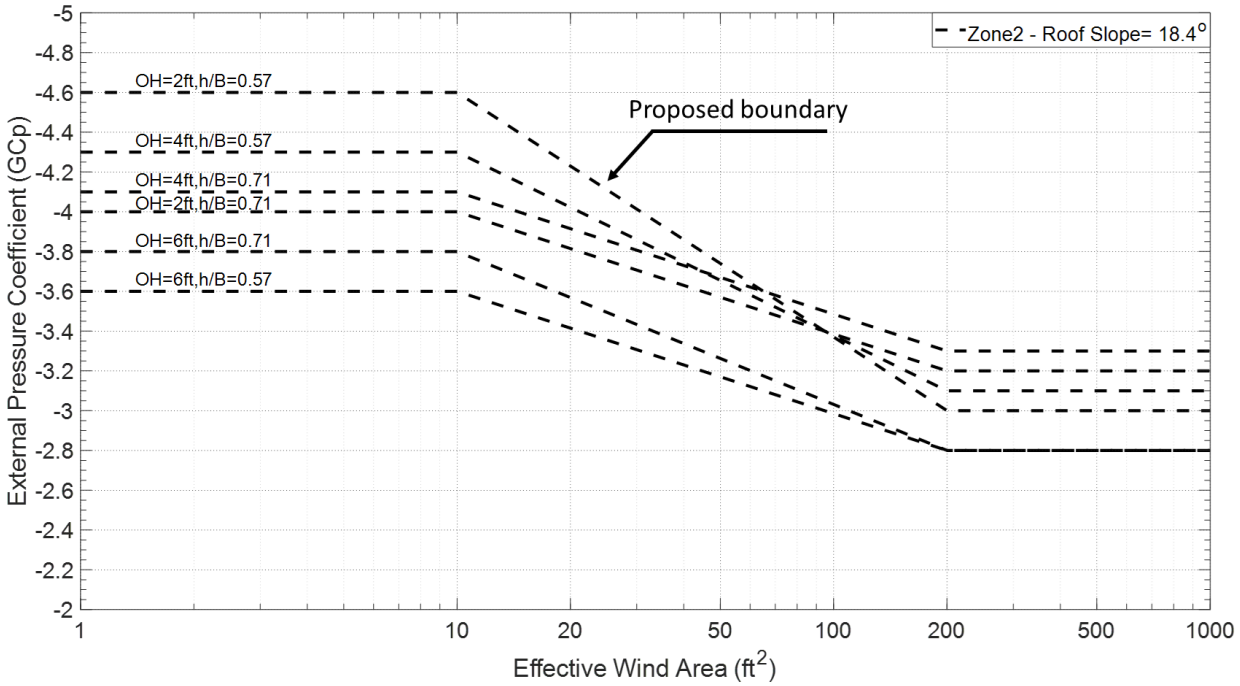

(a)

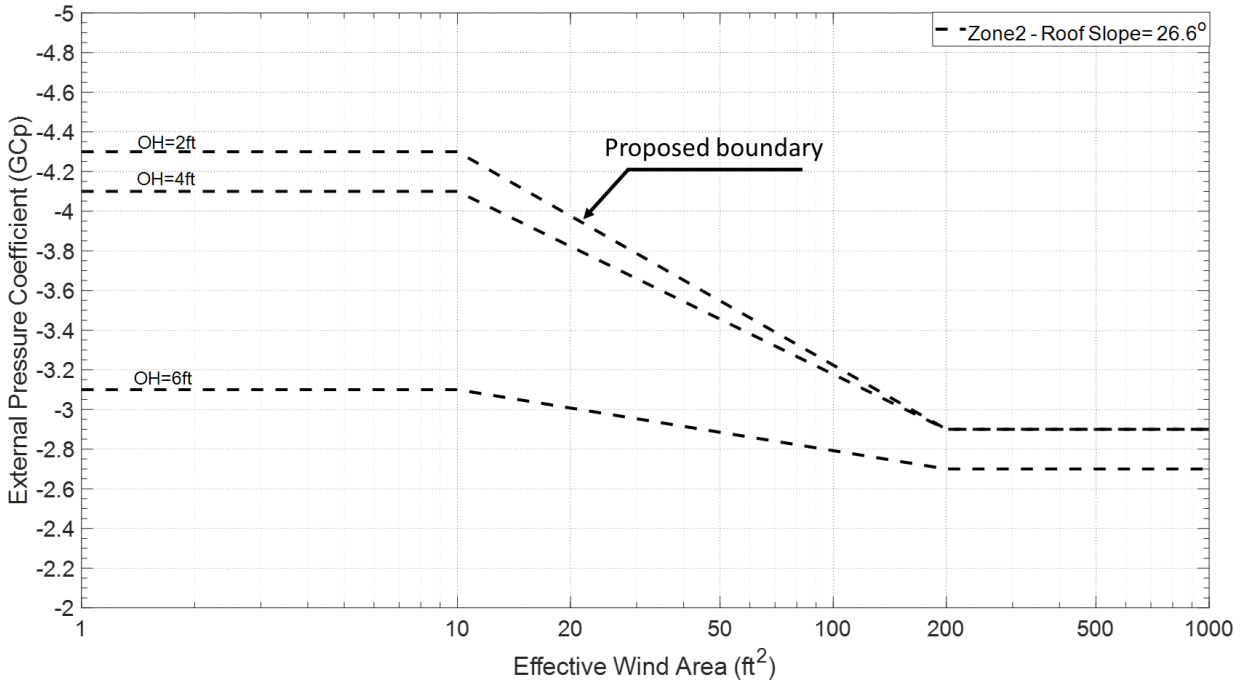

(b)

Figure 38 Area averaging envelope for corresponding ranges for all testing cases for zone 2

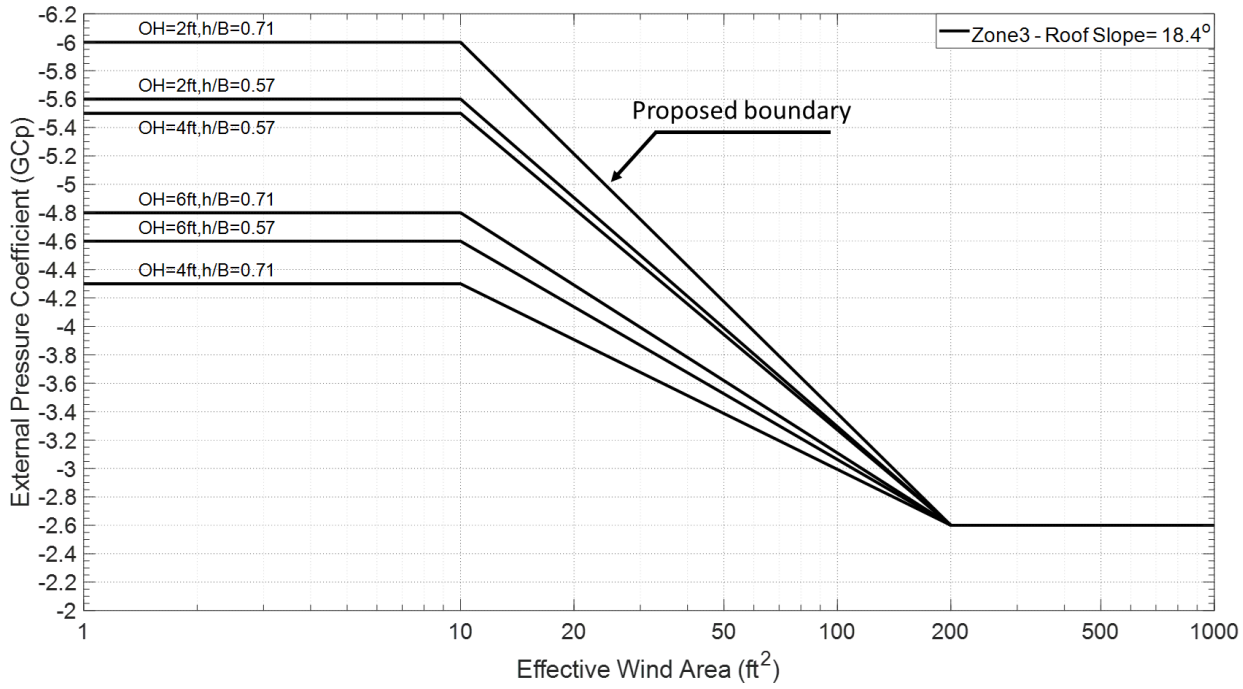

(a)

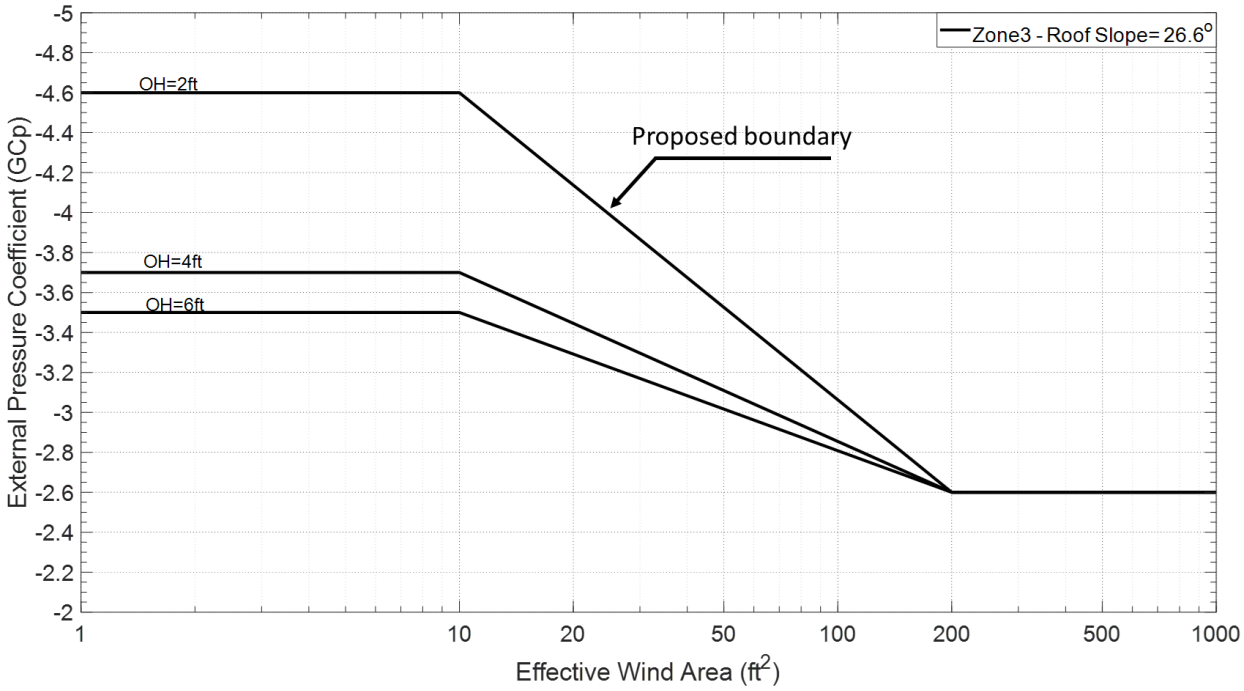

(b)

Figure 39 Area averaging envelope for corresponding ranges for all testing cases for zone 3

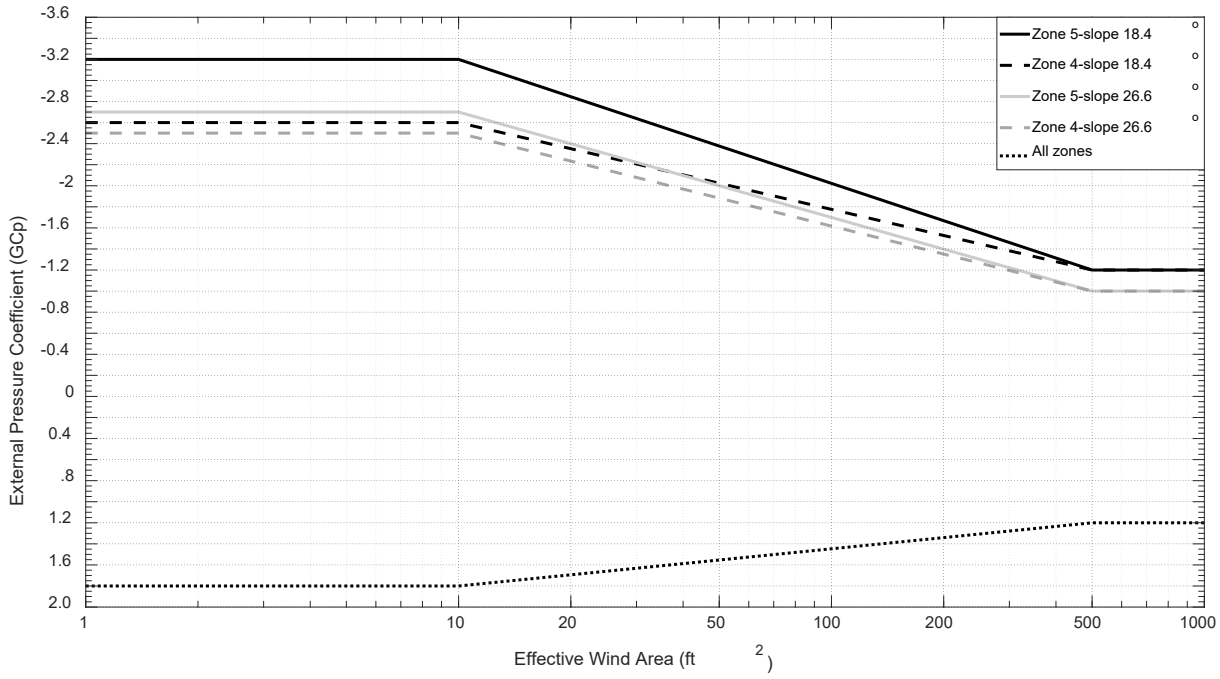

Figure 40 Area averaging envelope for corresponding ranges for all testing cases for walls

3.6.1 Recommendation

Based on the area-averaged pressure analysis with the plotted minimum envelope lines, and according to the latest three versions of ASCE 7, the following recommendations can be made towards codification:

- Zoning area for hip roof with overhangs shall not follow ASCE 7-22 and it is suggested to assign the edge of the overhangs to zone 2 and the corner to zone 3 as previous versions (Figure 41).
- Roof slope categories as specified in ASCE 7-16 and ASCE 7-22 (i.e., $7^\circ < \theta \leq 20^\circ$ and $20^\circ < \theta \leq 27^\circ$) shall be maintained.
- Eliminating h/B criteria for GC_p plots of roof angles $7^\circ < \theta \leq 20^\circ$ that was specified in ASCE 7-16, as it was found that the width of the building does not significantly affect the GC_p values.
- Wall zoning criteria shall be kept unchanged as specified in the last three versions.
- Figures 40 to 42 provide recommended provisions for the design guidelines of overhangs for hip roof and walls based on the present study.

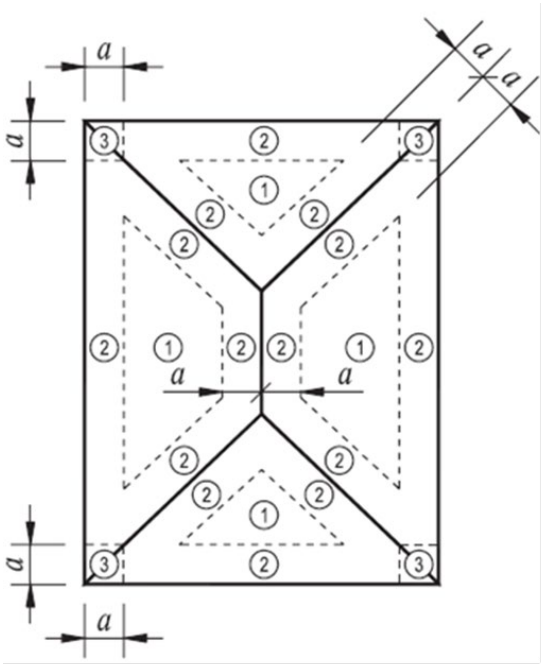

Figure 41 Proposed zoning area for hip roof with overhangs; same as ASCE 7-10

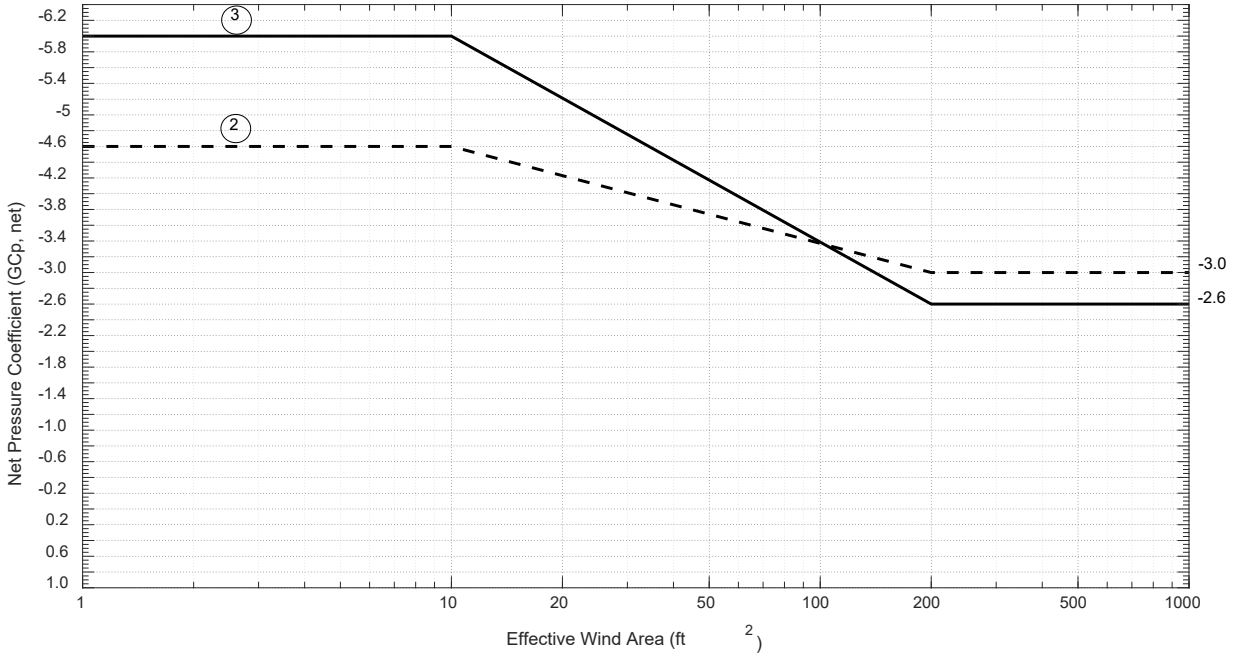

Figure 42 Proposed provisions for $GC_{p,net}$ on roof overhangs of hip roof of angles $7^\circ < \theta \leq 20^\circ$

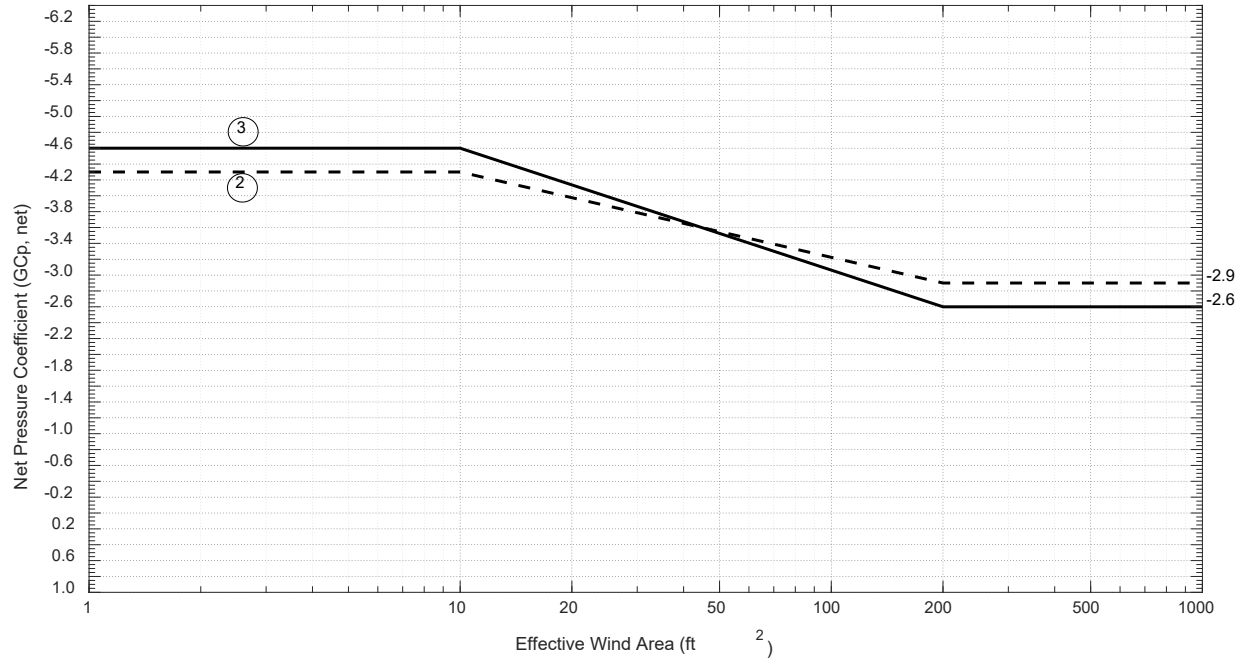

Figure 43 Proposed provisions for $GC_{p,net}$ on roof overhangs of hip roof of angles $20^\circ < \theta \leq 27^\circ$

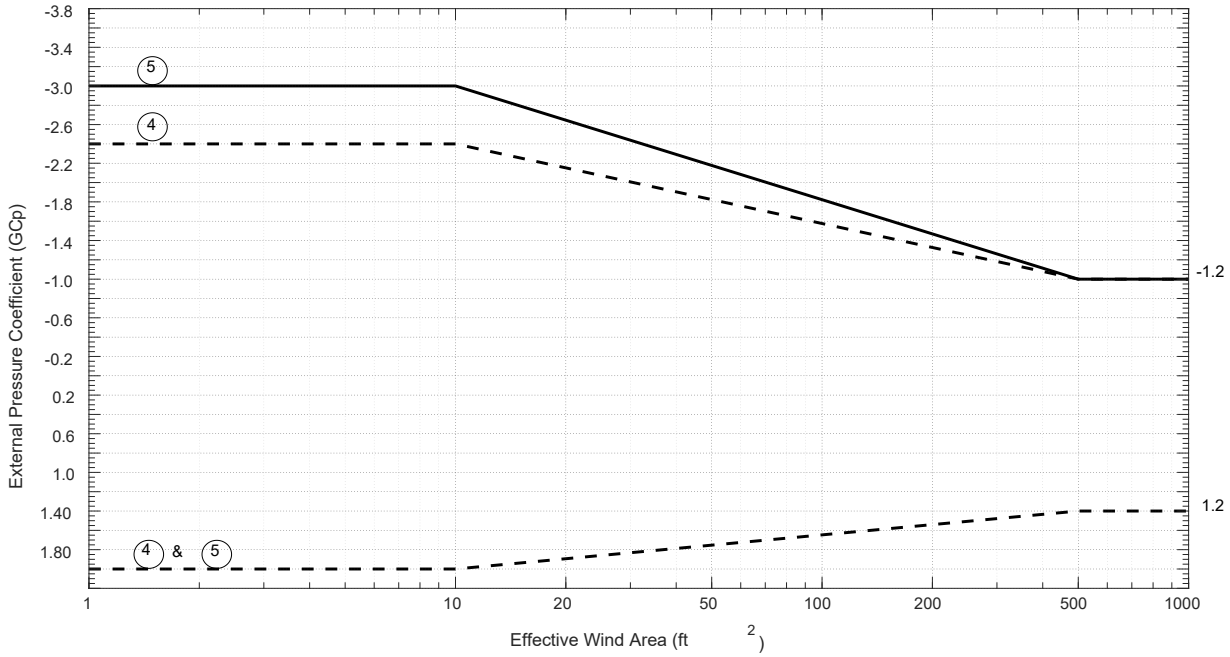

Figure 44 Proposed provisions for GC_p for walls of enclosed, partially enclosed, and partially open buildings

4. Overall summary, conclusion, and future works

4.1.Summary

Large scale wind tunnel experiments were conducted at the Wall of Wind Experimental Facility at Florida International University for six models of a residential building with hip roof and different overhang width. This phase testing completes the set of models that have been tested in phase 1 to end up having eight different models of large-scale testing. Two roof slopes of 18.4˚ and 26.6˚ were selected for building the models that have been tested during the two phases. Models of three different overhang widths (2 ft, 4 ft, and 6 ft) were tested for each roof slope. Peak and mean local surface wind coefficients were recorded for walls, soffits, and roofs with overhangs for all configuration cases. Moreover, correlation coefficients and regression analyses were considered to assess the correlation of soffit pressure coefficients to pressure coefficients of wall upper taps. The findings show that the 2 ft overhang experienced higher suction coefficients at the edges compared to the 4 ft and 6 ft overhang. In addition, the findings show that the steeper slope, the less suction experienced by the roof. Furthermore, the results confirmed that, for all models, soffit positive pressure coefficients may be taken as the adjacent wall external pressure, as stated by ASCE 7-16, but this is not valid for negative pressure coefficients. The width of the overhang did not seem to have a considerable effect on the positive pressure coefficient on walls and soffit. However, by carrying out correlation analysis and regression analysis between soffit pressure taps and upper wall taps, the 6 ft soffit seemed to be less correlated with the wall upper taps, than the 2 ft and 4 ft soffit. Uplift pressures were calculated for the aim of comparison between overhangs with covered and uncovered soffits. It was found that there is a negligible difference between the uplift pressure acting on the horizontal soffit (covered) or inclined soffit (uncovered). Also, no

significant difference was recorded between the covered and uncovered soffits in terms of regression analysis, correlation coefficients and contour plots. Area averaged pressure coefficients were measured for different combinations of taps and were compared to the GC_p plots in ASCE 7-10, ASCE7-16 and ASCE 7-22. Area averaging and pressure coefficients for overhangs, and adjacent roof areas were compared to the GC_p plots in the latest three versions of ASCE 7 for each specified zone. The Standards are less conservative regarding zone 2e/2 and zone 3 for most of the cases. Accordingly, a codification study has been proposed to account for the less conservative design guidelines in the previous versions of standards.

4.2.Observations and Conclusions

Based on experimental testing results and discussion, the following observed/concluded remarks can be drawn:

- The 2 ft inclined overhangs were found to have higher pressure coefficient at the edges compared to the 4 ft and 6 ft overhangs.
- Pressure taps at the soffit edge exposed to higher peak min Cp compared to the middle and inner taps.
- The width of the overhang did not seem to have a considerable effect on the absolute positive pressure correlation between walls and soffits.
- The width of the overhang has a recognized effect on the negative pressure correlation between walls and soffits.
- The 6 ft soffit appeared to be less correlated at the edge with the wall upper taps compared to the 2 ft and 4 ft soffit.
- The correlation coefficients for wider soffits with the wall significantly decrease compared to narrower soffits when the walls and soffits are exposed to suctions.
- The soffit pressure coefficients shall be taken as the adjacent wall external pressure, as stated by ASCE 7-16/7-22 for positive pressure only, while this shall not be applicable for suction pressure.
- Roof with steeper slope (i.e., 26.6˚) experience lower suction along the roof surface compared to roofs with less steep slope (i.e. 18.4˚)
- GC_p plots in the latest three versions of ASCE 7 for hip roof of both angle ranges $7^o < \theta \leq 20^o$ and $20^\circ < \theta \leq 27^\circ$ might be less conservative compared to the experimental results regarding zone 2e/2 and zone 3.
- GC_p plots in the latest three versions of ASCE 7 for walls might be less conservative compared to the experimental results regarding zones 4 and 5.
- It is important to include a revised codification approach in the upcoming version of wind codes and standards considering all previous wind load studies on roof overhangs.

4.3.Future work

The two phases of testing focused mainly on hip roofs with only two different roof slopes, and the findings have shown that some of the GC_p plots in the last three versions of the ASCE Wind Standard are less conservative compared to the experimental results. More comprehensive large scale testing may be needed for different roof shapes with overhangs (i.e. gable roofs), and

different roof angles ($27^{\circ} < \theta \leq 45^{\circ}$). In addition, many sets of models with different roof slopes and roof shapes will form large enough datasets for roofs with overhangs that may be used in developing robust machine learning models that can reliably automate the pressure prediction on low-rise building overhangs.

References

ASCE. (2010). "Minimum design loads for building and other structures." American Society of Civil Engineers, ASCE/SEI 7-10, Reston, VA.

ASCE. (2017). "Minimum Design Loads and Associated Criteria for Buildings and Other Structures." American Society of Civil Engineers, ASCE/SEI 7-16, Reston, VA.

ASCE. (2022). "Minimum Design Loads and Associated Criteria for Buildings and Other Structures." American Society of Civil Engineers, ASCE/SEI 7-22, Reston, VA.

ASCE. (2022). "Wind tunnel testing for buildings and other structures." American Society of Civil 593 Engineers, ASCE/SEI 49-21, Reston, VA.

Candelario, J. D., Stathopoulos, T., and Zisis, I. (2014). "Wind Loading on Attached Canopies: Codification Study." *Journal of Structural Engineering*, 140(5), 04014007.

Davenport, A. G., Stathopoulos, T., and Surry, D. (1985). "Reliability of wind loading specifications for low buildings." Proc., Int. Conf. on Structural Safety and Reliability, ICOSSAR 85, International Association for Structural Safety and Reliability.

Gan Chowdhury, A., Zisis, I., Irwin, P., Bitsuamlak, G., Pinelli, J.-P, Hajra, B., and Moravej, M. (2017). "Large-Scale Experimentation Using the 12-Fan Wall of Wind to Assess and Mitigate Hurricane Wind and Rain Impacts on Buildings and Infrastructure Systems." *Journal of Structural Engineering*, Vol. 143, Issue 7.

Irwin, H., Cooper, K. R., and Girard, R. (1979). "Correction of distortion effects caused by tubing systems in measurements of fluctuating pressures." *Journal of Wind Engineering and*

Mooneghi, M. A., Irwin, P., and Chowdhury, A. G. (2016). "Partial turbulence simulation method for predicting peak wind loads on small structures and building appurtenances." *Journal of Wind Engineering and Industrial Aerodynamics*, Elsevier, 157, 47–62.

Moravej, M. (2018). "Investigating scale effects on analytical methods of predicting peak wind loads on buildings." Florida International University.

Mostafa, Karim, Ioannis Zisis, Ted Stathopoulos "Wind Induced Loads on Roof Overhangs- Phase 1" Final Report- Florida Building Commission (2021). https://www.floridabuilding.org/fbc/commission/FBC_0621/HRAC/HRAC-06-21/Wind-Induced_Loads_On_Roof_Overhangs_Final_Report.pdf

Mostafa, K. Zisis, I. Chen, D. (2022) "Large scale testing for roof overhangs aerodynamic pressure 572 distribution using the wall of wind experimental facility", in Wind induced loads on hip roof 573 overhangs of low-rise building. DesignSafe-CI. https://doi.org/10.17603/ds2-8nyb-dm44.

Taher, R. (2007). “Design of Low-Rise Buildings for Extreme Wind Events.” *Journal of Architectural Engineering*, 13(1), 54–62.

Vickery, P. J. (2008). “Component and Cladding Wind Loads for Soffits.” *Journal of Structural Engineering*, 134(5), 846–853.

Wiik, T., and Hansen, E. W. M. (1997). “The assessment of wind loads on roof overhang of low-rise buildings.” *Journal of Wind Engineering and Industrial Aerodynamics*, 67–68, 687–696.

Zisis, I., and Stathopoulos, T. (2010). “Wind-Induced Pressures on Patio Covers.” *Journal of Structural Engineering*, 136(9), 1172–1181.

Zisis, I., Raji, F. and Candelario, J. D. (2017). “Large scale wind tunnel tests of canopies attached to low-rise buildings.” *ASCE Journal of Architectural Engineering*, Vol. 23 (1).

Appendix A

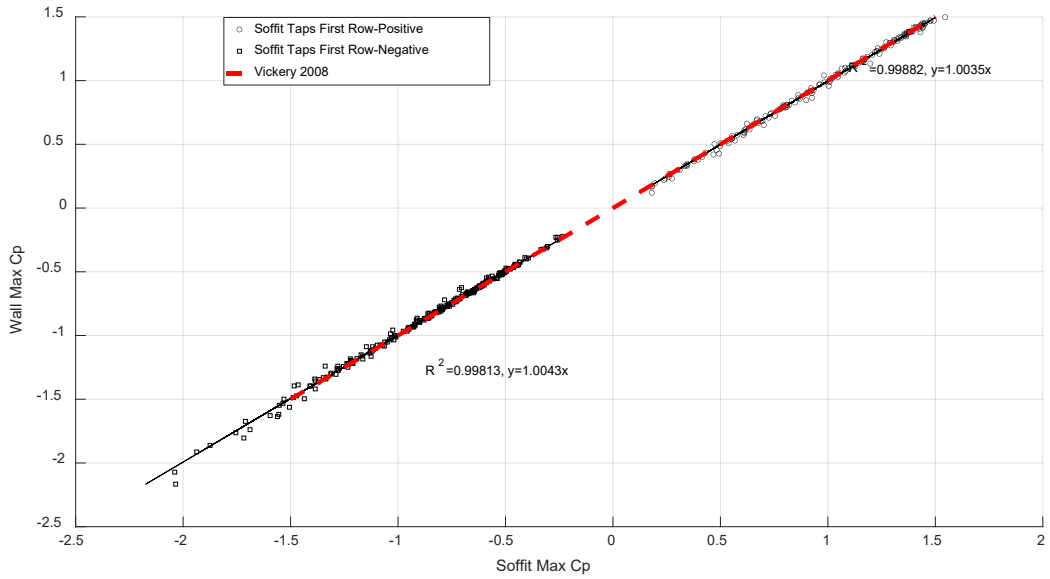

(a)

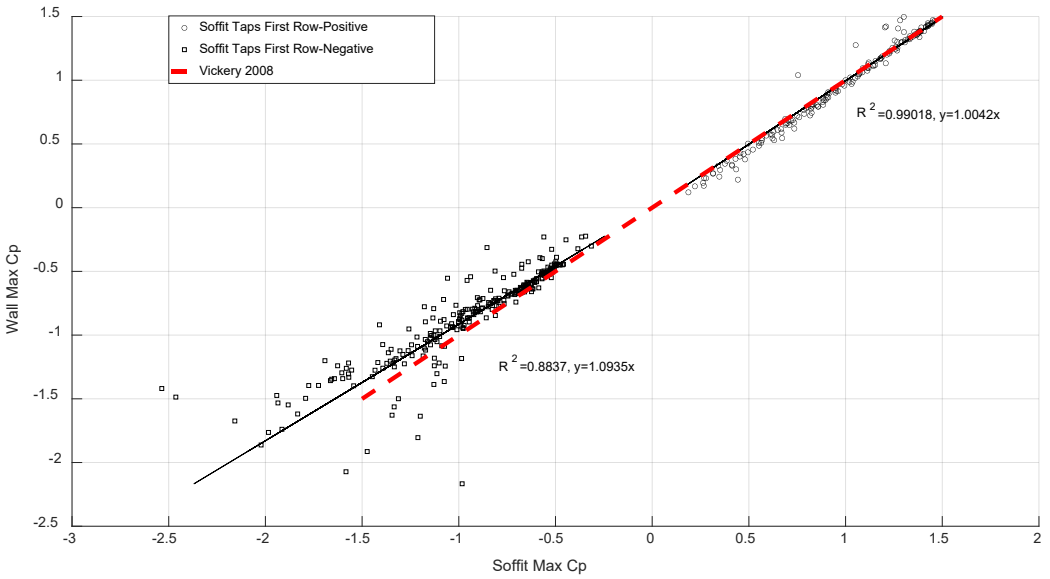

(b)

Figure 45 Linear Regression Relation between Upper Taps in South Wall and (a) first row of taps (b) fifth row of taps in soffit for model E

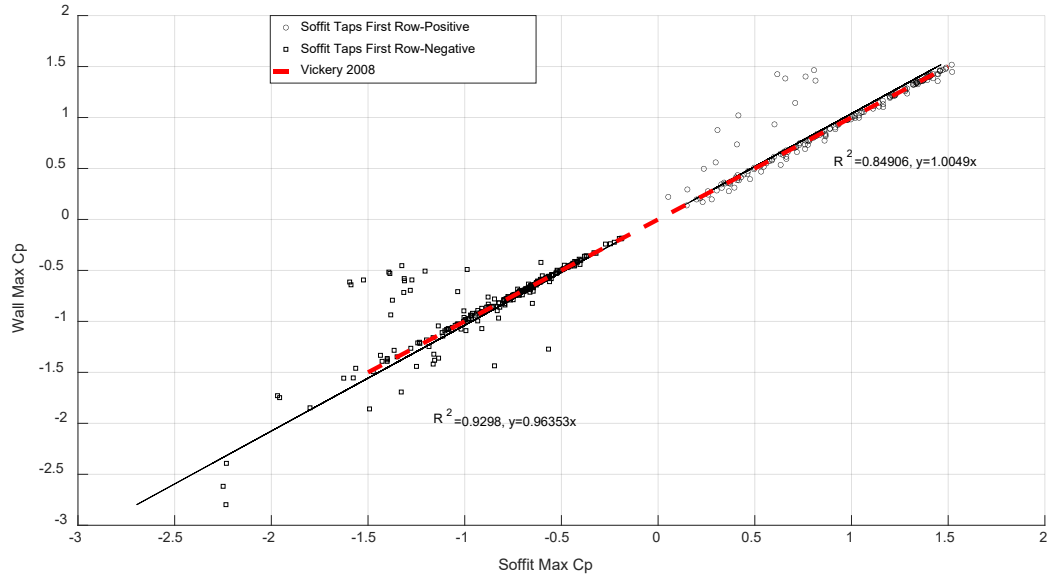

(a)

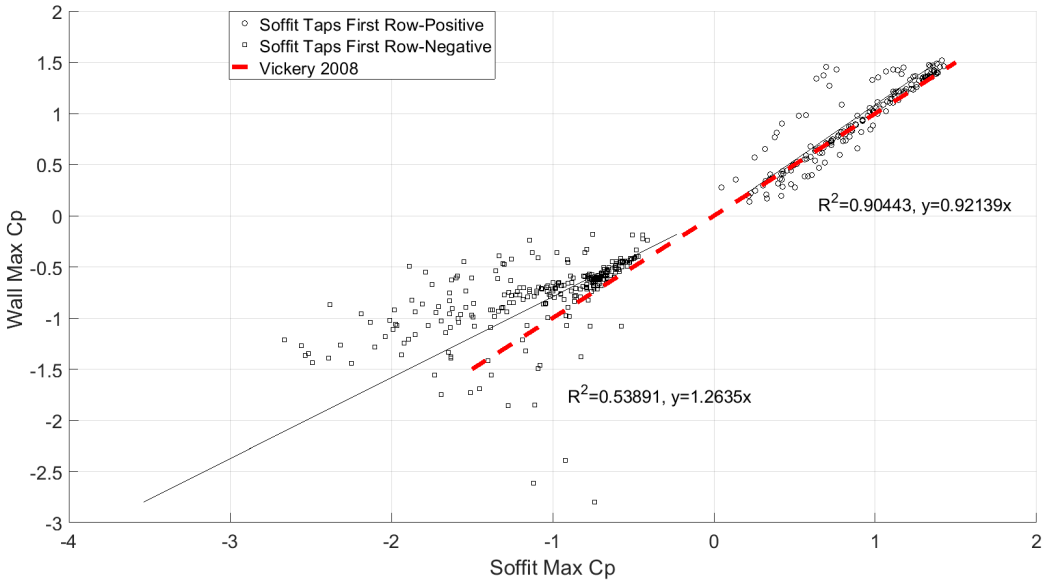

(b)

Figure 46 Linear Regression Relation between Upper Taps in South Wall and (a) first row of taps (b) fifth row of taps in soffit for model F

Appendix B

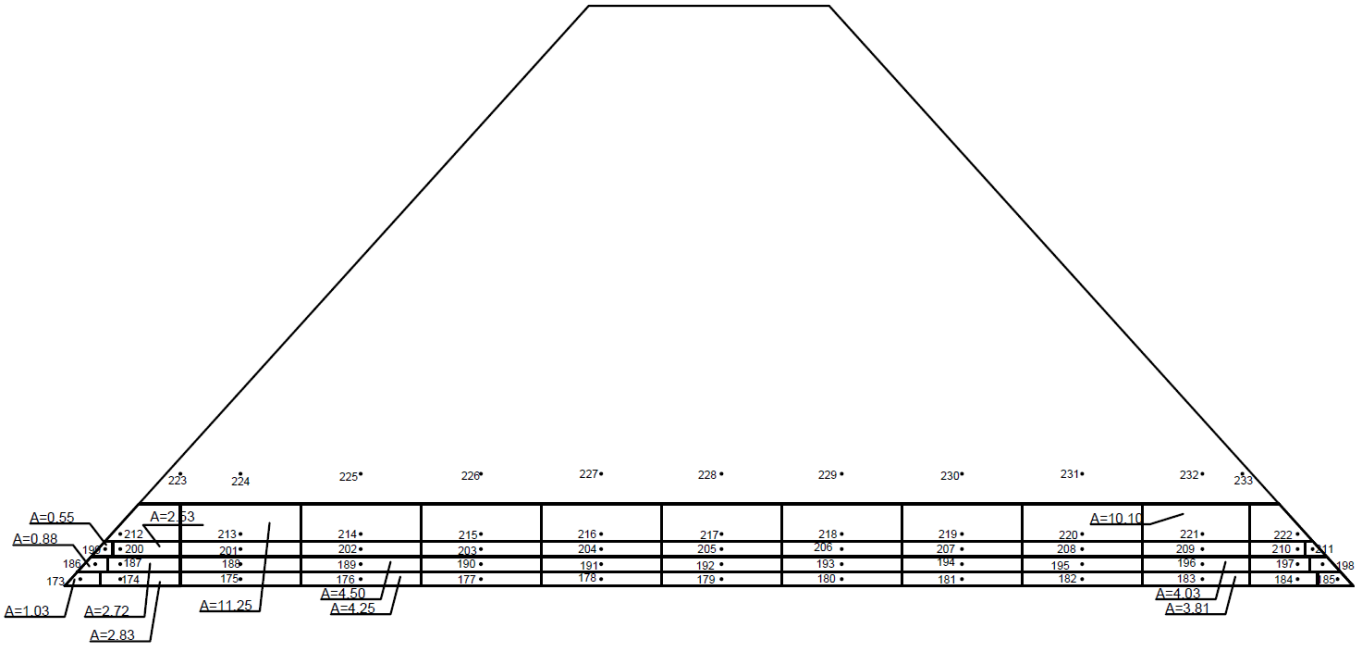

Figure 47 Pressure taps with their tributary area for Model B-south roof

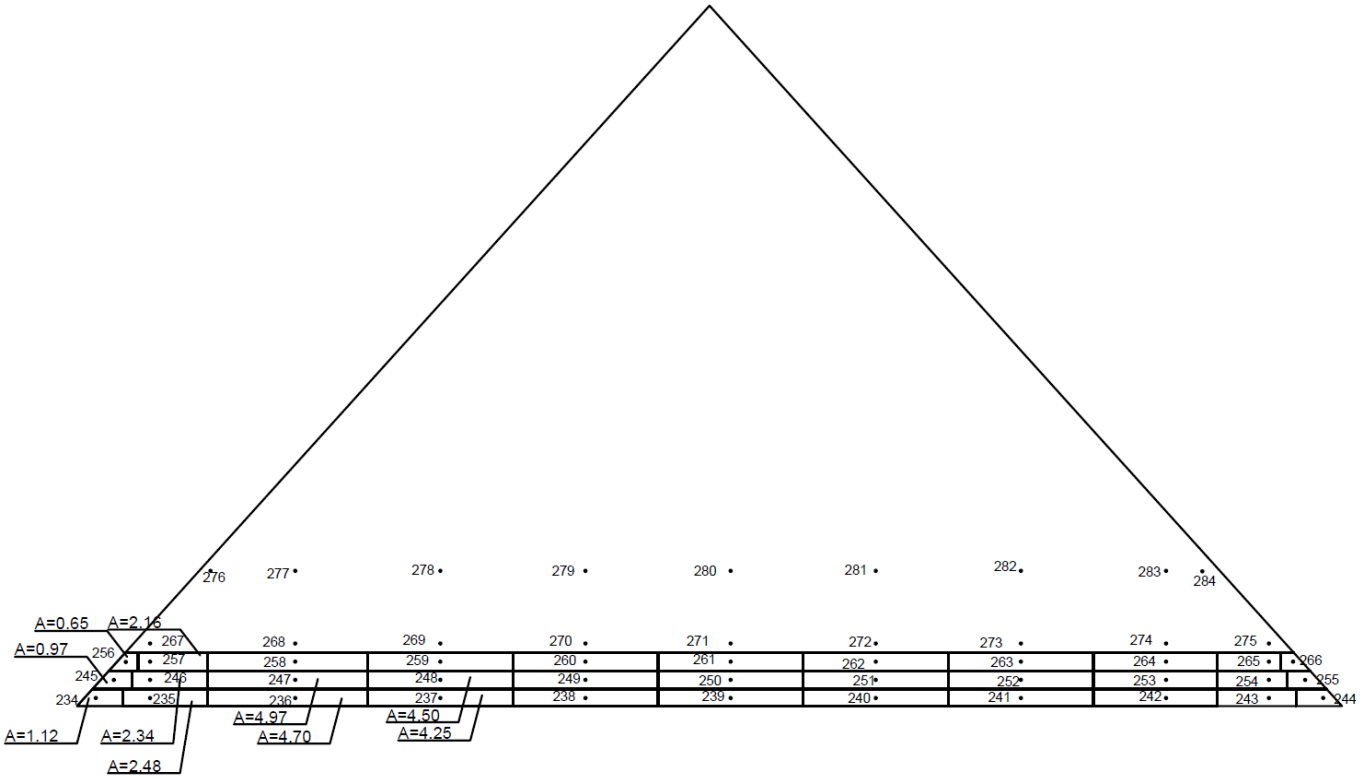

Figure 48 Pressure taps with their tributary area for Model B-East roof

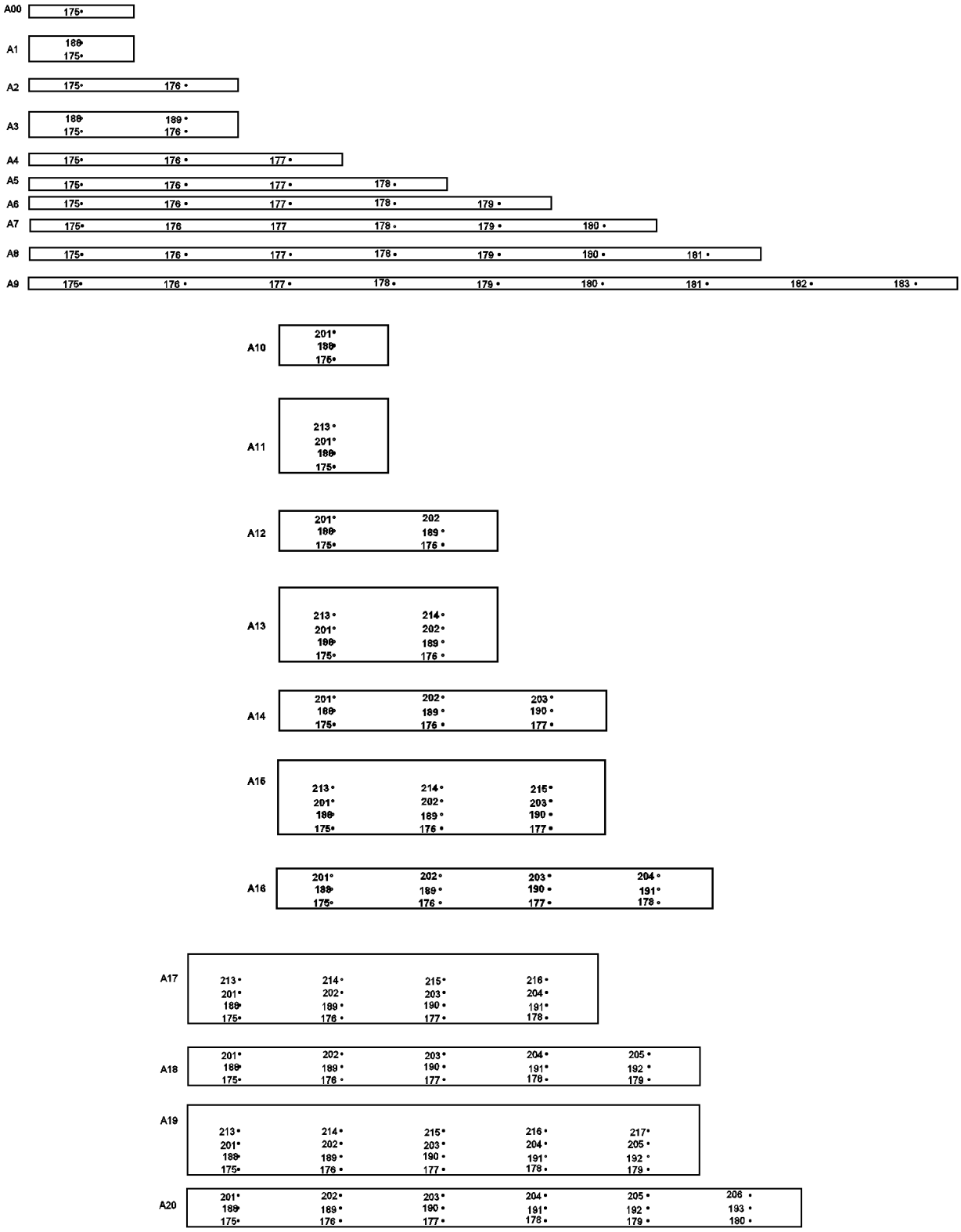

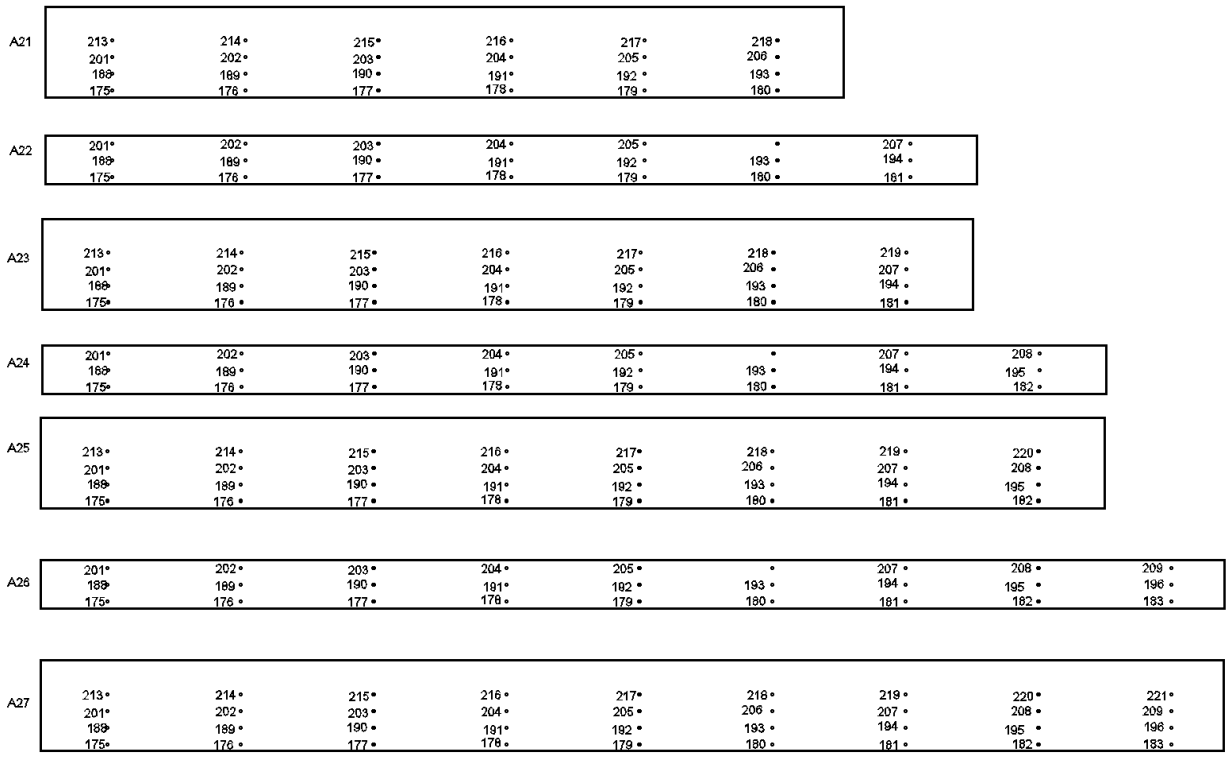

Figure 49 Sample of Area averaging pressure tap combinations for Model B-south roof